RADIOACTIVE FLOW CHARACTERIZATION FOR REAL-TIME DETECTION SYSTEMS IN UREX+ NUCLEAR FUEL REPROCESSING

A Thesis

by

THOMAS RUSSELL HOGELIN

Submitted to the Office of Graduate Studies of
Texas A&M University
in partial fulfillment of the requirements for the degree of

MASTER OF SCIENCE

December 2010

Major Subject: Nuclear Engineering

RADIOACTIVE FLOW CHARACTERIZATION FOR REAL-TIME DETECTION SYSTEMS IN UREX+ NUCLEAR FUEL REPROCESSING

A Thesis

by

THOMAS RUSSELL HOGELIN

Submitted to the Office of Graduate Studies of
Texas A&M University
in partial fulfillment of the requirements for the degree of

MASTER OF SCIENCE

Approved by:

Chair of Committee,	Sean M. McDeavitt
Committee Members,	William Charlton
	Miladin Radovic
Head of Department,	Raymond Juzaitis

December 2010

Major Subject: Nuclear Engineering

ABSTRACT

Radioactive Flow Characterization for Real-Time Detection Systems in UREX+ Nuclear Fuel Reprocessing.

(December 2010)

Thomas Russell Hogelin, B.M.E., Auburn University

Chair of Advisory Committee: Dr. Sean M. McDeavitt

The reprocessing of used nuclear fuel requires the dissolution and separation of numerous radioisotopes that are present as fission products in the fuel. The leading technology option in the U.S. for reprocessing is a sequence of processing methods known as UREX+ (Uranium Extraction+). However, an industrial scale facility implementing this separation procedure will require the establishment of safeguards and security systems to ensure the protection of the separated materials. A number of technologies have been developed for meeting the measurement demands for such a facility. This project focuses on the design of a gamma detection system for taking measurements of the flow streams of such a reprocessing facility.

An experimental apparatus was constructed capable of pumping water spiked with soluble radioisotopes under various flow conditions through a stainless steel coil around a sodium iodide (NaI) detector system. Experiments were conducted to characterize the impact of flow rate, pipe air voids, geometry, and radioactivity dilution level on activity measurements and gamma energy spectra. Two coil geometries were

used for these experiments, using 0.5 in stainless steel pipe wound into a coil with a 6 inch diameter; the first coil was 5.5 revolutions tall and the second coil was 9.5 revolutions tall. The isotopes dissolved in the flowing water were produced at the Texas A&M Nuclear Science Center via neutron activation of chromium, gold, cerium, and ytterbium nitrate salts. After activation, the salts were dissolved in distilled water and inserted into the radioactive flow assembly for quantitative measurements. Flow rate variations from 100 to 2000 ml/min were used and activity dilution levels for the experiments conducted were between 0.02 and 1.6 μCi/liter. Detection of system transients was observed to improve with decreasing flow rate. The detection limits observed for this system were 0.02 μCi/liter over background, 0.5% total activity change in a pre-spiked system, and a dilution change of 2% of the coil volume.

MCNP (Monte Carlo N-Particle Transport) models were constructed to simulate the results and were used to extend the results to other geometries and piping materials as well as simulate actual UREX stream material in the system. The stainless steel piping for the flow around the detector was found to attenuate key identifying gamma peaks on the low end of the energy spectrum. For the proposed schedule 40 stainless steel pipe for an actual reprocessing facility, gamma rays below 100 keV in energy would be reduced to less than half their initial intensities. The exact ideal detection set up is largely activity and flow stream dependant. However, the characteristics best suited for flow stream detection are: 1) minimize volume around detector, 2) low flow rate for long count times, and 3) low attenuation piping material such as glass.

ACKNOWLEDGEMENTS

I would first like to thank my committee chair Dr. Sean McDeavitt for his support and advice through this process. I would like to thank Braden Goddard whose work tied in directly with mine and who assisted me in my own work. I would like to thank the personnel at the Texas A&M Nuclear Science Center for supplying all the radioactive isotopes used in these experiments. I would like to thank Claudio Gariazzo for his assistance with the set up and calibration of my detector system. I would also like to thank the FCML personnel who assisted me in the construction of my experimental apparatus.

NOMENCLATURE

AFCI	Advanced Fuel Cycle Initiative
CCD-PEG	Chlorinated Cobalt Dicarbollide-Polyethylene Glycol
FPEX	Fission Product Extraction
HKED	Hybrid K-Edge/X-ray Fluorescence Densitometry
HPGe	High Purity Germanium
HRGS	High Resolution Gamma Spectroscopy
ICP-MS	Inductively Coupled Plasma Mass Spectrometry
IDGS	Isotope Dilution Gamma-ray Spectrometry
IDMS	Isotope Dilution Mass Spectrometry
KED	K-Edge Denitometry
KMP	Key Measurement Point
LSDS	Lead Slowing-Down Spectroscopy
LWR	Light Water Reactor
MBA	Material Balance Area
MCA	Multi-Channel Analyzer
MCNP	Monte Carlo N Particle
MIP	Multi-Isotope Process
MOX	Mixed Oxide fuel
NaI	Sodium Iodide
NRC	Nuclear Regulatory Commission
NRF	Nuclear Resonance Fluorescence
NSC	Nuclear Science Center
ORIGEN	Oak Ridge Isotope Generation and Depletion Code
PUREX	Plutonium-Uranium Extraction
SEID	Standard Error of the Inventory Difference
TALSPEAK	Trivalent Actinide Lanthanide Separations by Phosphorus- Reagent Extraction from Aqueous Complexes

TARIS	Thermal Atomization Resonance Ionization Spectroscopy
TBP	Tributyl Phosphate
TIMS	Thermal Ionization Mass Spectrometry
TMFD	Tensioned Metastable Fluid Detector
TRU	Transuranic
TRUEX	Transuranic Extraction
UREX	Uranium Extraction
XRF	X-Ray Fluorescence

Elements

Am	Americium
Au	Gold
Ba	Barium
Ce	Cerium
Cm	Curium
Cr	Chromium
Cs	Cesium
Pu	Plutonium
Rb	Rubidium
Sr	Strontium
Tc	Technetium
U	Uranium
Yb	Ytterbium

TABLE OF CONTENTS

Page

LIST OF FIGURES

FIGURE Page

FIGURE Page

LIST OF TABLES

1. INTRODUCTION

As the worldwide demand for electricity continues to climb, the need for a large-scale sustainable power source also continues to increase. Concern is also growing over finding an energy source that will not produce large quantities of harmful greenhouse gases.[1] For this reason advanced nuclear energy systems are being proposed to meet this increasing demand since the fuel is relatively abundant and “burning” nuclear fuel via the fission process produces no carbon dioxide emissions.

Nuclear power currently produces about 20% of the electricity consumed in the United States. This power is produced by over 100 nuclear reactors across the country, all of which contribute to the approximately 2,000 metric tons of high-level radioactive waste generated in the U.S. each year.[1] In order for nuclear energy to remain an attractive option for meeting the growing energy demands, practical solutions must be found for disposing of this waste. Currently high-level radioactive waste is stored either in cooling pools or large dry casks at nuclear reactor sites until a more permanent disposal location can be found. However, at the current rate of waste production, even a large-scale geological repository such as the formerly proposed Yucca Mountain site would be filled to capacity with the waste that will exist by 2015. Reprocessing has the capability to increase the capacity of a geological repository 40 to 60 times by reducing the volume and heat load of waste that requires long-term geological storage.[2]

This thesis follows the style of Journal of Nuclear Materials.

Approximately 96% of commercial used nuclear fuel consists of uranium oxide which when properly separated can be disposed of as a low level waste or re-enriched and reused as light water reactor (LWR) fuel.[1] The remainder of the waste can be divided into two main categories: fission products and transuranics (TRUs). Many of the fission products have half-lives on the order of 10 years or less. Some of the longer-lived fission products such as cesium-137 and strontium-90, 30.1 and 28.8 year half-lives respectively, also produce a great deal of heat. Separating them from the rest of the waste can greatly increase the storage density of waste in a long-term geological storage facility. [3] The TRUs, the majority of which consist of plutonium, pose a difficult long term disposal issue because of their relatively long half-lives, which are typically on the order of thousands to hundreds of thousands of years.[4] However, the plutonium that is separated from the used fuel may be recombined with uranium to produce a mixed oxide fuel (MOX), which can also be used to power the current generation of LWR plants.

Current large-scale commercial reprocessing facilities around the world make use of the PUREX (Plutonium-Uranium Extraction) method, which separates out a pure plutonium and pure uranium stream and puts all the remaining isotopes into the waste stream. PUREX is an aqueous solvent extraction separation process in which the fuel assemblies are first dissolved in hot nitric acid then mixed with certain chemicals in a series of liquid-liquid contactors to remove specific species from the used fuel. Because of the proliferation risk associated with producing separated plutonium in PUREX, a new separation technique has been developed known as UREX (Uranium Extraction) that has become the process of interest for reprocessing in the United States.[1]

The basic UREX process separates uranium (along with technetium) from all the other waste and then separates the two from one another. The plutonium is left mixed in with the high activity actinides, which makes it less desirable to be diverted for weapons purposes. A series of other separations can be performed on the UREX waste stream to divide up the remaining isotopes for recycle, low level disposal, high level disposal, or transmutation. This sequence of consecutive separations is often referred to as the UREX+ family of separation techniques. The particular UREX+ process that is adopted for a future reprocessing facility will depend on the fuel cycle strategy that is finally adopted in the U.S. The production of MOX fuel requires the separation of plutonium from the fission products. Cesium and strontium may be separated from the other fission products if the heat load of the long-term repository needs to be reduced. If fast reactors are employed, then the minor actinides may be isolated to allow them to be burned in a fast reactor.[4]

In the UREX+1a sequence, for example, uranium and technetium are first removed using tributyl phosphate (TBP), which is the typical solvent used in the PUREX process. Technetium is then separated from the uranium using an ion exchange process. The high heat load products Cs and Sr are removed from the UREX raffinate by a process connoted by the solvent CCD-PEG (chlorinated cobalt dicabollide); an alternative process connoted FPEX (Fission Product Extraction) is also being investigated [5]. This also removes the chemically similar fission products Rb and Ba. Then the TRUEX process separates off the transuranic actinides and rare earth metals from the remaining fission products. Finally the TALSPEAK process separates the

transuranics from the rare earth fission products.[6] Figure 1 shows a simplified diagram of the UREX+1a process. Even though the plutonium is kept well "protected" during this process by being mixed in with other isotopes, it is still important to keep track of it throughout this process to ensure no material can be stolen or diverted.

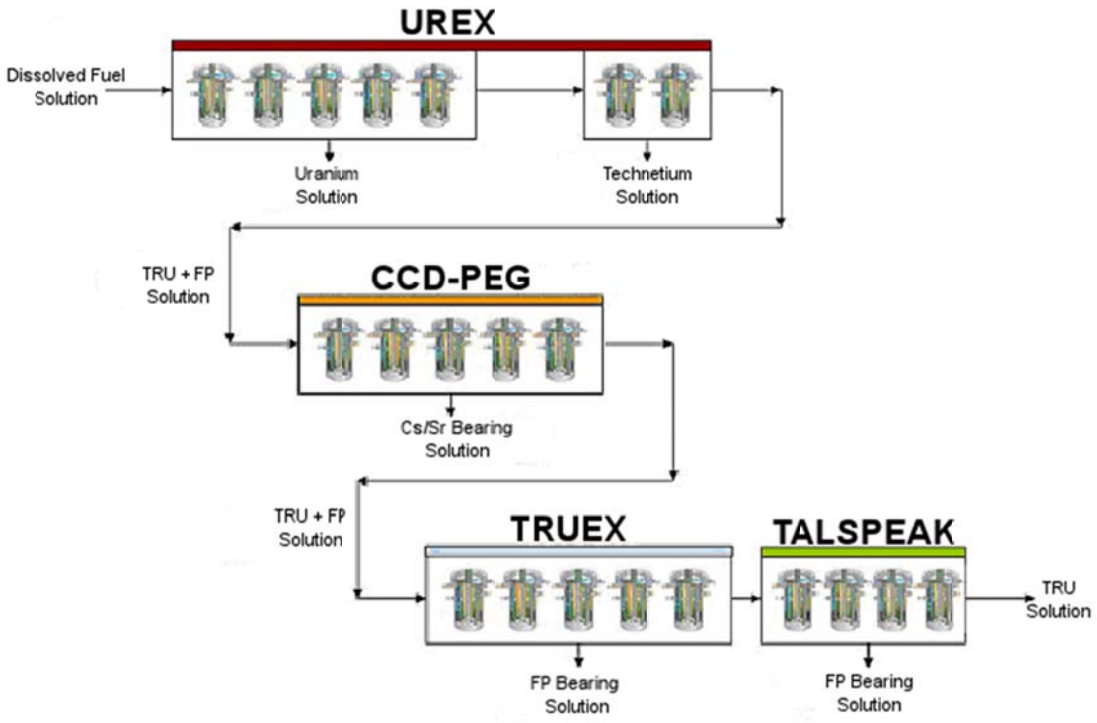

Figure 1. Simplified flow diagram for UREX+1a process.[7]

The focus of this project is to develop a real time detection system for use in a UREX reprocessing facility that can provide timely information on the constituents of each of the flow streams in the plant. This is to ensure that the materials are being separated to the levels required for disposal and that no special nuclear materials (such as plutonium) are being diverted or stolen during the process. In current large scale reprocessing facilities these measurements are performed by separating off a portion of

each stream and analyzing it in a lab using mass spectrometry.[8] This process can take several days or weeks to complete, thus a more timely measurement system would greatly improve the operations of such a facility. The measurement strategy of interest that is used for this project is High Resolution Gamma Spectroscopy (HRGS). Each radioactive isotope produces a characteristic spectrum of gamma ray energies as it decays. By measuring this spectrum with a high level of accuracy it can be determined which isotopes in what concentrations are present at various locations within the processing facility. This system could potentially be implemented within process flow streams so that measurements of the flow stream constituents can be taken in real time, or while the process is operating, without having to shut down the plant or remove and prepare samples from each stream.

The following sections will discuss the potential viability and advantages of using this type of measurement system in a UREX type reprocessing facility. Section 2 gives background on other measurement systems that have been used in reprocessing facilities and those being evaluated for future use in a reprocessing facility. The experiments that were performed for this particular project are discussed in detail in Section 3. The results are presented in Section 4 with discussion of those results following in Section 5. Finally, the last section presents the conclusions that were drawn from this study.

2. PREVIOUS WORK

The design of new measurement strategies and methods to improve materials accountancy in a reprocessing facility is an active area of research and development. [9] There are two major benefits that real-time materials accountancy can provide in a nuclear fuel reprocessing facility. The first arises from the need for improved precision and timely responsiveness such that special nuclear materials such as plutonium cannot be diverted or stolen for use in nuclear weapons. Second, the chemical operations of the facility must be monitored to minimize waste and optimize reagent insertion to ensure that separation efficiencies are high enough that the end products will meet the requirements for their future use or disposal. For example, if a large quantity of cesium carries over into the uranium stream it cannot be disposed of as low level waste and fuel that may be produced from that uranium would require special remote fabrication or additional treatment. The following sections describe briefly some of the new strategies and technologies being explored for implementation in a UREX facility.

2.1 Measurement Strategies

The accountancy goals that are currently used for modeling safeguards strategies for reprocessing facilities are the Nuclear Regulatory Commission's (NRC) regulation 10CFR74 [10], which is for material control and accounting of special nuclear materials. This requires a physical inventory to be taken every 6 months to calculate the "inventory difference" as well as the "standard error of the inventory difference" (SEID). A report is

required of any SEID that is greater than 0.1% of the total inventory and of an inventory difference greater than 3 times the SEID and 200 grams of plutonium. Also, systems are required to be in place that can detected the abrupt loss of 2 kg of weapons useable plutonium within 3 days and 2 kg of non-directly weapons useable plutonium within 7 days with a 95% accuracy. International safeguards standards require the detection of one significant quantity of plutonium (8 kg) with a 95% accuracy over a given material balance period. Current large scale reprocessing facilities do not meet these goals so additional safeguards are required.

The Advanced Fuel Cycle Initiative (AFCI) has established the following set of process chemistry goals for a UREX+1a type reprocessing facility.[6] TRU element recovery must be confirmed to be greater than 99.9% to meet future repository heat load standards. Uranium must be recovered to greater than 95% and contain less than 100nCi/g of TRU elements. Greater than 95% recovery is also required for technetium. The Cs/Sr stream must remove greater than 99% of the amount present in the fuel and also contain less than 100nCi/g of TRU elements. The criteria for the fission product raffinate is that it must follow the recovery rates required by each of the other product streams, such as less than 0.1% plutonium since the recovery rate required is >99.9% for plutonium[6]. These goals may vary depending on the UREX process that is chosen for a reprocessing facility and the final waste forms that are to be produced.

Traditional safeguards strategies of the currently operational PUREX reprocessing facilities are best exemplified by those used at the Rokkasho Reprocessing Plant in Japan.[11] This facility is divided up into 5 material balance areas (MBA) as

shown in figure 2 below. The circles with arrows indicate flow key measurement points that keep track of inventory changes into and out of material balance areas. The circles without arrows indicate the flow measurement points for losses that may occur within a material balance area and the boxes represent inventory key measurement points (KMP) within each area.

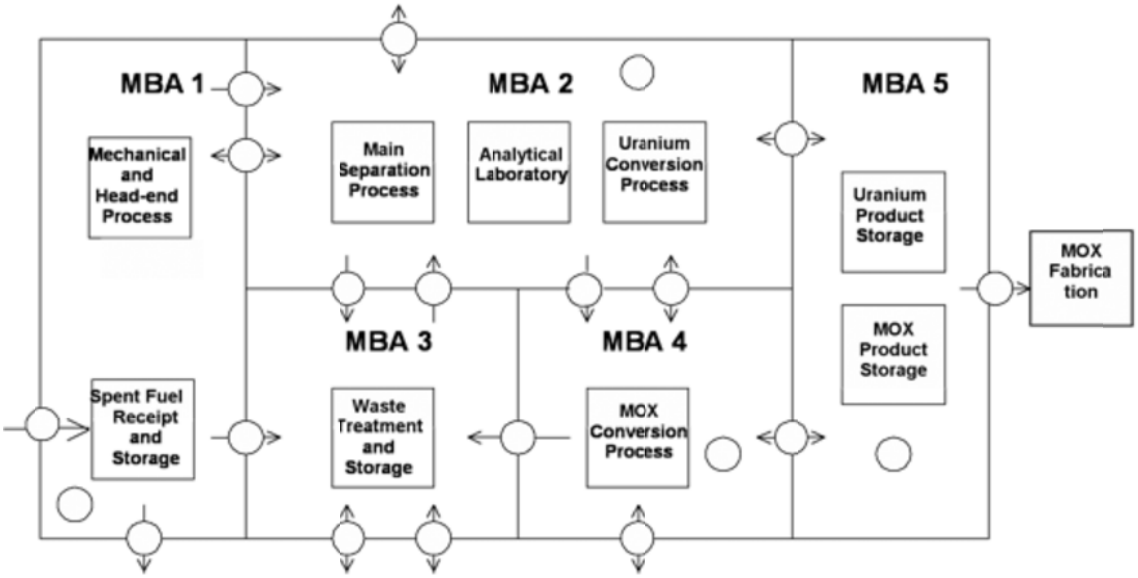

Figure 2. Safeguards Strategy for Rokkasho Reprocessing Plant. [11]

MBA 1 is where irradiated fuel assemblies are received and stored and then mechanically chopped and dissolved at the head end of the plant. Currently plutonium measurements in undissolved fuel assemblies are very poor due to material self shielding and inhomogeneities so heavy surveillance must be used in this area. Once dissolved, the plutonium concentration can be measured to with 0.3 to 1 percent uncertainty. Fuel cladding and other undissolved waste are transported to MBA 3 while the bulk of the

material is sent to the separations area in MBA 2. The PUREX separation process removes only the uranium and plutonium from the used fuel and sends the remaining isotopes into the waste in MBA 3. The purified plutonium stream in MBA can be measured to within 0.2 to 0.8 percent uncertainty. At least 99% of the separated uranium is converted to UO_3 and sent to MBA 5 for storage while the remaining uranyl nitrate is sent to MBA 4 for conversion to MOX powder. Laboratory measurements of the product powder are used to determine the plutonium concentration to 0.2% uncertainty. The MOX powder is then sealed into cans before being transported to storage in MBA 5 so that manual surveillance is sufficient to maintain the integrity of the measurements taken in MBA 4. Large process hold-up in MBA 2 creates the need for the periodic flushing of the entire facility. This makes detection of a protracted diversion of material difficult between flush out periods. Less than 0.5% of the total plutonium is lost into the waste stream into MBA 3. However, current measurement technologies of this stream create uncertainties in this measurement of 5 to 25 percent. [11]

Developing a safeguards approach to a UREX processing facility is more complex than the approach used in PUREX because of the additional separations steps required by UREX. A recent study by Sandia National Laboratory identifies the two biggest weaknesses of current safeguards as: 1) long time periods for taking precision measurements which limit the number of areas that can be sampled and 2) lack of precision measurements that are taken of process inventory. [9] As with the Rokkasho Plant, a periodic flushing of the facility would be required for a UREX plant to measure the in-process inventory. If a near real-time accountancy system is developed that can

measure process inventory with a high degree of precision then the need for plant flush out could be eliminated completely and a complete mass balance could be quantified for the plant on the order of every 8 hours. [9]

A study conducted by Feener in connection with this project developed a safeguards strategy for a UREX+1a facility using three types of safeguards systems: nuclear materials accountancy, containment and surveillance, and solution monitoring.[12] Figure 3 below indicates the material balance areas chosen as well as key measurement points inside of MBAs and between MBAs. The MBA 3 was divided into parts A through D to be better suited for having separate containment and surveillance systems for each separation step. Also, the solution monitoring systems for smaller MBAs have a higher probability of detection of a diversion faster than for a larger MBA.

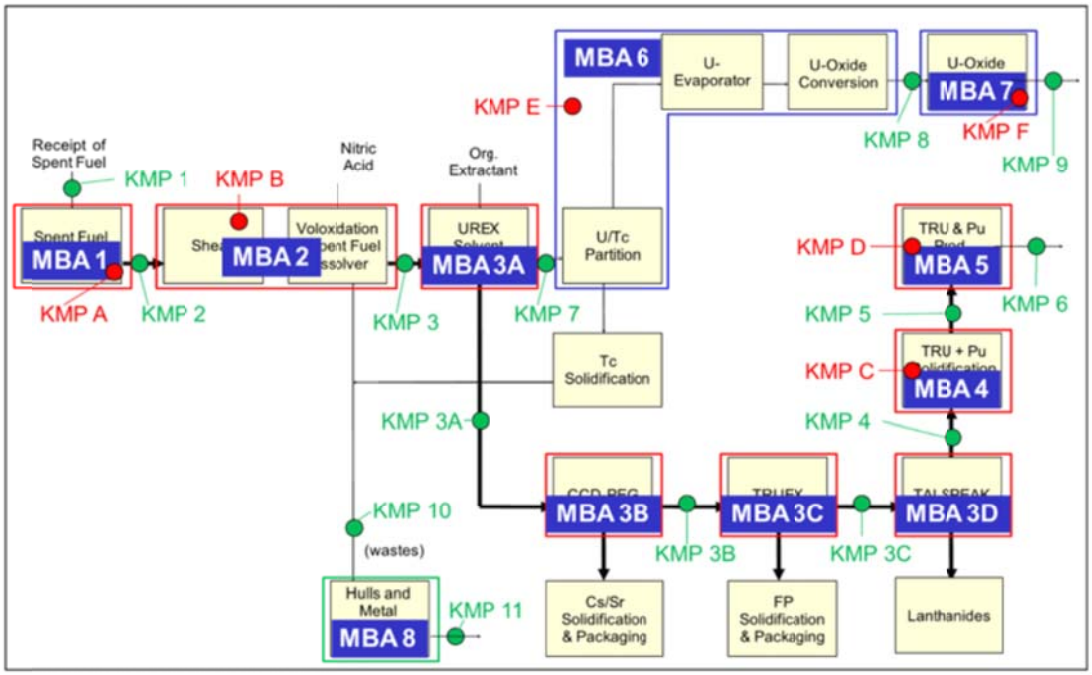

Figure 3. MBAs and KMPs for UREX+1a facility identified by Feener. [12]

A simulation was conducted by Sandia National Laboratories to determine the process locations and level of precision required for measurements to achieve the goal of near real time accountability. In this study, measurement at the head end of the plant was ignored due to the high uncertainties associated with measuring Pu content before the used fuel is chopped and dissolved. Figure 4 shows an expanded UREX+1a flow diagram and indicates the locations where additional measurements would be most effective. This study looked at a much more detailed view of each separation step and thus identified a different set of useful KMPs than the study conducted by Feener. The KMPs shown in red indicate the areas where the high precision of mass spectrometry would be required for determining plutonium concentration. The KMPs shown in green are located at the mixer-settler tanks where the concentration of nuclear material is expected to be very low. For this reason high precision is not required and a non-destructive measurement technique such as gamma and alpha spectroscopy may be used.

The remaining KMPs in blue are at locations of high plutonium concentrations. These points are located at the UREX feed tank, the UREX contactors, the TRUEX stripper, the TRUEX reduction vessel, and the TALSPEAK feed adjustment tank. These locations would require more advanced measurement technologies than the ones used in current plants. They require the high precision associated with IDMS but also require the timeliness offered by non-destructive measurement techniques. This measurement strategy only focused on keeping track of plutonium concentration and not the other actinides and fission products. Techniques such as hybrid K-Edge densitometry (HKED) or high resolution gamma spectroscopy (HRGS) should be adequate for tracking these

materials. [9] The new technologies that may be useful at each of these key measurement points will be discussed further in the following section.

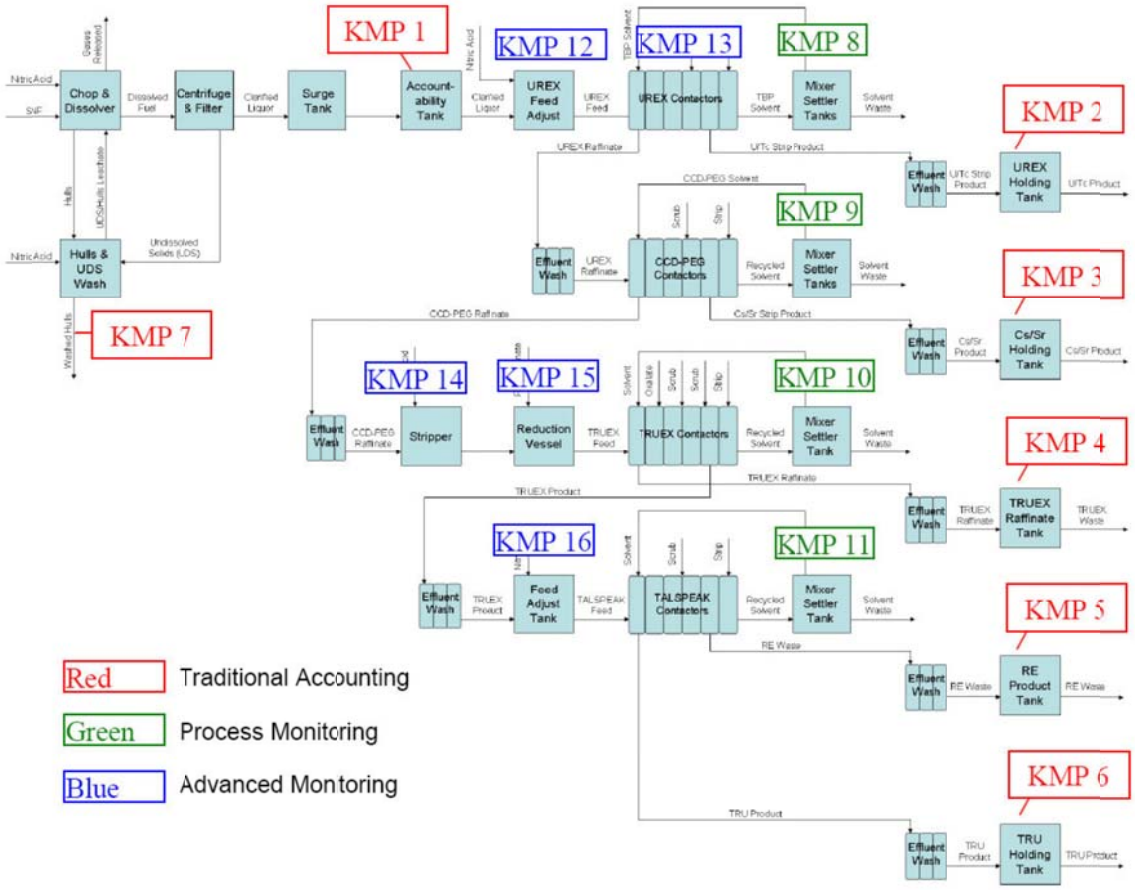

Figure 4. UREX+1a key measurement points required for near real time materials accountancy. [9]

2.2 Measurement Technologies

Mass spectrometry is the current standard for achieving high precision nuclear measurements.[13] However, it requires a relatively long sample preparation time since similar species which could create interference must be chemically separated from the sample before measurement. There are a number of different methods of mass

spectrometry including isotope dilution mass spectrometry (IDMS), thermal ionization mass spectrometry (TIMS), and inductively coupled plasma mass spectrometry (ICP-MS). IDMS requires the sample to be fully chemically separated and to have reached isotopic equilibrium before it is accelerated into the mass spectrometer. A standard of known concentration and known isotopic composition must be added to the sample before it is measured.[14] ICP-MS currently has the highest level of accuracy with the ability to give isotopic ratios of uranium and plutonium with an uncertainty less than 0.1%. The ICP-MS technique also involves faster sample preparation time and makes use of an argon plasma to ionize the sample before it is accelerated into the mass spectrometer. [13]

One measurement method that has the potential to replace mass spectrometry is Isotope Dilution Gamma-ray Spectrometry (IDGS).[15] IDGS works similar to IDMS but has the advantage of easier and faster sample preparation. With IDGS plutonium and uranium isotopic compositions and elemental concentrations can be measured simultaneously. This method is well suited for taking measurements of used fuel dissolver solutions. Methods have been developed for effectively separating all the other fission products and activation products leaving only plutonium and uranium in the sample. A control sample must be prepared that is spiked with a sample of well known concentration and isotopic composition of plutonium. Once the samples have been prepared, a planar high purity germanium (HPGe) detector is used to measure certain low energy characteristic gamma rays from the plutonium and uranium. The ratios of these gamma peaks can then be used to compute both isotopic compositions as well as

elemental concentrations. Tests have shown plutonium isotopic measurement precision for IDGS to be ~0.5% and plutonium concentration measurement precision to be less than 1% using a 1-hour count time. [15]

Several measurement techniques exist that have the potential to provide on-line near real time measurements but lack the precision required to be an effective replacement for mass spectrometry. K-edge densitometry (KED) involves bombarding a sample with an x-ray spectrum while a scintillation detector on the opposite side counts the x-rays passing through to determine the energy levels which were absorbed by the K-shell electrons in the sample. This is useful in determining the uranium concentration in the head end of a reprocessing facility and can achieve uncertainties of 0.2%. A similar method called x-ray fluorescence (XRF) uses x-rays to excite electrons which then give off characteristic x-rays of each particular element. The XRF method has the ability to determine the plutonium concentration in a given sample to within ±2% uncertainty. The combination of these two methods into HKED and using two HPGe detectors can give measurements of the plutonium concentration with ±0.7% uncertainty. [13]

The measurement technique of primary interest to this project is HRGS (high resolution gamma spectroscopy) which identifies radioactive isotopes based on the characteristic gamma energies they emit from decay. This technique is most effective for the flowing process streams after major separations steps have occurred as a large number of radioactive isotopes in a single stream can cause interferences. Also, highly active isotopes such as ^{137}Cs can mask out most other materials when it is present in a stream. The HRGS method has the potential to take real time measurements of materials

as they flow through process streams or in process holding tanks rather than having to remove samples for mass spectroscopy.[16] The uncertainty for measurements taken using HRGS is typically between 0.5 and 2% for separated material streams. [13] It has also been proposed that HRGS can be used to track changes in a well characterized spectrum for a flow stream rather than being used to track particular isotopes.[17] Changes in process chemistry associated with a diversion of material would show up as changes in the gamma spectrum of that particular flow stream. This tracking method is known as Multi-Isotope Process (MIP) monitoring and could be used to indirectly keep track of special nuclear materials like plutonium. Work is needed to identify which isotopes in each process stream that produce recognizable gamma energies are most chemically similar to plutonium to be used as trackers. Also, work is needed to determine how much fluctuation in the spectrum occurs under normal operating conditions and what changes would be indicative of a significant process chemistry change. [17]

Passive neutron coincidence counting (PNCC) is sometimes used alongside of HRGS for determining plutonium mass and isotopic ratios. Like HRGS, coincidence counting has also been proven effective in taking continuous automated measurements for real-time or near real-time material accountancy.[16] Neutron detectors are used in PNCC to count neutrons from the spontaneous fission of ^{240}Pu while HRGS is used to determine the ^{240}Pu to ^{239}Pu ratio. Active NCC uses a neutron source to cause plutonium isotopes to fission and then measures the resulting neutron release and decay. NCC

typically has uncertainties between 2 and 5% due to neutron attenuation and geometry effects. [13]

Currently there are no accurate methods for measuring fissile material in used fuel assemblies before the chopping and dissolution stage [17]. Typical methods involve measurements of gamma emissions from high activity isotopes such as ^{137}Cs and neutron emissions from ^{244}Cm to indirectly infer the nominal amount of plutonium in the fuel. These computations are often complex and rely heavily on data on the history of the operation of the reactor where the fuel was used. This data may be incomplete or incorrect due to mistakes or intentional changes made by the operators who recorded the data. Uncertainties in the total plutonium concentration in undissolved fuel assemblies are typically around 5%. One method that has been proposed to solve this issue and give direct plutonium measurements in the used fuel is lead slowing-down spectroscopy (LSDS). [17] In this method, the used fuel assembly is placed in a large lead pile that acts as a continuous slowing-down moderating media for a pulsed neutron interrogation source. The source must be of sufficient intensity to overcome the background from ^{244}Cm and must also have a pulse width of only a few microseconds. A series of fission chamber neutron detectors are located around the fuel assembly in the lead pile capable of giving a neutron energy spectrum. Simulations of this technique have demonstrated uncertainties in the same range as current techniques without the need for operator data. [17]

There are other new technologies currently under development that may hold the key to creating highly accurate measurements that can still achieve near real time

accountancy goals. One of these new technologies is thermal atomization resonance ionization spectroscopy (TARIS). [13] This works much like an automated version of mass spectrometry. The sample solution is atomized from a hot tantalum plate into a vacuum chamber where it is then ionized by a laser of a particular frequency which excites only a particular element group. The excited vapor species are then sent through a mass spectrometer to compute the isotopic ratios in the particular element group selected. TARIS has the capability to give measurements with precision on the same order as ICP-MS with a much faster, automated sample preparation. A tunable laser would give the system the ability to switch between measuring several different element groups. [13]

Another advanced measurement technology still undergoing development is nuclear resonance fluorescence (NRF). A compact electron accelerator is used to produce a high energy photon spectrum (2-8 MeV) which excites isotopes in the sample to unique nuclear states, each of which produces characteristic photon energies when they decay back to the ground state. NRF creates less interferences than atomic excitation since nuclear excitation states produce much fewer wavelengths. The penetration power of the high energy photons makes this method feasible for use on non-homogenous solid materials such as the undissolved fuel assemblies at the head end of the plant. Sufficient tests have not been performed using this method to determine the precision capabilities. Also, information on nuclear resonance states for all the isotopes of interest is not complete. A great deal of experimentation would be required to create this database before NRF could become a viable nuclear measurement option. [13]

A new detection system is currently being developed at Purdue University under the direction of Taleyarkhan for the detection of neutrons and alpha particles.[18] This system is known as the tensioned metastable fluid detector (TMFD). In this type of detector, a fluid is held at a negative pressure in such a way that an interaction of a nuclear particle with the fluid will break the molecular bonds causing a bubble to nucleate and collapse. This interaction can be measured both visually and audibly. The amount of negative pressure or tension applied to the fluid affects the range of particle energies that will nucleate bubbles in the detector. Since the detector response depends on the linear energy transfer from the incident particle, neutrons and alpha particles can be readily detected without any interference from gamma rays. This gives this type of detector system the ability to measure isotopic concentrations of nuclear materials based on neutron or alpha emission in the presence of a high gamma fields, such as those found in a reprocessing facility, without any gamma interferences. [18]

3. EXPERIMENT SETUP AND PROCEDURES

The purpose of the experiments described in this section is to create a knowledge base for the design of an in-line HRGS detection system to be used in a future UREX type reprocessing facility. These experiments demonstrate how such parameters as flow rate, flow geometry, and material attenuation affect the ability to measure the constituents of a flowing stream of radioactive liquid and to detect subtle changes in the process fluid. The intention is for these experiments to be general enough that they can be applied to any flow stream or holding tank in a reprocessing facility where they would be found useful. A number of radioactive isotopes were chosen that could be easily produced by activation in a research reactor and provide a range of gamma energies. The selected isotopes had half lives that were relatively short (1 to 35 days) so that they would not pose long term waste issues and they would not decay significantly during the experiments.

3.1 Selection of Isotopes

A list was draw up of materials that could easily be made into radioactive isotopes by neutron activation and which also had half-lives greater than 1 day. Materials were rejected from the list that created isotopes with half-lives greater than 35 days to minimize the long term waste produced by this project. Also materials that produced high energy (>2MeV) gamma or beta rays or posed possible toxicity hazards were removed from consideration. Finally calculation were made using ORIGEN to

determine if any of the natural isotopes of the selected elements posed any high activity hazards or had long half-lives when activated. The elements that were selected for activation were chromium, gold, cerium, and ytterbium. The major isotopes of interest that were produced by activation of these elements were ^{51}Cr, ^{198}Au, ^{141}Ce, ^{143}Ce, ^{169}Yb, ^{175}Yb, and ^{177}Yb. A summary of the associated half-lives and primary gamma energies of each of these isotopes is given in table 1.

Table 1. Half-lives and primary gamma energies of major isotopes used.

Isotope	Half life	Primary Gamma Energies (keV)		
Cr51	27.7 days	320.1		
Ce141	32.5 days	145.4		
Ce143	1.377 days	57.4	293.3	
Yb169	32.03 days	63.1	198	
Yb175	4.185 days	396.3	282.5	113.8
Yb177	1.911 hours	150.4	1080.2	
Au198	2.6952 days	411.8021		

These elements were procured in their nitrate form so that they would be easily dissolved in water and so they would be chemically similar to those elements in a reprocessing facility that have been dissolved in nitric acid. Samples of all the necessary chemicals were transferred to the Texas A&M Nuclear Science Center (NSC) were the needed amount of activity was produced in the NSC 1 MW research reactor by neutron activation before each experiment. The materials were delivered to the lab in plastic vials which were emptied into a beaker containing 500 ml of distilled water. Because of the large number of gamma peaks present, cerium and ytterbium were chosen for direct comparison studies between the different coil geometries. Gold nitrate presented

problems with dissolution in water but did produce an interesting result which will be discussed in a later section.

3.2 Experimental Apparatus

An enclosed fluid circulation system was designed and built for this project. The initial experimental consisted of a single tank, a peristaltic pump, and two flow meters connected with the stainless steel coil that surrounded a sodium iodide (NaI) detector. The system was modified in minor ways (described below) as the experiments progressed. The coil and the detector were surrounded by lead bricks to minimize background. Aluminum plates 3/8 inch thick were added between the bricks and coil/detector to reduce the number of lead x-rays produced. The pump, tank, valves and piping of the system were all located inside a sealed clear plastic enclosure with three glove ports that was designed to prevent the contamination of the laboratory in the unlikely event of a leak or spill during operation. A photograph of this set up is shown in figure 5 below.

Figure 5. Initial experimental apparatus (1) Reservoir Tank (2) Peristaltic Pump (3) Radioactive material fill port (4) Glove port (5) Access door (6) High and low end flow meters (7) Detector and steel coil in lead shielding.

For the initial proof of principle experiments, a sodium iodide (NaI) detector with multichannel data acquisition was adequate to enable spectra comparisons and model development. An actual system would require a detector of higher resolution such as an HPGe detector in order to distinguish the greater number of gamma peaks associated with an actual UREX flow stream. The system flow rate was controlled by the peristaltic pump and measured by one of the two flow meters, depending upon the flow regime for each experiment. Modifications were made after the first set of experiments and the low end flow meter (30-300 ml/min) was removed for simplification since the majority of experiments occurred in the range of the high end flow meter (300-3000 ml/min).

The pump model that was chosen was rated to operate over the flow rate range of 1-3400ml/min. Because of the chemical resistant tubing used in this set up, the maximum achievable flow rate for the experiments performed was around 2000ml/min. The experiment flow rate range was chosen based on flow rates found that are typically used for the centrifugal contactors that perform each separation. Since pipe sizes are scaled down to 1/2in inside diameter from the 2in inside diameter expected to be found in a real facility, flow rates were scaled accordingly. Large scale contactors first designed in the 1970s of 9cm rotor size are rated for flow rates on the range of 5 to 13 liters per minute.[19] Assuming these used 2 in piping between them, then the scaled flow rate falls within the appropriate range. Miniature 2cm rotor size contactors were rated at around 120ml/min. Another centrifugal contactor study used a pipe size of 3/8in for a 5cm rotor size with tests conducted between about 0.59 and 3 liters per minute [20].

During experiments radioactively spiked water or clean distilled water could be added through the funnel on top of the main tank. A secondary tank was added to enable the insertion of clean (non-radioactive) water directly into the system piping rather than through the main reservoir tank. This clean water tank is located higher than the water level in the main tank so opening the valve causes it to become the dominate source of flow to the coil. Figure 6 shows a diagram of the system after all system modifications were made and in which the majority of the experiments took place. Using the forward pump setting, water flows out of the bottom of the main tank to the coil and returns via the pump to the top of the main tank.

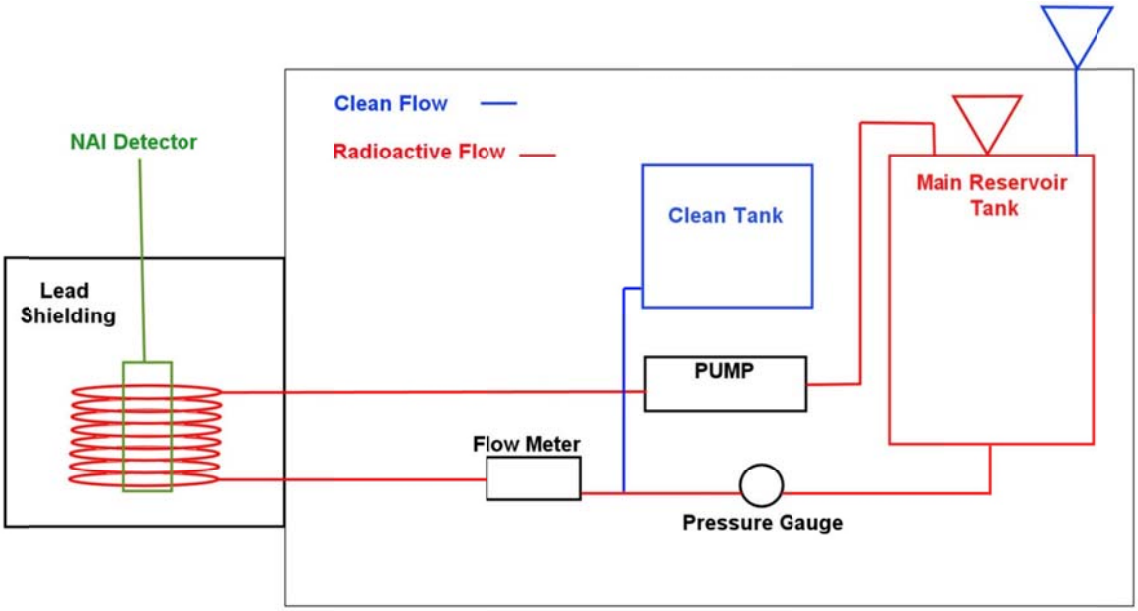

Figure 6. Schematic of the experimental apparatus for the circulation of radioactive fluid through a test coil.

Three stainless steel coils were fabricated to evaluate differences that arise using different geometries. The stainless steel pipe used to make the coils had an inside diameter of 0.5 in with 0.0625 in thick walls. The first two coils were wound around a 6in inside diameter. Coil 1 was 5.5 revolutions tall giving it a total volume of 370 ml and Coil 2 was 9.5 revolutions tall with a total volume of 630 ml. The third coil was wound 5.5 revolution around a 10” inside diameter for a 590ml total volume, but this coil was never installed because of the results from the experiments on the first two coils negated the need for further testing. A photograph of all three coils is shown in figure 7.

Figure 7. Detector coil geometries used from left to right: Coil 1 - 370ml, Coil 3 - 590ml, Coil 2 – 630ml.

The geometry comparison experiments also made use of a different multi-channel analyzer (MCA) connected to the NaI detector from the first experiments. A Lynx MCA was chosen to replace the Unispec MCA in these experiments because it has the capability to take time-stamped counts. This allows for viewing spectrum changes with time as well as total count changes over time. The basic Unispec system that was used in the initial experiments had the capability to take counts across 1024 channels which was sufficient for the resolution of the NaI detector. This MCA is capable of either measuring and reporting an energy spectrum or reporting the total counts over the entire spectrum as a function of time but it cannot do both at the same time. The NaI detector that was used both MCA systems had a cylindrical crystal 3 inches in diameter by 3 inches tall.

3.3 Initial Experiments

The initial experiments were all performed using Coil 1 and the Unispec MCA with the 3x3 NaI detector. The first experiment was performed using activated chromium which consists mainly of a 320 keV peak from ^{51}Cr. The first chromium experiment was used mainly to give an idea for the activity level and dilution level of that material in water that would be visible to the detector assembly. After this test, the activity level of the material produced by the NSC was increased to around 5 μCi total and the initial volume of water in the main reservoir tank was reduced to about 15 liters for further experiments. A summary of the initial set of experiments conducted on coil 1 is given in Table 2.

The first experiment performed each time, referred to in the table as “Spiking”, consisted of the addition of different percentages of the total material into the system running at constant flow rate. The “Flow Rate Variation” experiments consisted of changing the system flow rate in incremental steps over time with the material already in the system while holding all other variables constant. During the “In-line Dilution” experiments, the pump speed was kept constant while the valve connecting the clean water tank to the system was opening for varying intervals of time. Finally the “Void Comparison” experiments consisted of making a 15 min spectrum count under flow conditions in which the pipe was known to contain a low percentage of air voids and then making another spectrum count under flow conditions in which the air void percentage is known to be much higher.

The system was flushed out and rinsed in between each change of isotope for the initial set of experiments. The experiments conducted later for the comparison of the geometries used a different procedure and are described in detail in Section 3.4.

Table 2. Summary of initial experiments performed on Coil 1 using single isotopes.

Chromium	A) Spiking
	B) Flow Rate Variation 1
	C) Flow Rate Variation 2
Gold	A) Spiking
	B) In-Line Dilution
	C) Void Comparison
Cerium	A) Spiking
	B) In-Line Dilution
	C) Void Comparison
Ytterbium	A) Spiking
	B) In-Line Dilution
	C) Void Comparison

At the start of each experiment the activated materials would be delivered from the NSC in plastic vials. These vials would be placed directly beside the NaI detector and the gamma ray energy spectra would be collected for 15 minutes. The vials would then be dissolved into 500ml of distilled water and the beaker containing the solution would be placed by the detector and counted for 15 minutes. The counting of the vials and beakers occurred in less lead shielding than the actual experiments so 15 min. background counts were also taken in the same location. Similar 15 min. background

counts were also taken inside the coil with the system pump running to characterize the background activity of the system before the material of interest was added.

In each of the two experiments that used the activated chromium, the total counts over the entire gamma energy spectrum were acquired in 5 second intervals for the duration of the experiment. Half of the 500 ml beaker containing dissolved chromium nitrate was added to the tank at two separate points of time with a constant flow rate of around 620 ml/min. For the second chromium experiment total counts over time were taken while the pump speed was increased with time with all the chromium dissolved in the system. This experiment was then repeated with the flow rate being decreased over time.

In the activated gold nitrate experiment only about 17% of the gold delivered from the NSC (based on the measured activity) was dissolved in the 500 ml beaker of water. The remaining solid particles were filtered out and only the fully dissolved portion was used in the experiment. In this case, all of the gold was added to the system at once since the total activity in solution was significantly reduced from the planned level. After the activated gold was in the system, the flush valve on the clean water tank was opened for various time intervals at constant pump speed. The valve opening time durations for this experiment were 1 min, 30 sec, 15 sec, and then 1min again. The flow rate was carefully recorded on each opening to enable the calculation of the amount of clean water that entered the system at each point. The addition of clean water to the system had a slight effect on the flow rate even though the pump speed remained constant. Spectra were taken with the system under constant flow conditions to compare

the condition when the pipe was fully filled to when the pipe contained large amounts of air pockets. It was at this point that it was observed that the gold within the system was collecting inside the stainless steel coil over time. This observation is described in more detail in Section 4.

The next experiment conducted used the activated cerium nitrate which was added to the system 250 ml at a time just as in the chromium experiment. The flush valve on the clean water tank was opened for time periods of 1 minute, 30 seconds, 15 seconds, 5 seconds, and finally 1 second while the pump flow speed was kept constant. As in the gold experiment the flow rate changed as water was added to the system and the pump remained at constant speed. Spectra were collect for fully filled and partially filled pipe conditions just as in the gold experiments.

The experiments documenting ytterbium additions followed by and clean water flush was performed with a more complex solution insertion procedure than the previous experiments. This procedure is shown as the two sections of Table 3. The times are measured from the start of each particular experiment. The noted ytterbium portions come out of the 500 ml beaker of water into which the ytterbium was dissolved; water added indicates additional water added rather than total. Unlike the previous experiments, the in-line dilution experiments using ytterbium in the system were performed at various flow rates. A void comparison experiment was then done for the ytterbium spiked system as it had been done for the isotopes used in the system previously.

Table 3. Procedure of ytterbium experiment.

(A) Ytterbium Addition				(B) In-Line Clean Water Dilution		
Time (sec)	Yb added	Water added	Flow rate	Time (sec)	Duration (sec)	Flow rate
969	10ml	700ml	690 ml/min	430	30	700 ml/min
1760	100ml	700ml	700 ml/min	870	15	700 ml/min
2393	300ml	700ml	700 ml/min	1210	5	700 ml/min
3118	5ml	700ml	700 ml/min	1572	1	700 ml/min
3485	5ml	0ml	700 ml/min	1934	5	420 ml/min
3741	10ml	0ml	700 ml/min	2230	1	420 ml/min
4136	70ml	700ml	700 ml/min	2586	3	140 ml/min
4584	0ml	500ml	700 ml/min			

3.4 Geometry Comparison Experiments

The next set of experiments used both activated cerium and ytterbium in sequence and used the Lynx MCA for time stamped counting. A standard procedure was established for this set of experiments to enable side-by-side comparison between the performances of the different coil geometries. The first set of such experiments on Coil 1 ran into trouble when data inconsistencies were being observed. Further investigation found that there was a bad cable in the detector system so the coil 1 experiments had to be repeated.

Table 4 gives the standardized procedure as it was followed for the coil 1 experiments. The coil 2 experiments match this exactly except for the flow rates. These experiments are divided into 5 main sections: part A: ytterbium addition, part B: cerium addition, part C: tank dilution, part D: in-line dilution, and part E: flow rate variation. Times are measured from the start of each particular section of the experiments. After the results from coil 1 and coil 2 were reviewed, the decision was made not to use coil 3.

Because of the close geometric similarities between the coils, an MCNP model of coil 3 was chosen to be a sufficient basis for comparison over an experiment.

Table 4. Geometry comparison experiments standard experimental procedure.

A	*Flow rate=1030 ml/min
Yb added	Time (sec)
10ml	200
40ml	400
50ml	600
100ml	800
300ml	1000

*Flow rate= 1020 ml/min	
C	
Water added	Time (sec)
100ml	180
200ml	360
500ml	540
700ml	720

*Flow rate = 660 ml/min	
D	
Duration	Time (sec)
<1 sec	200
1 sec	400
5 sec	600
10 sec	800
20 sec	1000

B	*Flow rate=1030 ml/min	
Ce added	Water added	Time (sec)
5ml	0ml	200
25ml	0ml	400
50ml	0ml	600
70ml	0ml	800
150ml	0ml	1000
200ml	0ml	1200
0ml	500ml	1400

E		
pump speed	time	*Flow rate
9	0	1770 ml/min
8	200	1600 ml/min
7	400	1470 ml/min
6	600	1410 ml/min
5	800	1180 ml/min
4	1000	950 ml/min
3	1200	650 ml/min
2	1400	380 ml/min
1	1600	off scale

*Flow rate values differ slightly for coil 2 experiments

For this set of experiments, the ytterbium was added to the system first and then the cerium was added next with the ytterbium already completely dissolved in the system. The cerium addition experiment was the procedure of most interest of these experiments because it involved adding a radioactive material to a system already

containing radioactive material and watching for a spectrum change. The ytterbium addition, in-line dilution, and flow rate variation experiments were performed in a similar manner to those conducted in the initial experiments. The tank dilution experiments were novel to this set of experiments and involved adding specific amounts of non-radioactive water direction into the main reservoir tank. The void comparison experiments were done with these experiments just like the others and after all the cerium and ytterbium was in the system.

Instead of repeating the procedure in Table 4 for Coil 3, a new set of experiments was devised and carried out using Coil 2. In these tests, the flow rate was varied along with the addition of ytterbium and cerium to the system. This final experiment consisted of 4 parts: 1) ytterbium addition, 2) cerium addition, 3) tank dilution, and 4) in-stream dilution. Since the effects of the addition of the same amount of material each time is slightly different due to the change of the system with each addition, flow rate variation were performed in a random sequence as indicated in Table 5, rather than continuous increase or decrease. Flow rate changes were made approximately 20 seconds before a material addition occurred to allow the system to reach an equilibrium flow state. Only 300ml of the total 500ml of cerium was added to the system in that experiment. At the point 1200 sec which is shown to have 0 ml of cerium added, 500 ml of distilled water was added at this point instead. In the tank dilution experiment 300 ml of distilled water was added each time under various flow rates. The in-stream dilution experiment used only 1 second and 5 second valve opening durations for three different flow rates.

Table 5. Coil 2 flow rate variation experiments.

A) Ytterbium addition			
Yb added	Time	Pump speed	Flow rate
	0	2	440 ml/min
100ml	200		440 ml/min
	380	8	1730 ml/min
100ml	400		1730 ml/min
	580	4	1030 ml/min
100ml	600		1030 ml/min
	780	9.9	1930 ml/min
100ml	800		1930 ml/min
	980	6	1470 ml/min
100ml	1000		1470 ml/min

B) Cerium Addition			
Ce added	Time	Pump speed	Flow rate
	0	2	440 ml/min
100ml	300		440 ml/min
	500	8	1720 ml/min
100ml	600		1720 ml/min
	800	4	1000 ml/min
100ml	900		1000 ml/min
	1100	9.9	1900 ml/min
0ml	1200		1900 ml/min

C) Tank Dilution			
water added	Time	pump speed	Flow rate
	0	2	430 ml/min
300ml	240		430 ml/min
	420	8	1250 ml/min
300ml	480		1250 ml/min
	660	4	900 ml/min
300ml	720		900 ml/min
	900	6	1110 ml/min
300ml	960		1110 ml/min

D) In-Line Dilution			
Time	Duration	Pump speed	Flow rate
0		2	430 ml/min
200	5		430 ml/min
400	1		430 ml/min
600		8	1630 ml/min
700	5		1630 ml/min
900	1		1630 ml/min
1100		5	1230 ml/min
1200	5		1230 ml/min
1400	1		1240 ml/min

3.5 MCNP Simulations

After the experiments were complete, a series of MCNP [21] models were constructed and executed to confirm the spectra change of materials inside versus outside the system. It was also used to model attenuation and geometry effects as well as spectrum changes in the cerium addition to ytterbium spiked system experiments. A set of input decks used for these codes are provided in Appendix A.

The detector coils were modeled as a series of stacked tori (donut shaped). The detector was modeled as a 3x3 crystal surrounded by an aluminum can. The computer code ORIGEN [22] was used to estimate which isotopes and in what amount would be present from irradiation of the source material. The ORIGEN input decks used are provided in Appendix B. Precise irradiation data from the NSC reactor was not provided, so an estimation was made to achieve valves as close as possible to the declared activity amounts produced. The gamma energy values and relative intensities for each isotope that was used in the MCNP model were obtained from Janis 3.2 from the NEA of France. [23] The experimental procedure in Table 4 where activated cerium was added to the system already containing ytterbium was modeled for all three coil geometries including the one that was not used in experiment. The model of this experiment was repeated for coil 1 using an HPGe detector in order to separate the peaks that were combined using the NaI detector. Models of both glass and stainless steel straight pipes with inside diameters up to 2 in were modeled with varying amounts of air void in the center of the pipe and using the activated cerium spectrum in the working fluid.

Spectra of three different UREX+ streams were modeled inside of a beaker and inside of each of the three different coil geometries. The streams that were modeled were the U and Tc stream; the Cs and Sr stream; and the TRU stream containing Am, Cm, Pu and Np. The isotopic compositions of each of the streams were taken from the models used in work done by Goddard [24]. Goddard obtained this data through burn up and decay calculations on LWR fuel using ORIGEN. Because of the number and close

proximity of the peaks in the UREX streams, the NaI detector was replaced with an HPGe detector for this set of MCNP models.

4. RESULTS

This section describes the result from the experiments that were outlined in Section 3. The first section describes the experiments carried out to evaluate the behavior of the newly constructed gamma detection system containing flowing radioisotope solutions (the following 9 figures). These experiments also characterized the behavior of each of the isotopes selected for this study. Section 4.2 describes the experiments that were used to quantify the comparison between two coil geometries. Finally, Section 4.3 gives the results of the MCNP simulations that were created to confirm the experimental results and extend the results to other detection system geometries and applications.

The data for the majority of the experiments was recorded as total counts over the entire energy spectrum taken over time intervals that differed from one experiment to the next. In the first set of experiments, the count rate response to activity changes can be seem visually on a count rate over time plot. However, since this was not true of the later geometry comparison experiments, a quantitative statistical evaluation was performed for all the data to confirm the significance of the activity level changes. The standard deviation and standard error were computed over incremental time intervals for each data set. Because the data sets increased non-linearly by several orders of magnitude from beginning to end, the standard deviation evaluated over the entire set would not be useful. The count rate data was then averaged over selected time intervals that were chosen based on the amount of time between points in which activity changes

were made in the system, to smooth the data of statistical fluctuations. The changes in the average with time were compared with both the standard deviation and 3 times the standard error. The value of 3 times the standard error was chosen based on the NRC regulation presented in Section 2 that requires a report of all inventory changes greater than 3 times the SEID. The time intervals over which the standard deviation and standard error were computed were specific to each data set and chosen based on the time interval between activity insertion or dilutions made during each experiment. Graphical results of these comparisons among change in averaged count rate, standard deviation and 3 times standard error are given in Appendix C.

4.1 Isotope Selection Experiments

As described in Section 3.3, the first activated chromium experiment was used to give a basis for detectable dilution level for the rest of the body of experiments so the results were not significant. The second experiment, however, also used activated chromium and it provided clearly observable changes when the flowing solution was spiked with the radioisotope solution. These experiments used the Unispec MCA connected to the NaI detector and recorded data as total activity vs. time. The initial activity levels indicated in this set of experiments are based on the activity levels reported by the NSC after activation and before delivery to the lab.

Figure 8 shows a comparison between the energy spectrum measured of the activated chromium in the plastic vial it was delivered in from the NSC to the spectrum measured once the material had been dissolved in distilled water and diluted in the

system. The only attenuation that occurred was in the region of the x-ray peaks. Also, with dilution the count rate became low enough such that the high energy peak (~1400 keV) associated with the activated chromium was no longer visible.

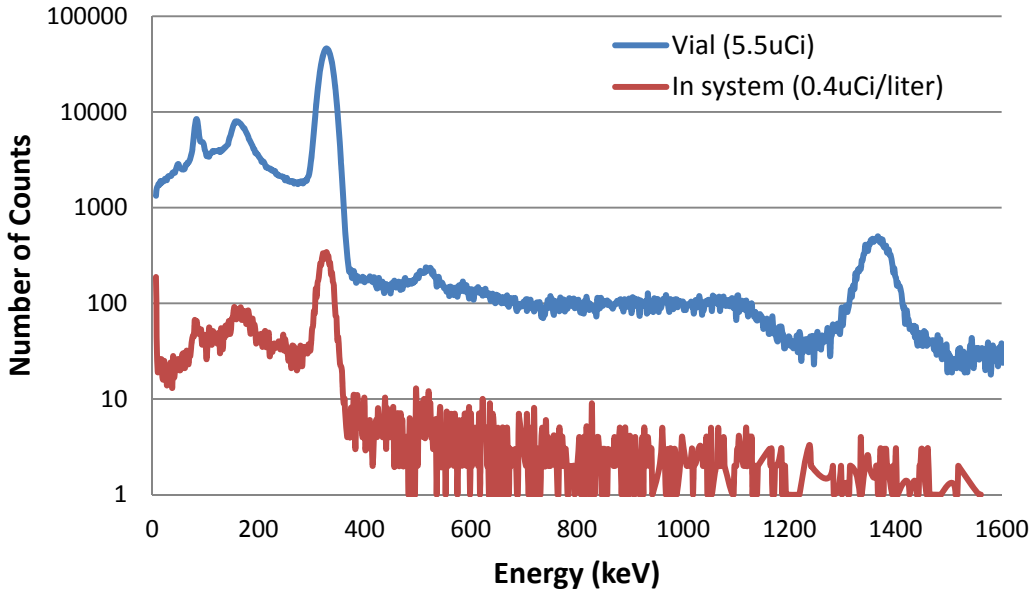

Figure 8. Comparison of gamma spectrum of activated chromium in vial to in system.

Figure 9 shows the plot of counts per second (normalized to per second from 5 second counting times) versus time with the two insertion points indicated in red where the 250ml spiked solution were added to the flow system. The total volume of the water in the system before the chromium addition was about 15 liters, making the total final system dilution about 0.3uCi per liter. The second addition of chromium to the system reached the detector before complete homogenization of the system fluid, creating a notable activity spike after insertion. Both points of insertion were indicated as being

statistically significant on the basis of the change in the average count rate being greater than one standard deviation at each point.

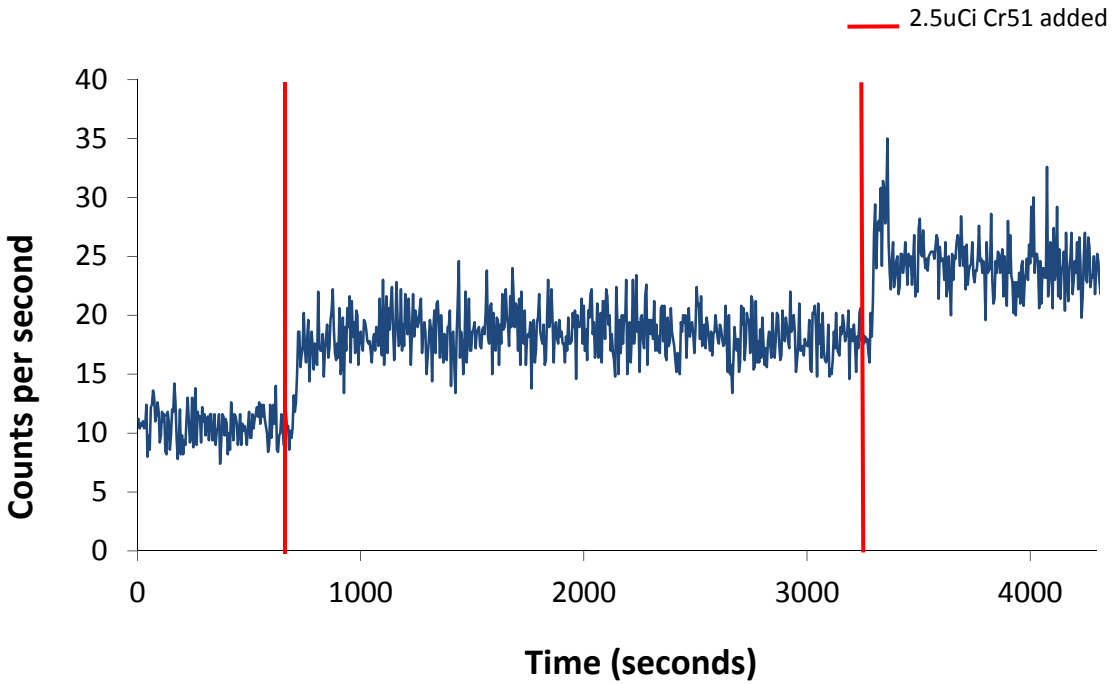

Figure 9. Total counts versus time for activated chromium spiking.

The next experiment was performed to characterize the impact of flow rate on the detector signal on the system containing chromium. The resulting count rate plot from this experiment, shown in Figure 10, appears to indicate a correlation between increasing flow rate and increased count rate measured by the detector. However the second stage of this flow variation experiment, in which flow rate was decreased with time, produced a relatively flat curve. This implies that the increasing total count rate was due to the elimination of air void space within the coil. Air was being forced out of the tubing as flow rate was increased during the first stage of the flow rate variation experiment. Once the system pipes had reached maximum liquid fill capacity the total count rate remained

relatively constant even as flow rate was once again decreased since air was not allowed to re-enter the coil and the volume of radioactive material was relatively constant.

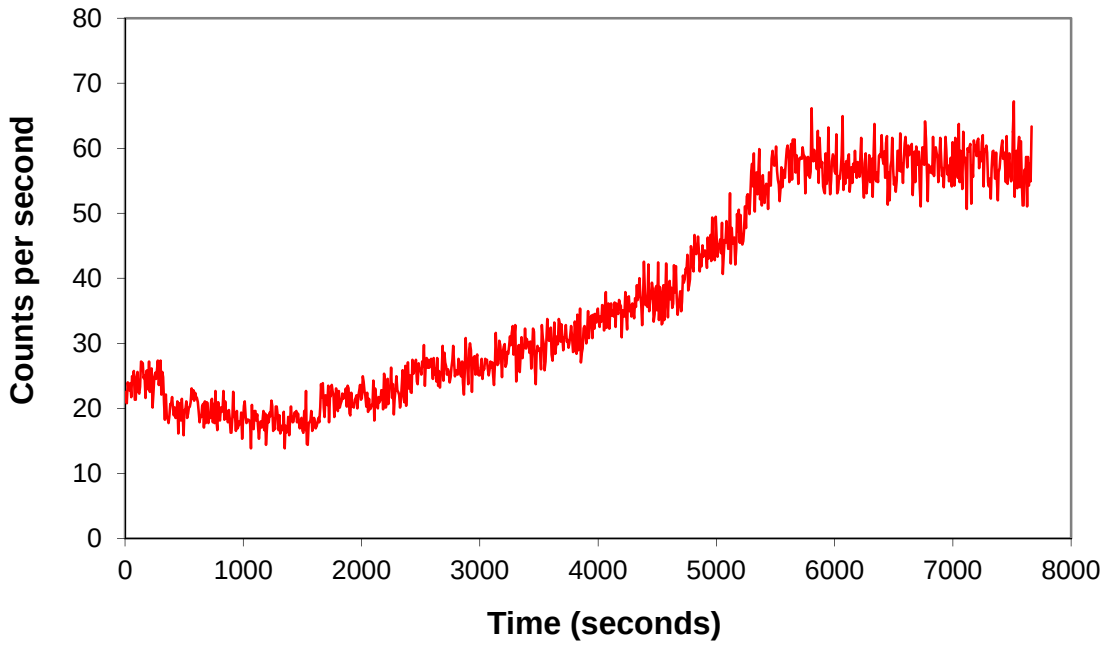

Figure 10. Total count rate increase with air removal using activated chromium in Coil 1.

The next experiment to consider from Section 3, Table 2 is the ^{198}Au spiking experiment in which gold was observed to collect inside of the detector coil over time. Like chromium, the activated gold only had one major gamma peak as shown in Figure 11. Only the x-ray peak was in the energy range low enough to experience significant attenuation by the stainless steel of the coil pipe. The majority of the minor high energy peaks proved too low to show up on the energy spectrum once the gold had been dissolved and diluted into the system.

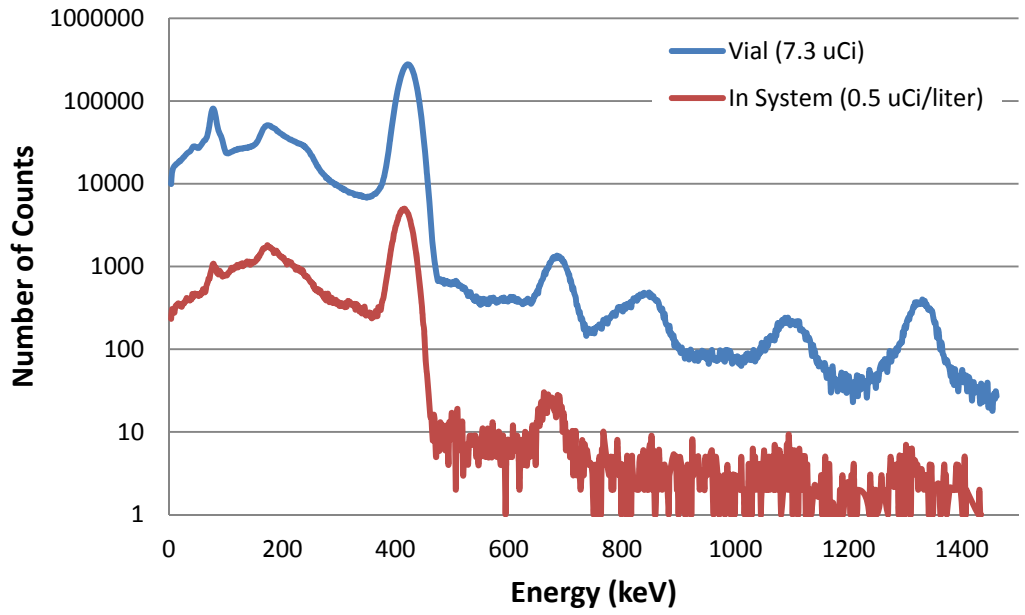

Figure 11. Gamma spectrum from activated gold nitrate in plastic vial vs. dissolved and diluted into system.

Figure 12 shows the total count rate versus time for the entire experiment. The entire solution containing the fully dissolved ^{198}Au gold was added to the system at point A, creating a spike as it reached the detector before uniform dilution. The other points represent the opening of the clean tank flush valve for various lengths of time. As clean water was added to the system the flow rate decreased slightly over time even though the pump speed remained constant. Therefore, even though points B and E both represent a valve opening time duration of 1 minute, point B represents the addition of more material since the flow rate was higher at the time. Points C and D represent valve opening durations of 30 seconds and 15 seconds respectively. Based on the flow rates observed during the experiment, the calculated volume of water input at each point is as follows: B – 970 ml, C – 420 ml, D – 203 ml, and E – 760 ml. Even though the dilution

of the system is increasing the total count rate at the detector continues to increase as the gold becomes held up in the coil. Since the solution is becoming more dilute over time, the steady increase in activity strongly implies the collection of activated gold on the pipe walls as the test progressed.

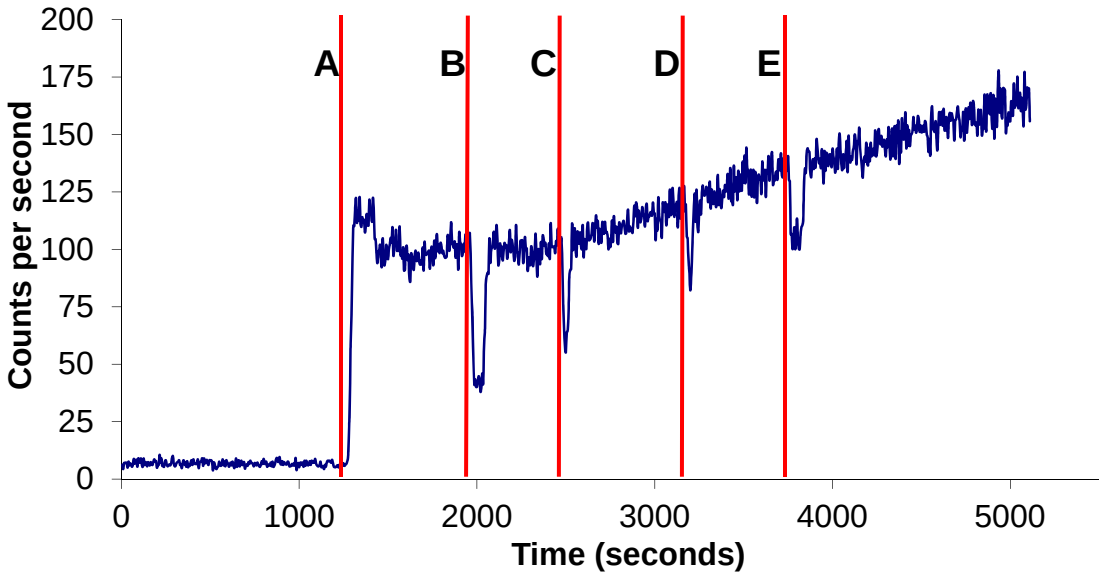

Figure 12. Gold spiking and in-line dilution experiment indicating hold up.

Unlike points C and D dilutions which show an abrupt turnaround upon valve closure, points B and E dilutions appear to be saturated at a point high above the original background, where no more gold can be removed. The point E saturation point is much higher than that at point B, indicating a continued build-up of gold between those two points. Each of the activity dilution and insertion points that appear visually in the plot indicated a change in activity that was greater than one standard deviation for the data set. Excluding the four points of dilution (B-E) from the calculation, the rise in activity

due to gold build up over time was also an activity change greater than the standard deviation for the data set. Because of the gold build up in the coil there was very little difference between the spectra taken at the fully filled pipe condition versus the partially filled pipe condition, so the void comparison results are not discussed further here.

The activated cerium experiments from Section 3, Table 2 showed the first indication of major attenuation of low energy peaks due to the stainless steel piping of the system. Figure 13 shows a comparison of a 900 second gamma energy spectrum measured using the NaI detector with the vial of solid activated cerium nitrate alongside a 900 second spectrum measured after the cerium nitrate was dissolved in water and inserted into the system. The cerium spectrum within the system is approximately a factor of 10 lower in magnitude due to the dilution in distilled water. On the low end (<100 keV) of the energy spectrum, only the higher of the two lowest (~36 keV and ~57 keV) energy gamma peaks is distinguishable through the stainless steel coil. However, the relative peak intensity has dropped even further due to attenuation as compared with the rest of the diluted spectrum. The third low energy peak visible in the vial spectrum completely disappears and was from the x-rays produced in the lead surrounding the vial during counting.

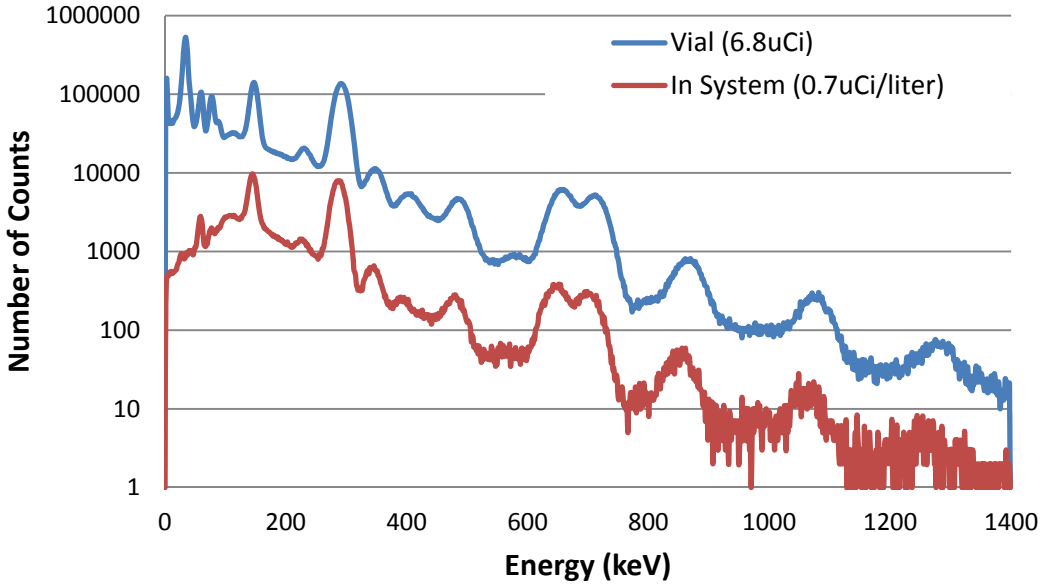

Figure 13. Cerium spectrum measured in plastic vial vs. dissolved and diluted in system.

A total count rate over time plot was constructed for the cerium spiking experiment and in-line dilution experiments together, similar to the way it was done in the gold experiment. This is shown below in Figure 14. Half of the cerium was added to the system at point A and the other half added at point B. Point B shows the similar spike from the material reaching the detector before uniform dilution occurred as seen previously. Points C through G indicate points of time in which the in-line clean tank valve was opened for the following time periods in order: 1 minute, 30 seconds, 15 seconds, 5 seconds, and 1 second.

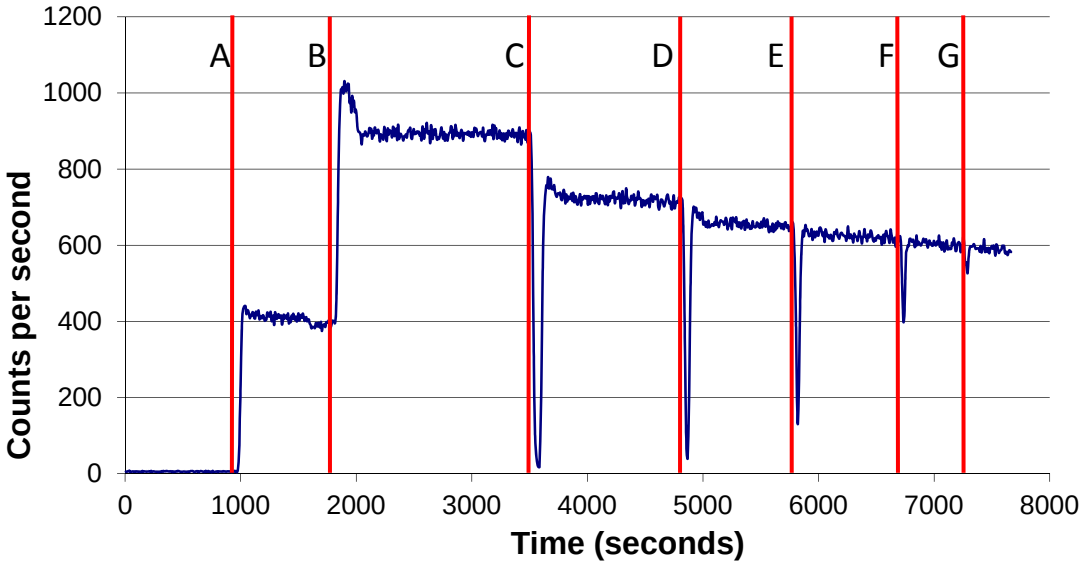

Figure 14. Cerium spiking and in-line dilution experiment total counts versus time.

Unlike the ^{198}Au experiments, the total count rate in the cerium test drops following the in-line dilution stages and the new equilibrium count rate gets lower with each insertion of clean water due to the additional dilution of the entire system. Taking into account the flow rate observed at each point of in-line dilution, the amount of water added into the system at each point is calculated to be the following: C – 930 ml, D – 470 ml, E – 248 ml, F – 105 ml, and G – 21 ml. The first two dilutions represent volumes greater than the total volume of the coil and thus would have been capable of clearing all the radioactive cerium out of view of the detector. The activity level at the insertion point drops to very near background levels indicating negligible or very small material hold up in the coil. The last dilution was only about 6% of the total coil volume and still shows up very clearly indicating that small in-line changes can easily be detected. All the visual changes in activity level observed on this plot were confirmed to

be statistically significant activity level changes (the data analysis plot is shown in Appendix C). Absolute activity level changes were greater than three times the standard error for each of the seven points as well as for the overall activity decrease with system dilution increase.

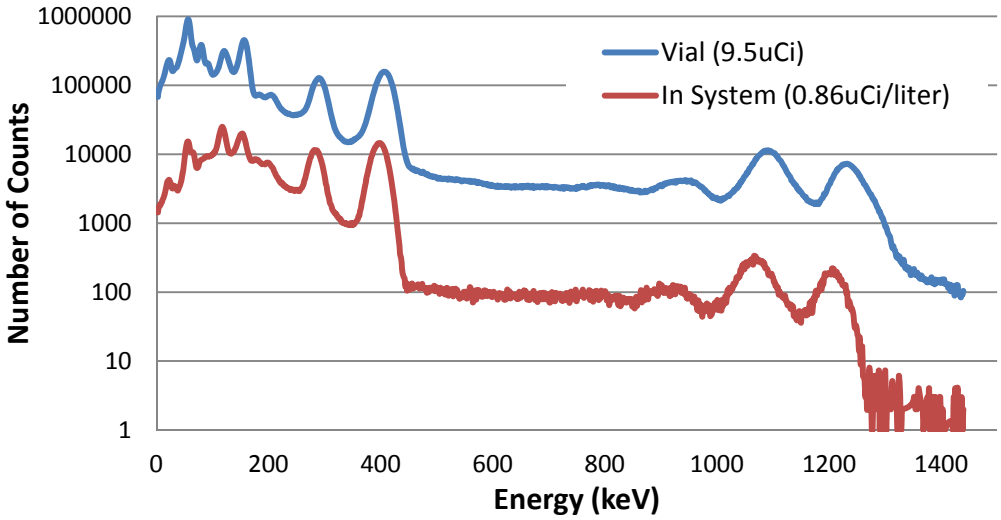

Figure 15. Ytterbium gamma spectrum measured in vial vs. dissolved and diluted in system.

Figure 15 shows the difference between the two 900 second counts measured of activated ytterbium inside and outside of the system. Ytterbium also has low energy gamma peaks in the range that are attenuated by the stainless steel coil. The ytterbium spiking experiment from Section 3, Table 3 was designed to be more complex than the previous spiking experiments in order to determine how well different dilution levels of ytterbium may be observed as compared to system dilution in a total count rate plot. The initial volume of the system was approximately 7 liters and the system contained no radioactive material. The resulting total count rate with time plot for this experiment is shown in Figure 16. Since the system was clean at the beginning a highly diluted

addition of ytterbium at point A showed up very clearly. However, after the large amount of material was added at points B and C, the material added at point D was then more diluted than the system and thus caused a net activity decrease. At points E and F, the volumes added were too small to show up as a significant change. A calculation of activity per liter indicates point G is less diluted than the system producing a net gain again. Point H was water only so an activity decrease is expected once again.

Table 6 shows the dilution level and volume of each material insertion as compared to the system dilution level at the point at which it was added. Statistical analysis of each of the insertion points indicated that all points except E and F showed activity level changes greater than one standard deviation. Activity levels were calculated based on the declared levels measured by the NSC after activation. Decay correction was made for the short lived isotope ^{177}Yb based on time of experiment after time of measurement by the NSC.

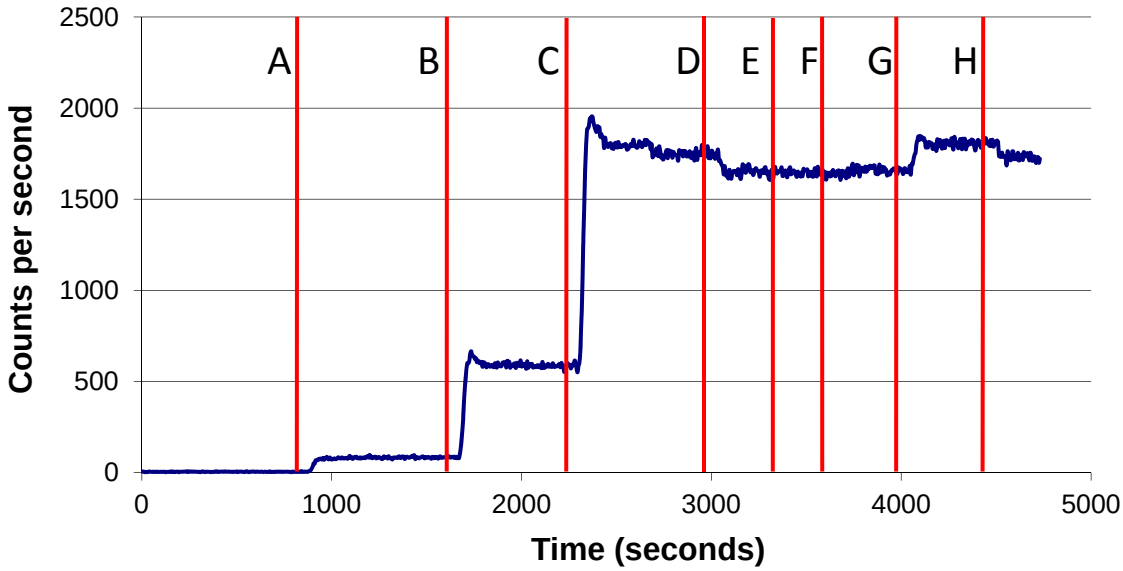

Figure 16. Ytterbium spiking experiment using varied dilution levels.

Table 6. Activity dilution amount added at each point in time for ytterbium spiking experiment.

Time	activity added (uCi/liter)	volume added (liters)	initial activity (uCi/liter)	initial total volume (liters)
A	0.23	0.71	0	7
B	2.05	0.8	0.021	7.71
C	4.92	1	0.212	8.51
D	0.12	0.7	0.707	9.51
E	16.4	0.005	0.667	10.21
F	16.4	0.01	0.674	10.215
G	1.49	0.77	0.690	10.225
H	0	0.5	0.746	10.995

The in-stream dilution experiment performed with the ytterbium was done at various flow rates and was also described previously in Table 3. Figure 17 shows the resulting total count rate with time from this experiment. The boxes represent regions of different flow rates: A to D=700 ml/min, E and F=420 ml/min, and G=140 ml/min. Using the flow rates and the open valve duration, the volumes of water inserted into the system at each point were calculated and the results are presented in Table 7. Note that point E shows up nearly as large as the large volume addition at point C. The same is true for points F and D. Also, point G shows up much larger than F despite being approximately the same volume. Statistical analysis (Appendix C) of the data indicated the absolute activity level change at each the dilution points were greater than three times the standard error. The two points of smallest dilution that were significant in this experiment represent in-stream volume additions of approximately 2% of the total volume of Coil 1.

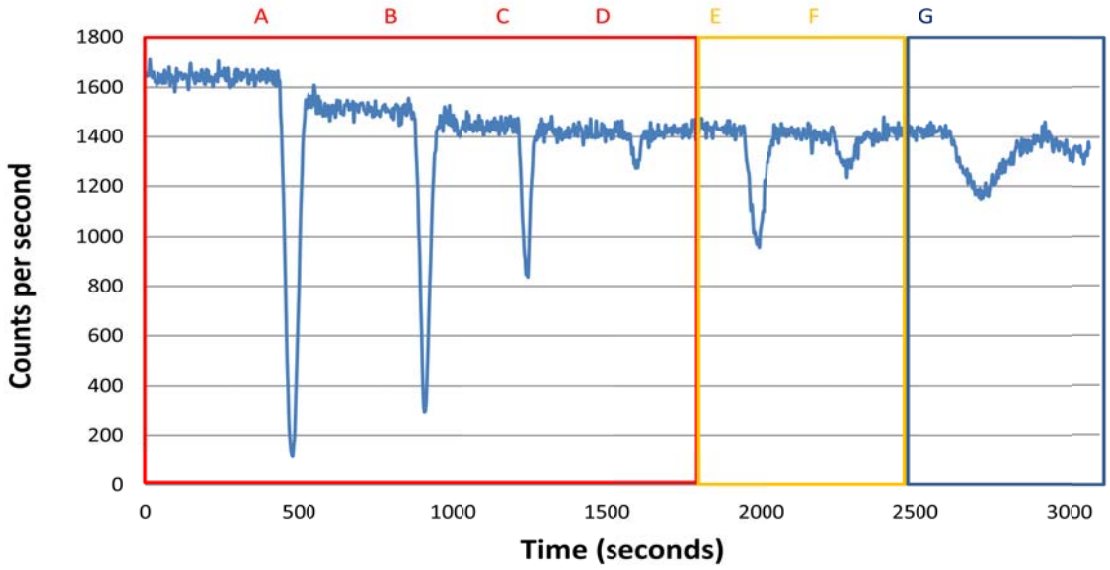

Figure 17. Ytterbium in-line dilution experiment at various flow rates.

Table 7. Calculated volume of water added at each point in ytterbium dilution experiment.

Time	Water added
A	350ml
B	175ml
C	58ml
D	12ml
E	35ml
F	7ml
G	7ml

The void comparison experiment was performed using every isotope except for chromium to see if the amount of fluid in the pipe caused any major attenuation of the low energy peaks. The results for all such experiments were the same and showed no major changes in relative peak heights on the low end of the energy spectrum. The spectrum comparison using ytterbium is shown below in Figure 18. Ratios were computed for the area of each peak at full-width half maximum (FWHM) to the total

counts in the entire spectrum. Also, ratios were computed of the area at FWHM to the sum of the areas of all five peaks studied at FWHM. The variation of these ratios between this experiment and the two later experiments that used ytterbium were used to establish a standard deviation and standard error value for these ratios. All five peaks examined on the two spectra in Figure 18 were less than 3 standard error difference from one another. A table summarizing the results of these calculations is provided in Appendix C.

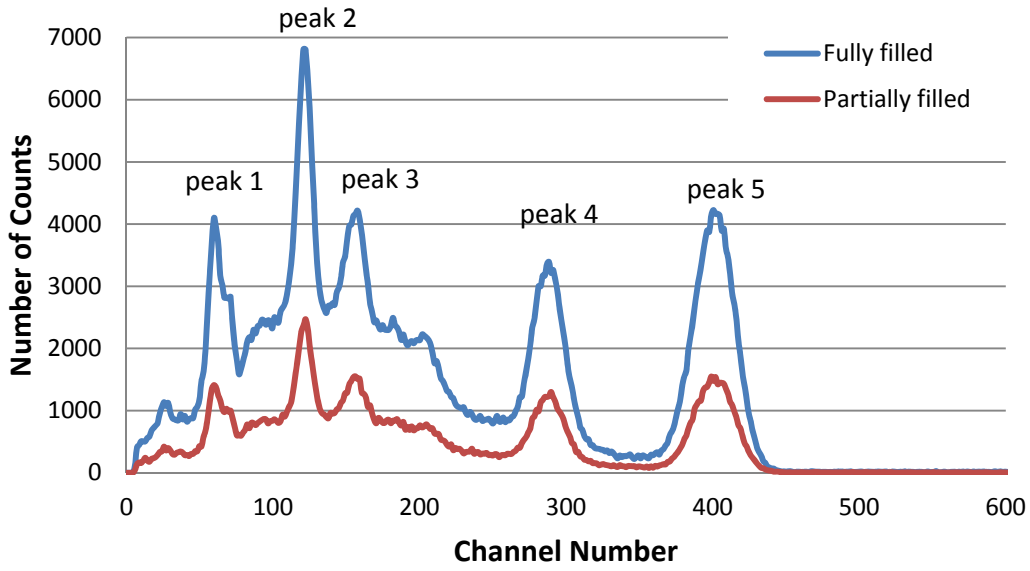

Figure 18. Pipe filling effects on spectrum from ytterbium.

4.2 Geometry Comparison Experiments

The experiments from Section 3.4 were completed using Coil 1 and repeated as closely as possible using Coil 2. However, the activity of the activated materials received for the Coil 2 experiments were slightly higher than those used in the Coil 1 experiment. In order to correct for this, more water was added to the system for the Coil 2

experiments to dilute that solution to a comparable level. According to the activity levels declared by the NSC, Coil 1 tests had about 7.4uCi of cerium and 6.5uCi of ytterbium in 8.5L initial system volume, while the coil 2 had about 9.3uCi of cerium and 7.6uCi of ytterbium in 9.5L initial system volume. This made the dilution level nearly identical for the ytterbium addition experiment but it remained slightly higher for the cerium addition experiment. Figure 19 below shows a comparison of total count rate over time for the ytterbium addition experiment on Coil 1 and Coil 2 following the procedure outlined in Table 4. Each of the vertical lines indicates a point of material insertion. The most noticeable difference between these two experiments is the slightly slower ramp rate for the large coil whenever ytterbium is added. Statistical analysis (Appendix C) confirms the significance of each activity spike after material was added based on the average activity change exceeding the value of three times the standard error at each point. However, the slower ramp rate with activity insertion observed visually on the plot for Coil 2 did not appear to be statistically significant.

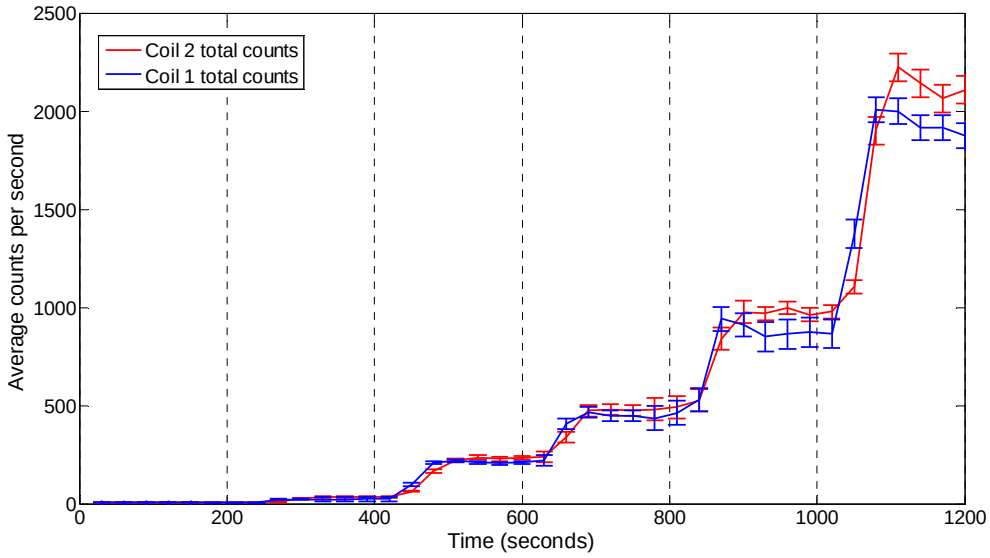

Figure 19. Average total counts over time for ytterbium spiking experiment for Coil 1 vs. Coil 2 including error bars of 3x the standard error. (Table 4 part A)

In a clean system, a very small activity addition at the beginning shows up very clearly on a total counts over time plot. Once the ytterbium was completely dissolved in the flowing system, the statistical variation in the count rate over time increased, which made the detection of small activity changes more challenging. In the cerium addition experiment the data from the different coil experiments diverge from one another over time due to the higher activity levels used in the coil 2 experiment. The total count rate plots for the cerium addition experiments are compared in Figure 20 with the vertical lines indicating points of cerium insertion. While the activity level changes at each point are difficult to see visually on this plot, statistical analysis (Appendix C) of these data sets indicate activity level changes greater than three times the standard error for all points of material insertion for both coils. Therefore, both coils were able to detect an addition of 1% of the total cerium activity to the system.

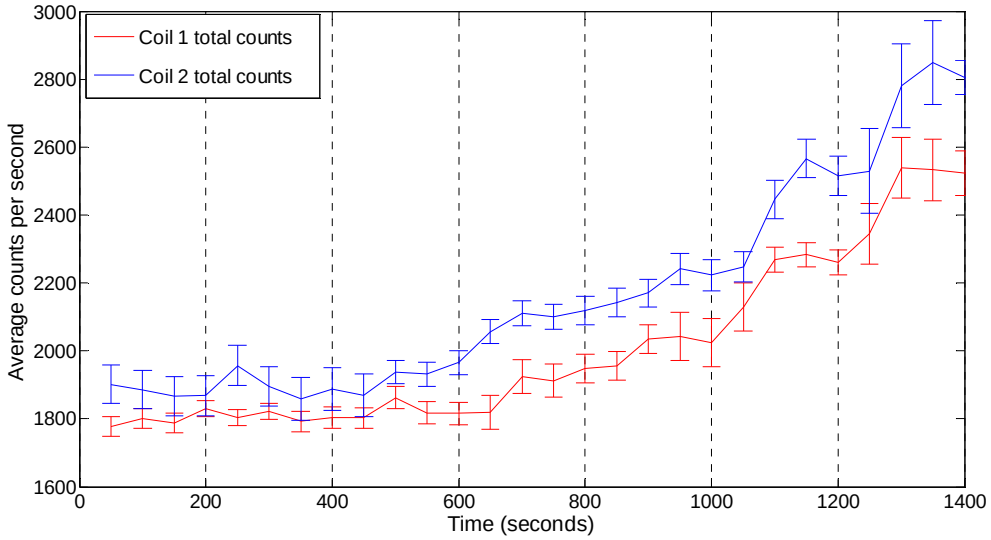

Figure 20. Average total count rate over time for cerium spiking experiment on Coil 1 versus Coil 2 with error bars of 3x the standard error. (Table 4 part B)

Because of the difference in gamma production rate between cerium and ytterbium, the activity values declared by the NSC were suspected to be different from the actual activity levels. The cerium and ytterbium were therefore compared on the basis of the gamma counts taken before each experiment with the background count rate subtracted out. For both coils, the total counts from the activated cerium were found to be approximately one half of the total counts from the activated ytterbium. So the minimum activity level change that was observed to be detectable on both coil sizes was approximately 0.5% of the total gamma production activity in the system.

Because of the large number of peaks shared by cerium and ytterbium when using the resolution associated with a NaI detector, the analysis of activity changes on the basis of spectrum changes proved more difficult than the analysis that focused solely on change in total count rate. Analysis of spectrum change over time was done in the

same way that spectra were compared between the partially filled and fully filled pipe flow conditions. The naming convention for the peaks (shown previously in Figure 18) that was used in the previous spectra comparison calculations was retained also. Since the spectra were assumed to only change in magnitude during the ytterbium experiments after a significant amount of ytterbium was in the system, the peak areas from these experiments were used to establish the standard deviation and standard error associated with the peak area ratios. The 900 second counts taken of the ytterbium in the system were used to establish average values for the peak ratios to which peak ratios from the cerium addition experiments would be compared.

Peak areas were computed at FWHM for each of the five peaks in spectrum intervals of 100 seconds each. Ratios were computed for each of the peak areas to the total counts over the entire energy spectrum and to the total of the peak areas. Ratios were also computed between several of the peaks. The highest magnitude of change from the mean was seen by the ratios of peak 5 to both the total area and peak area as well as the ratios of peak 4 to the total area and peak area. Since peak 5 was unique to ytterbium and not located in the Compton continuum region, the ratio of its area to the total was seen to decrease significantly with time. Both peaks 3 and 4 were common to both ytterbium and cerium and were thus observed to have increasing ratios as cerium was added. However, the peak 4 ratio had the greater magnitude of change and also a lower standard deviation from other peaks and thus gave the earliest indication of a statistically significant change in the spectrum. For both coils this indication occurred after 600 seconds at which time 16% of the total cerium activity had been added to the

system. Figure 21 shows the difference of the ratio of the area of peak 4 to the total area of the peaks from the average of this ratio in the ytterbium spectrum. A significant change in this ratio is observed to occur when the differences of these ratios from the average is greater than three times the standard error for the average.

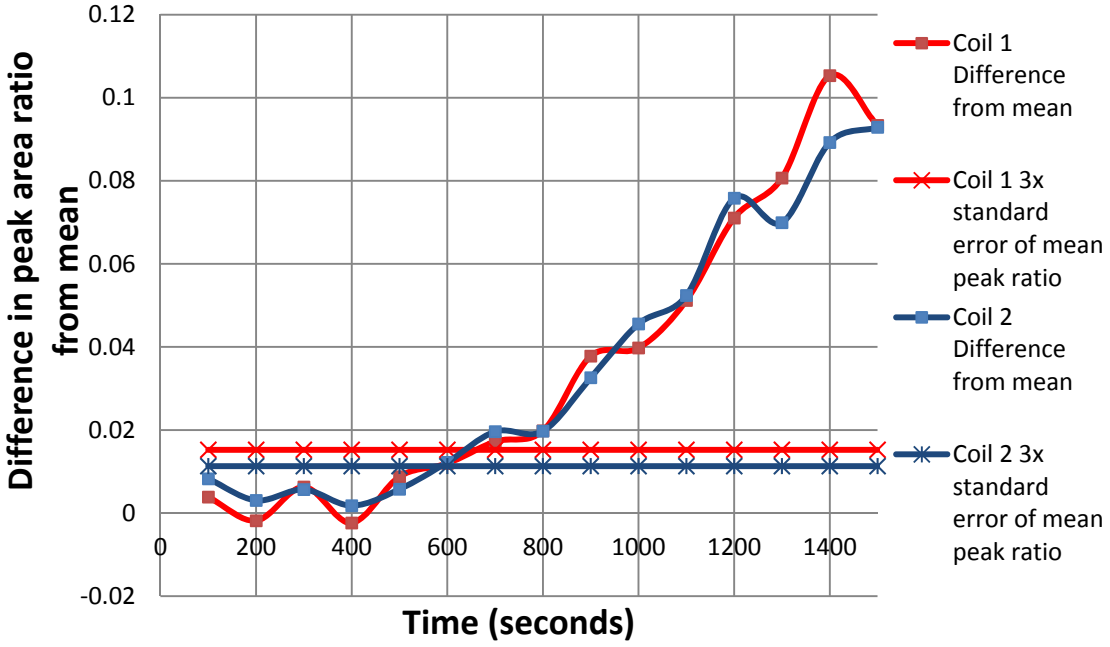

Figure 21. Change in ratio of peak 4 to sum of peak areas from average for Coil 1 and Coil 2. (Table 4 part B)

As expected from the results of the initial set of experiments, none of the flow variation experiments (Table 4 Part E) caused any activity changes since the system had all the air pockets forced out prior to these experiments. In the experiments using the Lynx MCA in the coil geometry comparisons there were no significant spectrum changes in these experiments either. The tank dilution experiments (Table 4 Part C) had relatively high standard deviation values for the experiments on both coils. Using the three times the standard error value, Coil 1 indicated significant activity decreases at

both the 500ml and 700ml additions. Coil 2 only indicated a significant change at the point of 700ml of water dilution. Graphical details of the statistical analysis of these experiments can be found in Appendix C.

The results from the in-line dilution experiments (Table 4 Part D) between the two coils proved more significant. The most recognizable difference between the experiments on the two different coils is the extra delay that Coil 2 experiences at each valve opening. Figure 22 shows a side by side comparison of the total counts over time for the in-line dilution experiments for the two coils. The vertical lines represent the points in time that the clean tank valve was opened. As mentioned before, the solutions used for the Coil 2 experiment had a slightly higher activity than the Coil 1 experiment as evident by the slightly higher curve.

The data from this experiment set was evaluated against the three times the standard error value to locate the points of significant activity decrease. All the dilution points except for the first opening of less than 1 sec appeared significant for the in-line dilution experiment on Coil 1. The Coil 2 experiment on the other hand did not indicate significant activity decrease in either the <1 sec or the 1 sec (located at 200 and 400 sec respectively) dilution points. The last three dilution points were significant for both Coil 1 and 3. For these particular experiments Coil 1 detected a minimum dilution of about 3% of the coil volume while Coil 2 detected a minimum dilution of about 9% of the coil volume.

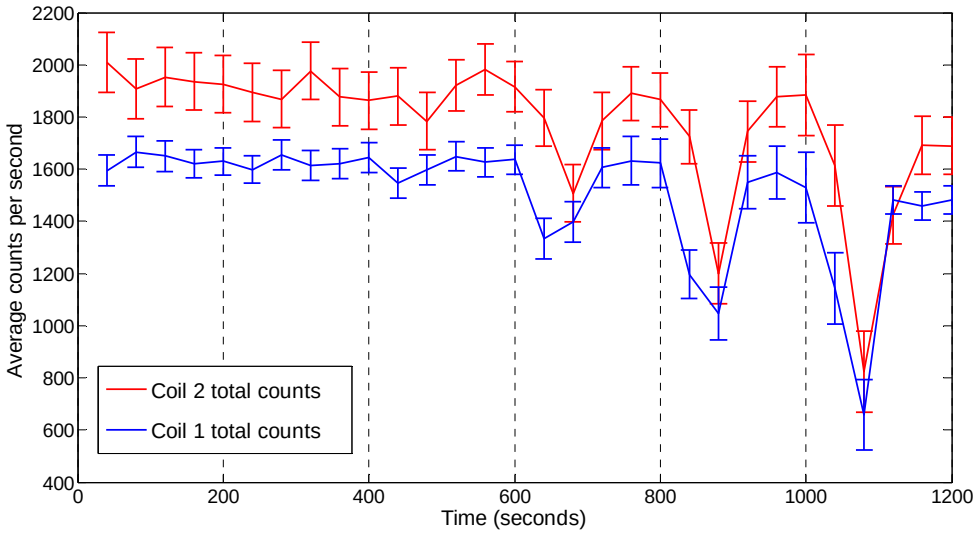

Figure 22. Average total counts over time for in-line dilution experiments on Coil 1 versus Coil 2 with error bars of 3x the standard error. (Table 4 part D)

The final set of experiments (Section 3, Table 5) were flow rate variation tests conducted with Coil 2 only. For each experiment in this set the amount of activity addition or dilution at each point in time remained constant while the flow rate was altered each time. The purpose of this procedure was to quantify the effects of the flow rate on the detection of the activity changes and to observe any effects of flow rate on the gamma energy spectrum with time that were not quantifiable without the Lynx MCA. There is no direct comparison for the Coil 2 flow rate variation experiments to Coil 1 (Section 4.1), but the results from both experiments are still significant. Both the ytterbium addition experiment and cerium addition experiment showed similar effects from the flow rate changes.

The total counts over time for the ytterbium spiking experiment are shown in Figure 23. Statistical analysis confirms the significance of the activity change at each

point of material insertion. At each of the vertical grid lines 20% of the total ytterbium activity prepared for this experiment was added to the system. The total activity of ytterbium used in this experiment as declared by the NSC measurements was approximately 8.3uCi and the initial volume of the system was approximately 8 liters. The flow rate mainly affected the time it took for the resulting activity change spike to appear.

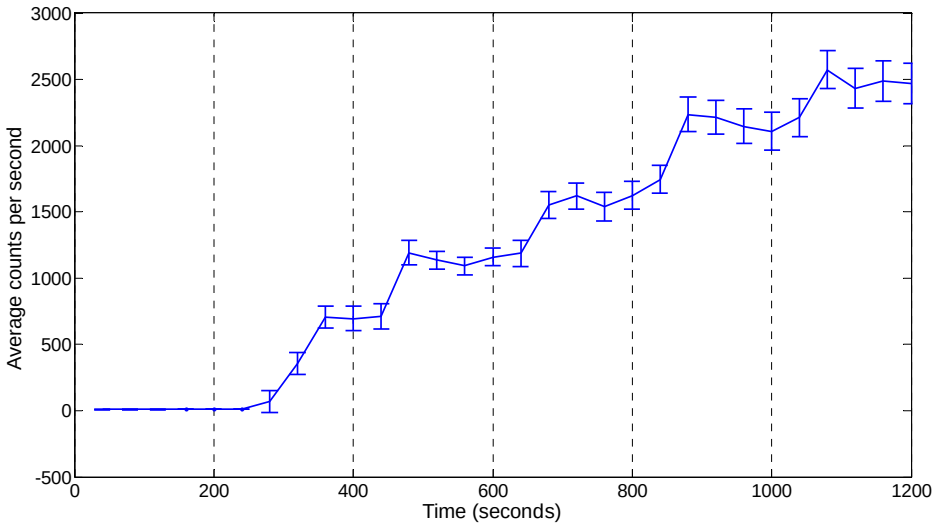

Figure 23. Average total count rate over time for ytterbium flow variation spiking in Coil 2 with error bars of 3x the standard error. (Table 5 part A)

The same effect is seen in the cerium spiking portion of the experiment (Figure 24). A significant spectrum change is seen at the first addition of material, but there is a slight delay between the time of material addition and the appearance of a significant activity level change. The vertical lines in the plot represent the points in time in which material was added. Cerium was only added at the first three points and 500ml of distilled water was added at the final point. This was performed at maximum flow rate

and showed up as a more significant drop than all the previous tank dilution experiments. Previous tank dilution experiments indicated no significant activity level change for coil 2 at dilution insertions below 700ml. One-third of the total 4.6uCi of cerium was added at each of the three points of material insertion. On the basis of gamma production rate the activity for cerium was approximately 30% of the ytterbium activity used in this experiment.

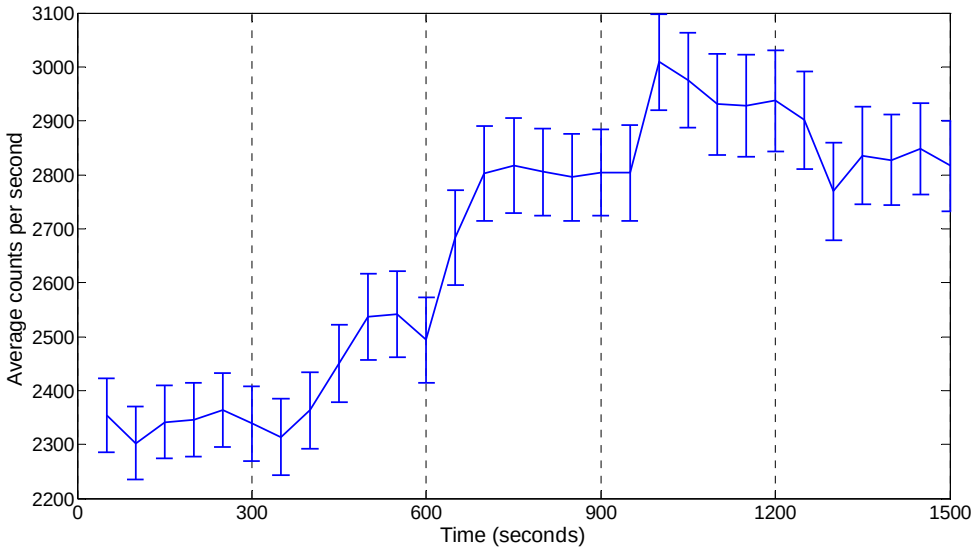

Figure 24. Average total counts over time for flow variation cerium spiking in Coil 2 with error bars of 3x the standard error. (Table 5 part B)

The next portion of the Table 5 experiments performed using variable flow rate conditions were the tank dilution experiments. Previous tank dilution experiments showed no significant activity level change for insertions less than 500ml. The standard deviation was fairly high for this set of experiments and none of the 300ml additions of distilled water to the tank showed any significant activity level changes.

Similar results to those done previously using only ytterbium in Coil 1 were found during the in-stream dilution experiments. Decreasing the flow rate was found to make the dilution much more visible than at higher flow rates. Figure 25 shows the total counts over time for this portion of the experiment. As before, the vertical lines represent points in time in which the clean tank valve was opened. Statistical analysis indicated that all points of dilution except the 1 second dilution at 430ml/min flow rate produced activity drops greater than three times the standard error. The three largest drops represent 5 second valve opening for three different flow rates. Since the middle of the experiment had the highest flow rate, that drop represents the largest water addition. The approximate volumes added in stream at each point in time in the order in which they occurred are as follows: 36ml, 7ml, 136ml, 27ml, 103ml, and finally 21ml. Therefore, for this experiment the lowest volume to produce a significant activity level change was about 3% of the total volume of the coil.

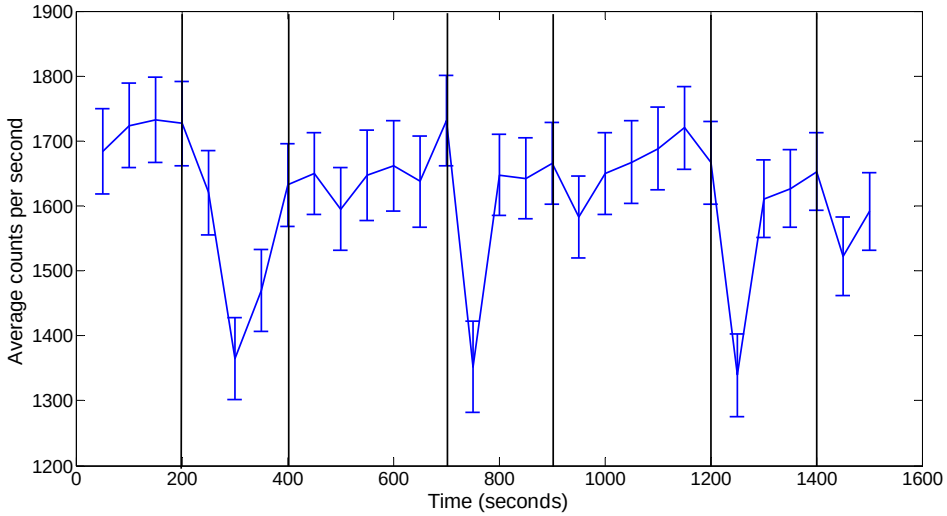

Figure 25. Average total counts over time for in-stream dilution with flow rate variation in Coil 2 including error bars of 3x the standard error. (Table 5 part D)

4.3 MCNP Simulations

The purpose for performing the MCNP simulations described in Section 3.5 was to create a modeling methodology that reliably reproduced the experimental results so that they could be extended to predict the behavior of Coil 3 and also the flow of actual UREX process streams through the system. The model was also used to study attenuation effects due to various pipe sizes as well as from the volume of air voids present in the pipe.

The first step was to simulate the individual behavior of cerium and ytterbium inside of a large diameter glass pipe to represent the measurements taken when the materials were first dissolved into beakers. Figure 26 shows the comparisons of the spectra of both ytterbium and cerium taken in the beakers to the MCNP simulations for them. The simulations showed all the correct peaks in the correct locations, but the relative peak heights were slightly different. The simulation output was given in units per activity per sec per cubic cm. Because factors such as detector efficiency were not taken into account in the simulation a correction factor was used to scale the simulation spectrum to the same magnitude as the experimental data. The low energy peaks were significantly higher in the MCNP calculation than they were observed experimentally.

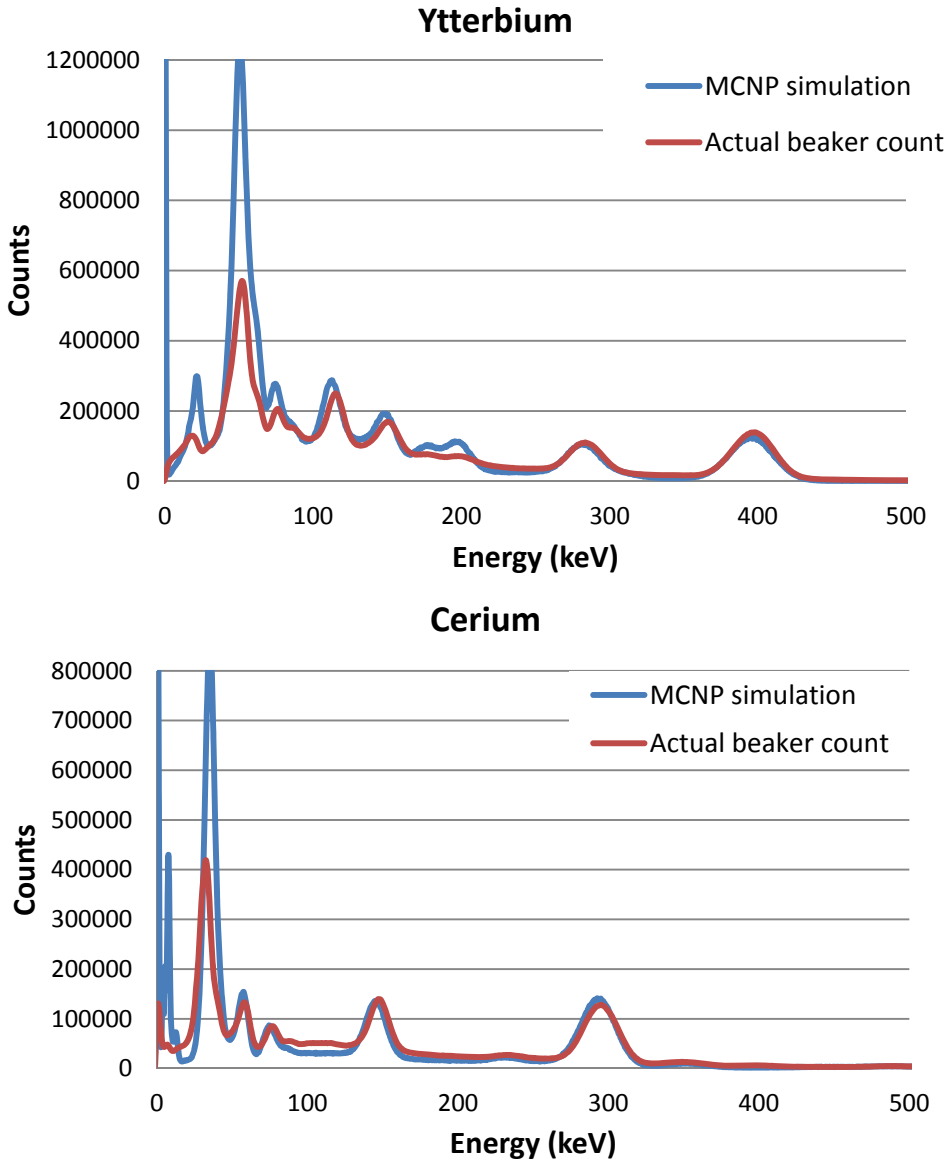

Figure 26. Cerium and ytterbium 900 second beaker counts compared to MCNP simulations.

The ytterbium solution was then simulated inside a series of stainless steel tori the size of Coil 1 with the detector in the center. The measured spectrum was a much closer much to the simulation in this case. A comparison is shown below in Figure 27. Only the peaks in the Compton continuum are shown to not match the measured data

after the data from the simulation was scaled to the same magnitude as the experiment data.

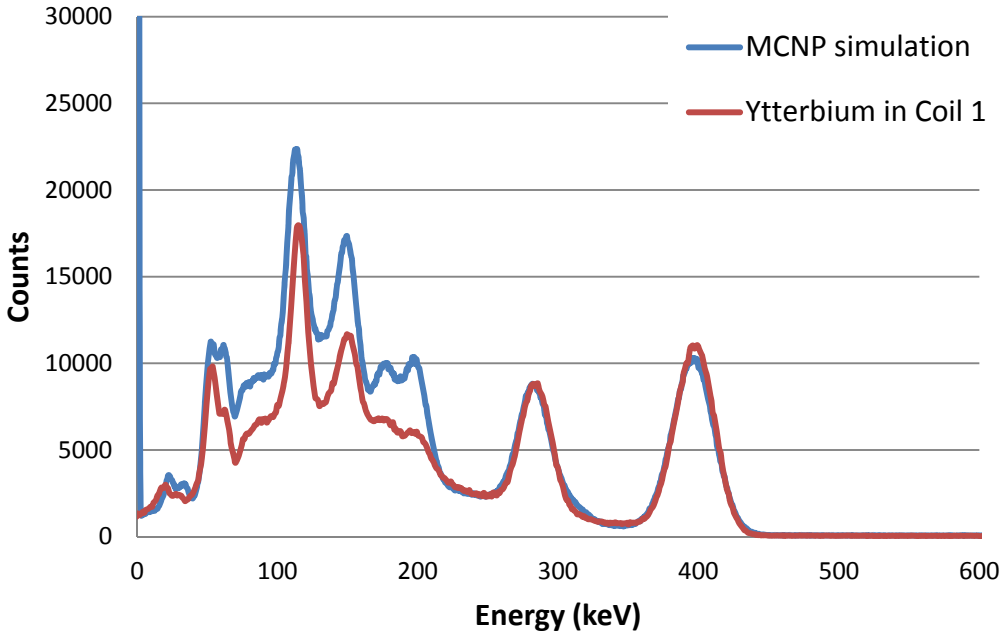

Figure 27. MCNP simulation for ytterbium compared to ytterbium dissolved in Coil 1.

Another set of simulations was completed to reproduce the cerium spiking experiment into the system with ytterbium (Table 4 part B) for all three coil geometries, including the one not used in the experiments. It was found that due to the higher gamma production rate by the isotopes of cerium, the actual amount of activity in terms of number of decays was much less than that declared by the NSC. For the purpose of these simulations, the total amount of cerium was reduced to half of that declared for the first coil experiment. For the purpose of comparison between the simulation data, the output from each coil simulation was scaled by a factor proportional to the volume of each coil. Plots of the results of these simulations and the comparative experimental results for the

first two coil experiments can be found in Appendix D. Each of the curves on each plot represent a point after the addition of a particular percentage of the total cerium.

The simulation for Coil 3 gave count rates that were lower than both the other two coils even though it was nearly the same volume as Coil 2. This demonstrates the important (and expected) geometry effect arising from locating the source further from the detector; the detector was farther from the coil wall and thus the count rate was lower.

The cerium spiking experiment was simulated for Coil 1 an addition time using an HPGe detector instead of the NaI that was used in the experiments. The graphical results of this simulation are also provided in Appendix D. This highlighted the fact that using a HPGe detector the peaks from cerium and ytterbium that were combined are visible individually allowing for a faster detection of spectrum change. Figure 28 below shows a comparison between the measured spectrum of ytterbium in Coil 1 and the simulations using a NaI and HPGe detectors.

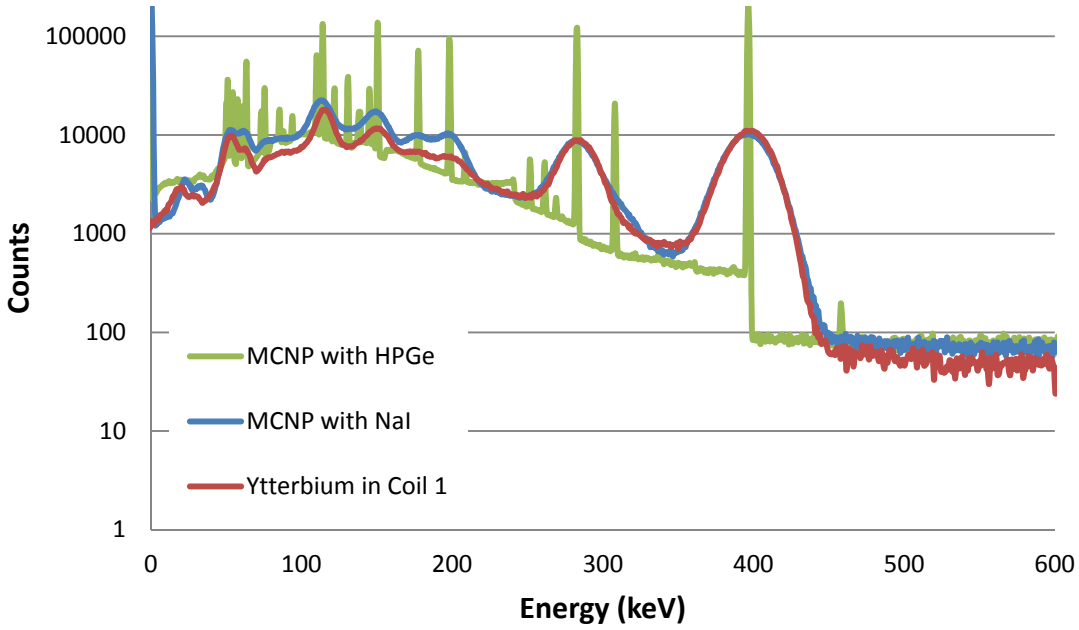

Figure 28. Actual ytterbium spectrum compared to MCNP simulations using NaI and HPGe detectors.

Simulations were also completed for ytterbium and cerium separately inside 2 inch inside diameter glass pipes with 1/8 inch thick walls. Comparisons were made between the pipe being fully filled and the pipe having a central air void 1.5 inches in diameter with the spiked fluid in an annular region. The change in pipe filling is seen to affect the attenuation of the low energy peaks in both the ytterbium and cerium spectra. The peaks affected were the peaks that were not able to be seen clearly through the stainless steel piping of the system due to their attenuation. Figure 29 shows the drop in the spectrum due to self shielding for cerium.

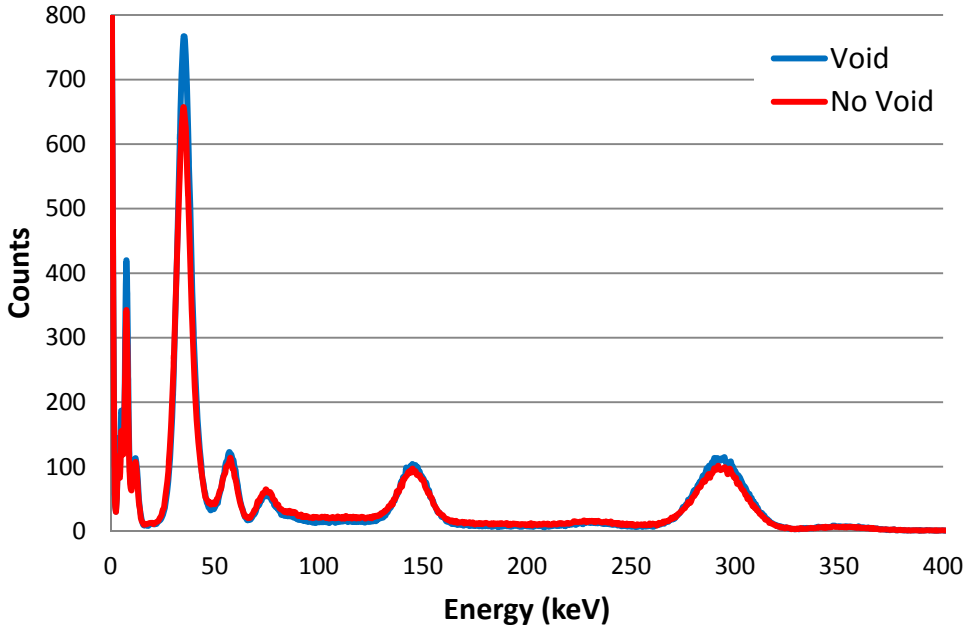

Figure 29. Cerium spectrum change due to self shielding.

The final set of simulations that were performed used three simulated UREX flow stream compositions as computed by Goddard[24]. The three streams that were simulated consisted of the product from the UREX separation (U and Tc), the product of the CCD-PEG separation (Cs and Sr), and the product of the TRUEX separation (Pu, Np, Am, and Cm). Each of the three streams were simulated inside of a glass beaker and inside of each of the three coil geometries just as the materials used in the experiments had been. Because of the large number of gamma peaks associated with the actual UREX streams, the NaI detector was replaced with an HPGe detector for these simulations. It is also true that an NaI detector would not be practical for a UREX processing facility and that an HPGe detector would most likely be used in such a facility. The simulation of the TRU stream showed the most significant attenuation of the low energy gamma peaks when simulated inside the system. The resulting simulation

of the TRU stream as measured using an HPGe detector in each of the three coils is shown in Figure 30. The low energy attenuation that occurred in the other two streams only affected the x-rays peaks in those spectra. The spectra from the other two UREX streams that were simulated are provided in Appendix D.

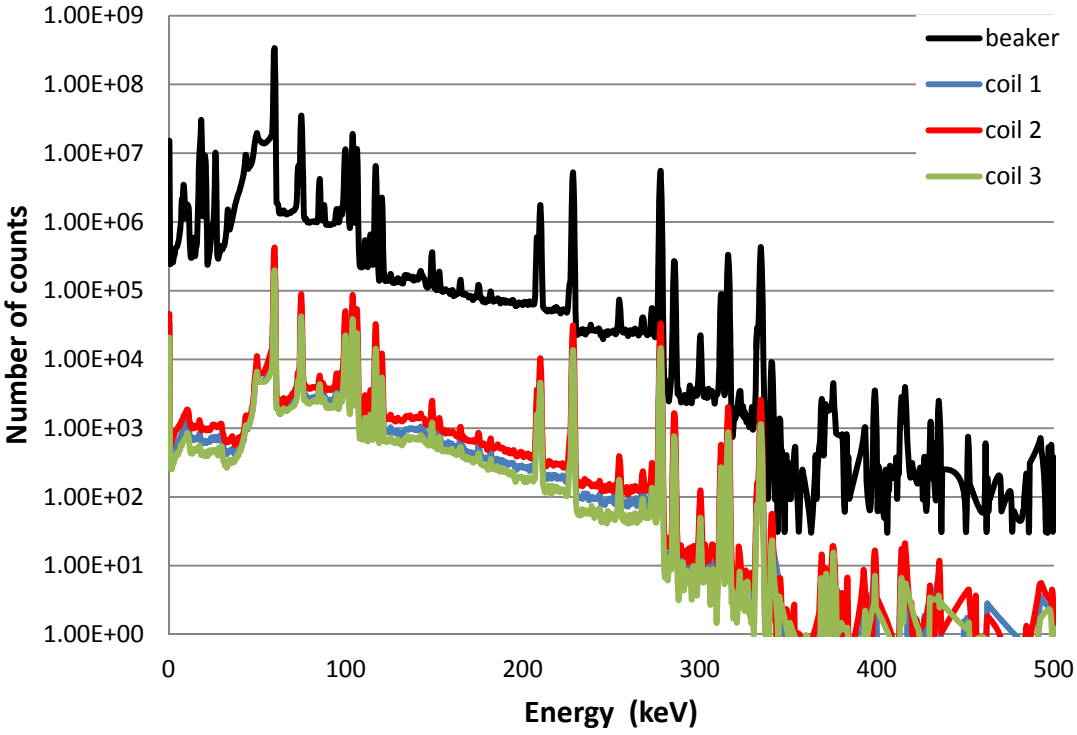

Figure 30. MCNP simulation of TRU flow stream inside coil system using HPGe detector.

The beaker spectrum was multiplied by a higher factor than the spectra simulated in the coils to simulate dilution and to make the spectra more easily comparable. There was little difference between each of the spectra in each of the three coils. The main difference between the coils was the count rate difference as observed in the previous simulations. There is a significant amount of attenuation of the low energy peaks in all

of the coils as compared with the spectrum in the beaker. Most of the peaks below 50keV become completely indistinguishable. However most of these peaks come from x-rays that would not be useful in identification of the constituents of the flow stream. One of the peaks that was significantly affected by attenuation was the ~60 keV peak that was identified by Goddard as belonging to ^{241}Am. Because of the low number of counts in the higher energy region, gamma peaks become difficult to identify and measure in the region above about 450 keV for this particular spectrum.

5. DISCUSSION

The radioactive flow system assembled for this research was able to detect very small activity changes when the spiked solutions were inserted into a clean system, as low as 0.02 μCi per liter. Once the activity level of the system was increased by the initial spiking of the solution, the sensitivity of the system was reduced and activity changes on the order of 0.5% were necessary before a significant change in the total count rate was observed. This was significantly more sensitive than attempts to detect difference in the gamma energy spectra where activity changes on the order of ~8% were necessary to induce an observable change in the spectrum. As shown by the MCNP simulations, using a higher resolution detector that breaks up the combined peaks has the potential to improve to detectability of small spectrum changes. (Percentage activity changes were based on gamma production rate activity rather than decay rate activity due to differences in the gamma production rates of the isotopes used.)

The detection system was also more sensitive to the in-stream addition of non-radioactive water at lower flow rates. There were two flow rates common to both Coil 1 and Coil 2 at which in-stream dilution experiments were performed. At both of these points Coil 1 detected lower total volume additions than Coil 2. When these are computed on the basis of percentage of the particular coil volume, the detection limits of the two coils appear to converge. Figure 31 shows points where in-line dilution showed significant activity change and points where in line dilutions did not show significant activity change as a function of flow rate for Coil 1 and 2. The in-stream dilution volume is given on the basis of percentage of total coil volume. Because of the limited number

of points that were measured, the exact point of detection limit for each coil cannot be determined. The detection limit as a function of flow rate for Coil 1 lies between the two blue lines, the lower being the points where activity change was not significant and the upper being the points where activity change was significant. However, the detection limit curve for Coil 2 is more indefinite, lying somewhere between the red squares and red X's. Since the minimum detectable volume insertion is expected to decrease with decreasing flow rate, the detection limit curve for Coil 2 would be expected to lie closer to the red X's in the lower flow rate region. Therefore, in terms of percentage of coil volume, the detection limit curves for the two coils lie in relatively the same region.

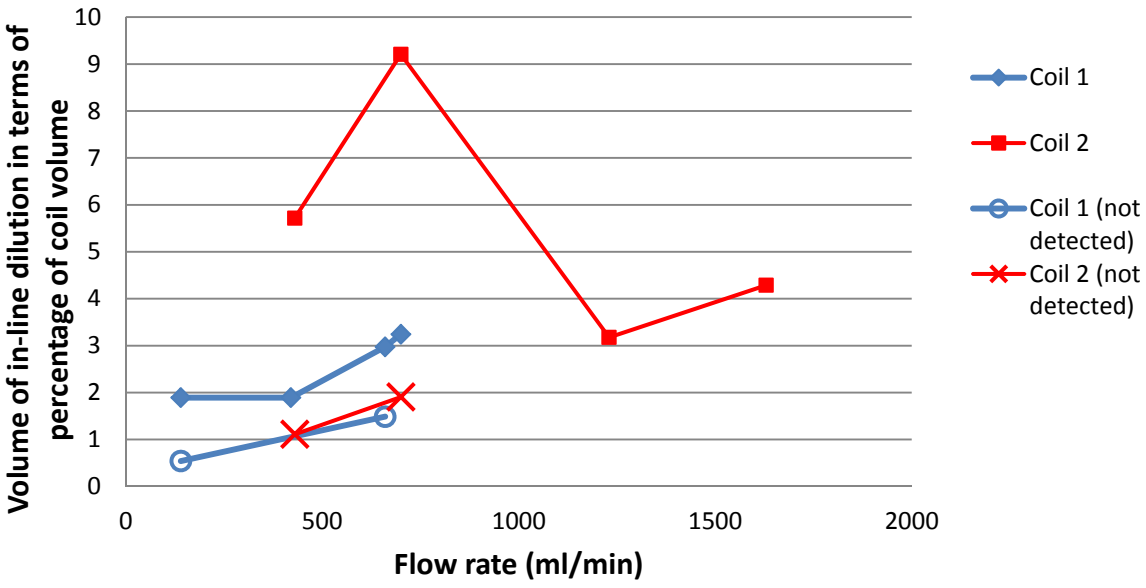

Figure 31. Observed in-line dilution volumes of detected activity change and activity change not detected as a function of flow rate for Coil 1 and Coil 2.

Because there were no statistically relevant results from the flow variation tank dilution experiments, there is little indication of the flow rate dependence of that type of

activity change. The only evidence for this is the appearance of a significant activity change with a 500ml in tank dilution using Coil 2 at a flow rate of 1900ml/min when it did not show up at 1000ml/min. However, because the system volume was greater in the second case it represented an addition of material that was about 4% of the system volume while the dilution that was detectable represented more than 5% of the system volume. The lowest detectable tank dilution observed for Coil 1 was similar at approximately 4.5% of the total system volume.

The installation of the Lynx MCA to the system improved the ability to see both total counts versus time as well as spectral changes with time. As stated before the total counts over time proved much more sensitive to small activity changes. Using a detector with a higher resolution will help to reduce the number of combined peaks that occur and thus increase the ability to detect small spectrum changes. Also, having the ability to view spectral changes with time would be important in an actual system to determine whether activity level changes simply indicate dilution changes or changes in the constituents of the flow stream. As seen in the spectral plots taken from the Lynx system experiments (Figure 32), the count time divisions used for this activity level were too low to give completely smooth, statistically relevant spectra. Longer spectrum count times of 5 minutes and 15 minutes that were often measured to characterize the entire system under its static state were much more statistically relevant for the activity levels used. An actual system would have flow streams with much higher activity levels so shorter count times will be able to provide statistically relevant spectra.

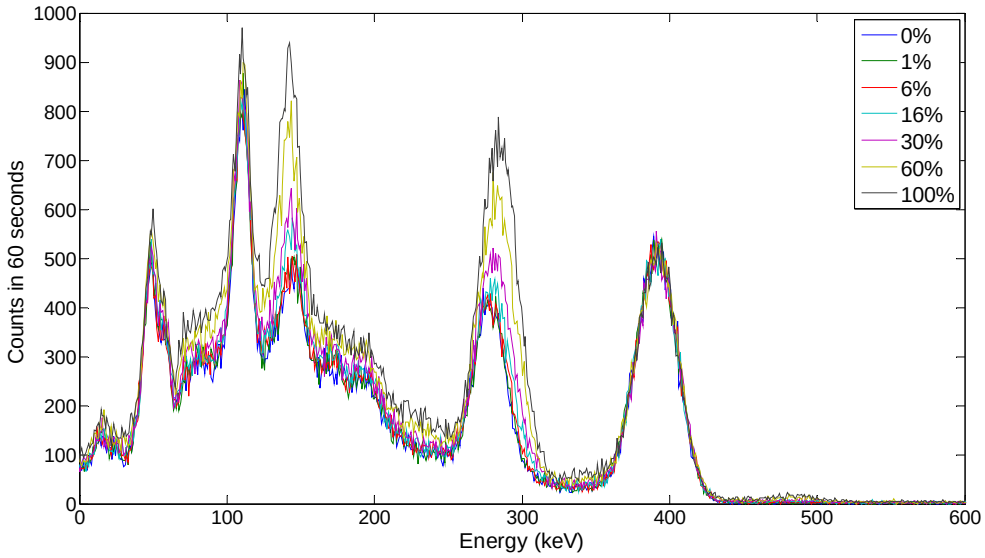

Figure 32. Experimental results for cerium addition to system containing ytterbium using Coil 1.

The count data from the Lynx system was parsed for analysis by considering the coil volumes and flow rates. When determining changes in the spectrum with time, it is necessary to choose time periods which are as long as allowable to give statistically relevant spectrum results for comparison. However these time periods also need to be short enough so that small or sudden changes in the isotopic composition of the flow stream are not over-looked or hidden within long counting periods. With this in mind, a strategy for taking spectral counts of a flow stream with a given flow rate and detector coil size was developed. The coil size and flow rate should be decided based on the flow stream activity which would determine the count time required.

It was deduced that using a count time that is twice the average dwell time for an average particle inside the detector coil will maximize the amount of material that is counted for the maximum amount of time possible using a given flow rate and coil

volume. If the computer system is sophisticated enough to take time stamped counts then the data can be divided into spectra in such a way that one starts halfway into one division and ends halfway into the next. If a spectrum count time that is twice the dwell time is used in this instance then all material passing through will be counted for its maximum possible time in at least one spectrum. An example of this counting strategy is shown in Figure 33.

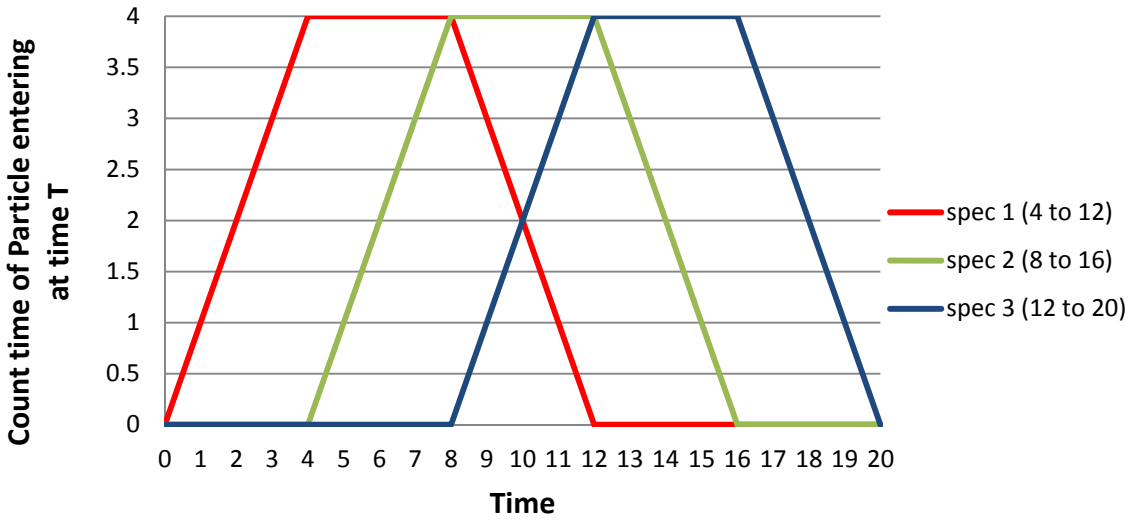

Figure 33. Counting study for detection system particle duration of 4 units and count time of 8 units.

In this example the length of time an average particle spends in view of the detector is 4 units and so the spectrum count time is 8 units. The maximum time a particle can be counted is 4 units. The plot shows three separate spectra being taken that overlap one another. Each point indicates the period of time that a particle entering the detection system at that time is counted in a particular spectrum. Spectrum 1 does not start until time 4 units so particles entering the system before that time are counted for

less than their total dwell time in the detection system. Particles that enter less than 4 units from the end of spectrum 1 also do not get the full count in that spectrum. Among the spectrum, all particles entering between 4 and 16 are counted for their maximum possible time in at least 1 spectrum.

Even though the two coil geometries proved to be very similar in these experiments, there was still useful information obtained from the differences that were observed. In the larger coil, it took slightly longer to observe changes in the activity within the system. The larger coil also appeared to be less sensitive to very small dilutions. However, in an actual facility a smaller coil might be overcome by small variations in flow streams that are normal to system operations. For example, if the coil volume were chosen to be on the same order as normal system variations then the detector would constantly measure drastic activity level changes and be incapable of distinguishing an actual significant change in the stream. Finally, larger coils would allow for longer count times for the same flow rate than the smaller coils.

Although most of the low end of the energy spectrum is often dominated by x-ray peaks there are still several low energy peaks (~50keV), such as the peak for ^{241}Am observed in the UREX flow stream simulation, that are important for flow stream characterization. The stainless steel piping used in these experiments was thinner than those that would likely be used in an actual facility and yet they caused significant attenuation losses for low energy gamma rays. The linear attenuation of gammas is dependent on the thickness of the material and a material specific factor called the linear attenuation coefficient (μ). This is also sometimes given in terms of the mass attenuation

coefficient (μ_m), which is simply the attenuation coefficient over the density. Using this, the intensity decrease of a particular gamma beam passing through a material can be given by the equation: $I = I_0 e^{-\mu_m \rho x}$, where I_0 is the original intensity, I is the resulting intensity, ρ is the density, and x is the material thickness. [25] Figure 34 shows a plot of linear attenuation coefficients as a function of gamma energy for the three main materials of interest for this project. The stainless steel is approximated by iron, the glass used is borosilicate, and the UREX flow stream is approximated as water.

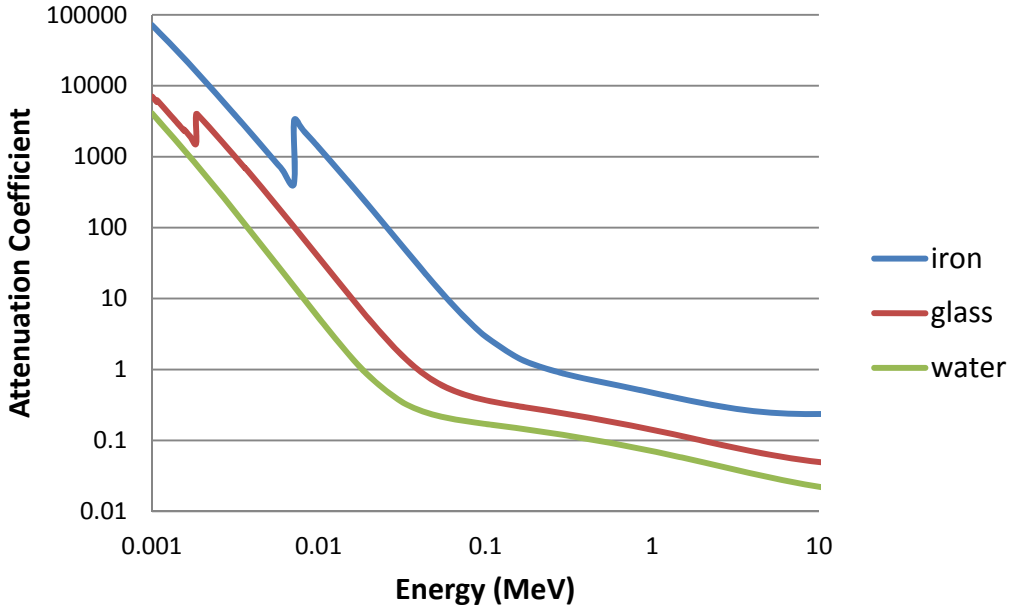

Figure 34. Linear attenuation coefficients for main components of concern. [26]

The magnitude of the attenuations produced by each of the materials used in these experiments can be attained by plugging the material thicknesses into the preceding equation. The stainless steel was 1/16” thick, the glass was estimated to be 1/8” thick and the average linear thickness of the water in the 1/2” inside diameter pipe is approximately 0.125 cm thick. It is also worth evaluating larger pipes such as a 2”

inside diameter pipe that is proposed for use in an actual reprocessing facility. Figure 35 shows an estimate of the fractional intensity as a function of energy where a fractional intensity of 1 means no attenuation and 0 means complete attenuation. It is clear that the low energy photons are easily attenuated. The crucial area of focus is between 10 and 100 keV. When the steel is used all gamma peaks below 80 keV are reduced by more than half. For the proposed pipe size of an actual reprocessing facility peaks below 100 keV are reduced in half. However when the glass is used, the working fluid of the process stream becomes the dominate source of attenuation causing the self shielding effects seen previously in the MCNP simulation. Therefore, a glass detection coil would be more capable of detecting the low energy gamma rays than a similar-sized stainless steel coil.

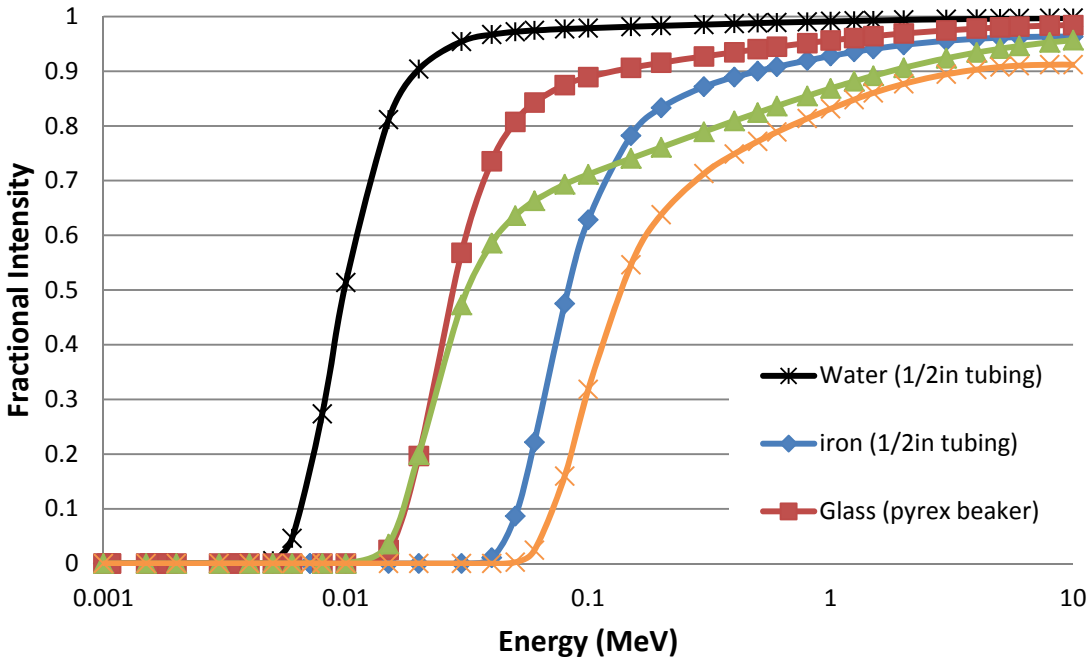

Figure 35. Fractional intensities computed using experimental and simulated material thicknesses.

6. CONCLUSIONS

A fully enclosed system was designed, built, and used as an experimental platform to measure the effects of flow rate, geometry, flow conditions, and activity level on the detection of transients in a flowing radioactive fluid stream. The purpose was to develop a model that can be used for the design of a High Resolution Gamma Spectroscopy (HRGS) system for the real time measurement of flow streams in a UREX type reprocessing facility.

The first set of experiments that were conducted used activated chromium, gold, cerium, and ytterbium nitrates dissolved in distilled water and inserted into the flowing working fluid. The fluid was pumped through coils around a single detector and an array of transient conditions were tested. From these experiments the minimum detectable activity dilution level above background for this system was found to be 0.02uCi per liter. The use of activated isotopes of cerium and ytterbium showed significant gamma attenuation in the energy range below 80 keV. The system proved more sensitive to activity changes that occurred directly in the process stream over changes that occurred within the large system holding tank. Clean water dilutions made in-stream with as low as 2% of the detector coil volume were detectable in this system. System transients that occurred under low flow rate conditions (~200 ml/min) proved more easily detectable than those at higher flow rates. The effects of process hold-up inside of the detection system were seen in the ^{198}Au experiments though they were not fully quantified.

Standard experimental procedures were used in the comparison of two detection system coil geometries. Differences between the two chosen coils were small yet significant. The smaller volume coil proved better suited for detection of small activity changes and small dilution changes. The larger coil also had a slightly longer response time to transients than the smaller coil. Count times for spectrum changes with time proved too low to give clear results as opposed to total counts over time. Use of a high resolution detector such as an HPGe detector as well as use of higher activity levels should improve the ability of the system to detect spectral changes. A method was developed for choosing flow rate and detection coil size based on the needed count time for statistical relevance.

Simulations were completed to verify results from the geometry comparisons, create a comparison to a third coil geometry, and extend the results to a simulation of three UREX process streams (UREX product, CCD-PEG product, and TRUEX product). Also, simulations were completed to compare attenuation and self shielding effects from piping material and flow stream fluids for different materials. These simulations indicated a much lower counting efficient from the third coil geometry which was larger in diameter and thus further from the detector. In an actual system the detector should be as close as possible to the system piping without over-whelming the detector with too large of a count rate. Material attenuation simulations indicate that it would be more effective to use a material such as glass around the detector in order to avoid attenuation of important low energy gamma rays. Additional simulations using the spectra that would be expected to be found in UREX flow streams indicated significant attenuation

would occur of some of the important low energy gammas such as the 60 keV peak for ^{241}Am.

The experiments documented in this thesis lay the foundation for further development of a HRGS real time detection system for a reprocessing facility. The recommendations for producing a more efficient detection system of this type are: 1) minimize flow rate, 2) maintain low volume around detector while maximizing count time, and 3) build the detection system using materials that reduce attenuation yet still tolerate the chemicals and radioactivity levels present in a reprocessing facility. Flow rate minimization may not be possible as flow rate will likely be dependent upon the flow rate required of each particular stream through a given set of centrifugal contactors. Future projects should seek to use actual UREX process stream material in experiments to progress the design of this detection system.

REFERENCES

[1] G. Suppes,T. Storrick, Sustainable Nuclear Power, Elsevier/Academic Press, Amsterdam, 2007.

[2] J. J. Laidler, J.C. Bresee, The advanced fuel cycle initiative of the U.S. department of energy: development of separations technologies, in: Proceedings of Waste Management 2004 Conference, Tucson, AZ, 29 February – 4 March 2004.

[3] L.H. Ortega, S.M. McDeavitt, Precursors for the immobilization of radioactive Cesium and Strontium from spent nuclear fuel, in: Proceedings of Global 2007: Advanced Nuclear Fuel Cycles and Systems Conference, Boise, ID, 9-13 September 2007, pp. 1385-1388.

[4] David Bodansky, Physics Today, 59, (12), (2006), p. 80-81.

[5] J. D. Law, R. S. Herbst, D. H. Meikrantz, D. R. Peterman, et. al., Development of technologies for the simultaneous separation of Cesium and Strontium from spent nuclear fuel as part of an advanced fuel cycle, in: American Institute of Chemical Engineers 2005 Spring National Meeting, Atlanta, GA, April 2005, p.182d.

[6] Candido Pereira, George F. Vandegrift, Monica C. Regalbuto, et al, Lab scale demonstration of the UREX+1a process using spent fuel, in: Proceedings of Waste Management 2007 Symposium, Tucson, AZ, 25 February – 1 March 2007.

[7] Private Communication, Sean McDeavitt, Diagram created for "Real time detection methods to monitor TRU compositions in UREX+ process streams," 2007 NERI Consortium Proposal, (2007).

[8] T. K. Li, S. F. Klosterbuer, H. O. Menlove, M. M. Pickrell, T. R. Wenz, H. Ai, S. Uehara, et. al, Conceptual designs of NDA instruments for the NRTA system at the Rokkasho reprocessing plant, in: Nuclear Materials Management 37th Annual Meeting 25, Naples, FL, 28-31 July 1996, pp. 1036-1045.

[9] B. B. Cipiti, N. L. Ricker, Advancing the state of the art in materials accountancy through safeguards performance modeling, United States Department of Energy, Washington, DC, (2008).

[10] U.S. Code of Federal Regulations, 10CFR74, accessed May 2010, available at www.nrc.gov/reading-rm/doc-collections/cfr/part074/html, July 2007.

[11] S. Johnson, The safeguards at reprocessing plants under a fissile material (cutoff) treaty, International Panel on Fissile Materials, Available at www.fissilematerials.org, February 2009.

[12] J. S. Feener, Safeguards for the uranium extraction (UREX) +1a process, MS Thesis, Texas A&M University, College Station, TX, May 2010.

[13] B. B. Cipiti, Advanced instrumentation for reprocessing, United States Department of Energy, Washington, DC, (2005).

[14] P. Bedson, C. Harrington, R. Harte, M. Sargent, Guidelines for Achieving High Accuracy in Isotope Dilution Mass Spectrometry (IDMS). Cambridge, Royal Society of Chemistry, 2002.

[15] T. Kuno, O. Kitagawa, S. Sato, A. Kurosawa, Y. Kuno, Simultaneous measurements of Plutonium and Uranium in spent-fuel dissolver solutions, in: Proceedings of 38th Annual Meeting of the Institute of Nuclear Materials Management, Phoenix, AZ, 20-24 Jul 1997.

[16] J.E. Stewart, C.R. Hatcher, La Verne L. Pollat, W.C. Harker, et. al., Development of an integrated, unattended assay system for LWR-Mox fuel pellet trays, Institute of Nuclear Materials Management 35th Annual Meeting, Naples, FL, July 1994, pp. 842-849.

[17] L.E. Smith, J.M. Schwates, J.J. Ressler, M. Douglas, K. A. Anderson, et. al., Next generation online MC&A technologies for reprocessing plants, in: Global 2007: Advanced nuclear fuel cycles and systems conference, Boise, ID, September 2007, pp. 1657-1666.

[18] J.R. Lapinskas, S.M. Zielinski, J.A. Webster, R.P. Taleyarkhan, S.M. McDeavitt, Y. Xu, Tension metastable fluid detection systems for special nuclear material detection and monitoring, in: 17th International Conference on Nuclear Engineering *(*ICONE17*)*, Brussels, Belgium, v4, 12-16 July 2009, pp. 607-614.

[19] G.J. Bernstein, R.A. Leonard, A.A. Ziegler, M.J. Steindler, An improved annular centrifugal contactor for solvent extraction reprocessing of nuclear reactor fuel, in: 84th National Meeting American Institute of Chemical Engineers, Atlanta, GA, 24 Feb. 1978.

[20] J. Law, D. Meikrantz, T. Garn, N. Mann, S. Herbst, T. Todd, The testing of commercially available engineering and plant scale annular centrifugal

contactors for the processing of spent nuclear fuel, in: 15th Pacific Basin Nuclear Conference, Sydney, Australia, 15-20 October 2006, pp. 219-225.

[21] J. Sweezy, T. E. Booth, F.E. Brown, J.S. Bull, R.A. Forster, et. al., Monte Carlo N-Particle Transport Code, Los Alamos National Laboratory, Los Alamos, NM, (2008).

[22] A.G. Croff, Oak Ridge Isotope Generation and Depletion Code, Oak Ridge National Laboratory, Oak Ridge, TN, (1980).

[23] Janis version 3.2, , Nicolas Soppera, OECD Nuclear Energy Agency, Issy-les-Moulineaux, France, available at http://www.nea.fr/janis/, May 2010.

[24] B. Goddard, Development of a real-time detection strategy for material accountancy and process monitoring during nuclear fuel reprocessing using the UREX+3a Method, MS Thesis, Texas A&M University, College Station, TX, December 2009.

[25] M. F. L'Annunziata, Radioactivity: Introduction and History, Elsevier, Amsterdam, The Netherlands, 2007.

[26] J.H. Hubbell, S.M. Seltzer, & National Institute of Standards and Technology (U.S.), Tables of X-ray mass attenuation coefficients and mass energy-absorption coefficients 1 keV to 20 MeV for elements Z=1 to 92 and 48 additional substances of dosimetric interest, NISTIR, 5632. Gaithersburg, MD: U.S. Department of Commerce, Technology Administration, 1996.

APPENDIX A

Sample MCNP input deck for cerium in glass container

```
C This deck is a glass pipe/beaker with cerium only
c
C    ccccccccccccccccccccccccccccccccccccccccccccccccccccccccccccccccccccccccccccc
C    Cell cards
1    8 -1.000    -1     19  -18                  imp:p=1     $source
2    9 -2.634     1  -2  19  -18                  imp:p=1     $source tubing, 0.125 in
3    7 -3.67     -3  -4  5                        imp:p=1     $detector
4    1 -.0012     -28 #1 #2 #3 #9 #10 #11 #12     imp:p=1     $air inside shielding
7    3 -11.34     -27 28                          imp:p=1     $shielding pb 4.0 in
8    0            6:-7:8:-9:10:-11                imp:p=0     $void
9    5 -2.7       -22 21 -23 24                   imp:p=1    $can
10   5 -2.7       -22 -25 23                      imp:p=1    $can
11   5 -2.7       -22 26 -24                      imp:p=1    $can
12   1 -.0012     3 -21 -23 24                    imp:p=1    $air

C    Surface cards
1    cz    2.54        $source, 0.5 inch inside diamiter
2    cz    2.69875     $source tubing, SS-316 0.154 in (0.39116 cm), for Schedule 40 pipe
[in]: id=1 => t=0.133, id=2 => t=0.154, id=3 => t=0.216, id=4 => t=0.237, id=6 =>
t=0.280, id=6 => t=0.322
3    c/y   10  0 3.81   $detector
4    py    3.81         $detector
5    py   -3.81         $detector
6    pz    20           $outer boundary
7    pz   -20           $ob
8    py    20           $ob
9    py   -20           $ob
10   px    25           $ob
11   px   -25           $ob
12   pz    10           $inside Pb boundary
13   pz   -10
14   py    10
15   py   -10
16   px    15
17   px   -15
18   pz    9
19   pz   -9
20   cz    2
21   c/y   10 0 3.91
22   c/y   10 0 3.96
23   py    3.91
24   py   -3.91
25   py    3.96
26   py   -3.96
27   rpp  -25 25  -20 20  -20 20
28   rpp  -15 15  -10 10  -10 10

C    Materials Cards
mode p                                                  $consider photons only
m1   007014 .72 008016 .28                              $air, density 0.0012 g/cm^3
m2   26000 0.68 24000 0.17 28000 0.12 42000 0.02 25055 0.01 $stainless steel 316, density
7.950 g/cm^3
m3   82000 1                                            $lead, density 11.34 g/cm^3
m4   32074 1                                            $germanium, density 5.323
g/cm^3
m5   13027 1                                            $aluminum, density 2.7 g/cm^3
m6   29063 .6917 29065 .3083                           $copper, density 8.96 g/cm^3
m7   11023 0.5 53127 0.5                               $NaI, density 3.67 g/cm^3
m8   01001 -0.112 08016 -0.888                         $water containing source
m9   14028 0.30743 14029 0.01561 14030 0.0103 08016 0.66504
     08017 0.00025 08018 0.00137                       $glass density 2.634g/cm^3
```

```
C    Data cards
C
sdef   cel=1   par=2   erg=d2   ext=d3   pos=0 0 0   axs=0 0 1   rad=d4   $source is cell
1 with energy according to d2 with sampaling cyliender of height d3 centered at (0,0,0)
extending in the Z-axis direction with a radius according to d4
C      discrete lines (in MeV) and their probabilities
si2    l 4.65000E-03 3.30340E-02 3.34420E-02 3.77200E-02 3.78010E-02 3.87260E-02
         5.11000E-01 1.06100E-02 1.48830E-01 2.17030E-01 4.33220E-01 4.36590E-01
         4.47150E-01 4.79120E-01 4.82470E-01 4.93030E-01 5.29300E-01 6.31380E-01
         6.78260E-01 6.98720E-01 7.09300E-01 7.24400E-01 7.70970E-01 7.81570E-01
         9.15800E-01 9.26350E-01 1.16085E+00 2.54290E-01 8.72000E-02 1.69260E-01
         7.62300E-01 8.24820E-01 8.35380E-01 9.06840E-01 9.17450E-01 9.93810E-01
         1.00449E+00 1.65858E-01 4.65000E-03 3.30340E-02 3.34420E-02 3.77200E-02
         3.78010E-02 3.87260E-02 1.45443E-01 5.03000E-03 3.55500E-02 3.60260E-02
         4.06530E-02 4.07480E-02 4.17640E-02 5.03000E-03 3.55500E-02 3.60260E-02
         4.06530E-02 4.07480E-02 4.17640E-02 5.73560E-02 1.22400E-01 1.39742E-01
         1.97600E-01 2.31550E-01 2.93266E-01 3.38300E-01 3.50619E-01 3.57800E-01
         3.71290E-01 3.89640E-01 4.16570E-01 4.32999E-01 4.38430E-01 4.46020E-01
         4.47450E-01 4.90368E-01 4.97810E-01 5.23000E-01 5.56870E-01 5.69910E-01
         5.87200E-01 6.14220E-01 6.64571E-01 6.70120E-01 6.75500E-01 6.82820E-01
         7.09590E-01 7.21929E-01 7.29870E-01 7.67700E-01 7.87400E-01 7.91070E-01
         8.06340E-01 8.09980E-01 8.80460E-01 8.91470E-01 9.07100E-01 9.37820E-01
         9.56900E-01 1.00285E+00 1.01430E+00 1.03122E+00 1.04678E+00 1.06022E+00
         1.10325E+00 1.16058E+00 1.32448E+00 1.34010E+00 1.38200E+00 5.03000E-03
         3.55500E-02 3.60260E-02 4.06530E-02 4.07480E-02 4.17640E-02 3.35680E-02
         4.09800E-02 5.33950E-02 5.90300E-02 8.01200E-02 9.99610E-02 1.33515E-01
         4.84000E-03 3.42790E-02 3.47200E-02 3.91700E-02 3.92580E-02 4.02280E-02
         5.08800E-01 6.42000E-01 1.57560E+00 5.23000E-03 3.68470E-02 3.73610E-02
         4.21660E-02 4.22720E-02 4.33350E-02 7.42100E-01 5.23000E-03 3.68470E-02
         3.73610E-02 4.21660E-02 4.22720E-02 4.33350E-02 6.24700E-01 6.74950E-01
         6.96510E-01 8.14100E-01 8.64450E-01 1.18200E+00 1.37627E+00 1.38802E+00
         1.48916E+00 1.56097E+00 1.97882E+00 2.04630E+00 2.07290E+00 2.18566E+00
         2.36830E+00 2.65490E+00
sp2    d 3.41140E-02 3.92857E-02 7.15397E-02 6.89410E-03 1.32990E-02 4.29544E-03
         3.08685E-05 1.44880E-03 1.61606E-06 7.11066E-06 9.40546E-05 4.81586E-04
         3.23212E-03 2.16552E-05 8.30654E-05 1.90695E-05 6.46423E-07 2.42409E-05
         1.61606E-06 5.65620E-05 1.93927E-06 1.29285E-06 1.09892E-05 5.49460E-06
         9.34082E-05 6.14102E-05 2.71498E-06 1.31311E-04 1.65165E-06 8.21694E-05
         3.59233E-05 8.25823E-05 1.93243E-05 5.20268E-07 2.39489E-06 3.71620E-07
         4.21170E-06 1.45797E-04 2.19491E-05 4.13742E-05 7.53429E-05 7.26061E-06
         1.40060E-05 4.52379E-06 7.83548E-02 3.99262E-03 7.82235E-03 1.41162E-02
         1.38165E-03 2.66739E-03 8.63156E-04 4.43173E-02 8.64688E-02 1.56041E-01
         1.52728E-02 2.94855E-02 9.54138E-03 5.80293E-02 4.23572E-05 3.81215E-04
         1.27071E-05 1.01657E-02 2.11786E-01 4.23572E-06 1.59898E-02 2.96500E-06
         1.22836E-04 1.80018E-04 3.38857E-05 7.85725E-04 2.11786E-05 7.41251E-05
         2.96500E-04 1.06952E-02 2.20257E-04 8.47144E-06 1.56722E-04 2.54143E-05
         1.31943E-03 5.93001E-05 2.81675E-02 4.02393E-05 4.23572E-06 4.23572E-05
         4.23572E-05 2.66850E-02 1.48250E-05 1.56722E-05 1.27071E-05 6.56536E-05
         1.41897E-04 1.54604E-04 5.10404E-03 4.02393E-05 6.35357E-06 1.29189E-04
         6.35357E-06 3.72743E-04 6.35357E-06 9.95393E-05 5.93001E-05 1.80018E-04
         2.05432E-03 1.18600E-05 7.83608E-06 1.52486E-05 1.90607E-06 4.35947E-12
         7.39280E-12 1.33410E-11 1.30578E-12 2.52092E-12 8.15758E-13 6.25840E-13
         8.06638E-13 3.12920E-13 6.18438E-16 4.27657E-12 1.25168E-13 3.47689E-11
         6.79616E-16 1.32268E-15 2.40024E-15 2.33385E-16 4.50938E-16 1.45036E-16
         8.83714E-15 8.55162E-16 1.42535E-12 1.97445E-13 3.65213E-13 6.57941E-13
         6.48184E-14 1.25037E-13 4.16790E-14 3.78687E-10 2.57344E-15 4.75181E-15
         8.56052E-15 8.43356E-16 1.62686E-15 5.42287E-16 3.49185E-15 9.14532E-15
         4.15696E-12 9.97671E-15 7.48253E-15 1.66279E-16 1.20552E-15 2.08264E-14
         8.60491E-13 6.23544E-16 2.70203E-15 8.31393E-16 7.06684E-16 2.14915E-12
         1.66279E-16 4.57266E-16
si3      -10 10                        $the lower and upper height from pos location
si4      0.0 2.69875                   $r1 r2, inner radius and outer radius
sp4      -21 1                         $distribute the source radialy with the correct
probability
c
f4:p 3                                 $give the photon flux for cell 3
f8:p 3                                 $give the photon counts per cm^3 for cell 3
```

```
e8   0 3999i 2.0                      $gives the energy bins for cell 3, 4000 bins at
0.5 Kev per bin
nps 200000000                           $run this many particles, 20 million particles
c
c Things to change in newer version of this deck.
sd8 1                                 $would give the result in counts instead of counts
per cm^3
ft8 geb -0.00152 0.035018 4.188                       $brodens the results resolution to
simulate a read detector for peramiters a=1, b=2, c=3.  FWHM=a+b*SQRT(E+c*E^2), E is in
MeV.
```

Sample MCNP input deck for ytterbium in coil 1

```
This deck is coil 1 geometry with ytterbium only
c
C    ccccccccccccccccccccccccccccccccccccccccccccccccccccccccccccccccccccccccccccccc
C    Cell cards
1    8 -1.000    -26:-33:-34:-35:-36:-37      imp:p=1     $source
2    2 -7.950    -28 33                       imp:p=1     $source tubing
4    2 -7.950    -29 34                       imp:p=1     $source tubing
5    2 -7.950    -30 35                       imp:p=1     $source tubing
6    2 -7.950    -31 36                       imp:p=1     $source tubing
7    2 -7.950    -32 37                       imp:p=1     $source tubing
8    2 -7.950    -27 26                       imp:p=1     $source tubing
3    7 -3.67     -3  -4  5                    imp:p=1     $detector
9    1 -.0012    -40 28 29 30 31 32 27 #3 #13 #14 #15 imp:p=1     $air inside shielding
10    5 -2.7      40 -39                      imp:p=1     $shielding al 0.25in
11    3 -11.34    -38 39                      imp:p=1     $shielding pb 4.0 in
12    0            38                         imp:p=0     $void
13    5 -2.7       -7 6 -8 9                  imp:p=1    $can
14    5 -2.7       -7 -10 8                   imp:p=1    $can
15    5 -2.7       -7 -9 11                   imp:p=1    $can

C    Surface cards
3    cz    3.81         $detector
4    pz    3.81         $detector
5    pz   -3.81         $detector
6    cz    3.91
7    cz    3.96
8    pz    3.91
9    pz   -3.91
10   pz    3.96
11   pz   -3.96
26   tz   0 0 0.79376 8.41375 0.635 0.635
27   tz   0 0 0.79376 8.41375 0.79375 0.79375
28   tz   0 0 -0.79376 8.41375 0.79375 0.79375
29   tz   0 0 -2.38127 8.41375 0.79375 0.79375
30   tz   0 0 2.38127 8.4175 0.79375 0.79375
31   tz   0 0 3.96878 8.4175 0.79375 0.79375
32   tz   0 0 -3.96878 8.4175 0.79375 0.79375
33   tz   0 0 -0.79376 8.41375 0.635 0.635
34   tz   0 0 -2.38127 8.41375 0.635 0.635
35   tz   0 0 2.38127 8.4175 0.635 0.635
36   tz   0 0 3.96878 8.4175 0.635 0.635
37   tz   0 0 -3.96878 8.4175 0.635 0.635
38   rpp  -21 21  -21 21  -18 18      $outer boundary
39   rpp  -11 11  -11 11  -8 8        $inside Pb boundary
40   rpp  -10 10  -10 10  -7 7        $inside Al boundary

C    Materials Cards
mode p                                                    $consider photons only
m1   007014 .72 008016 .28                                $air, density 0.0012 g/cm^3
m2   26000 0.68 24000 0.17 28000 0.12 42000 0.02 25055 0.01 $stainless steel 316, density
7.950 g/cm^3
m3   82000 1                                              $lead, density 11.34 g/cm^3
m4   32074 1                                              $germanium, density 5.323
g/cm^3
m5   13027 1                                              $aluminum, density 2.7 g/cm^3
m6   29063 .6917 29065 .3083                              $copper, density 8.96 g/cm^3
m7   11023 0.5 53127 0.5                                  $NaI, density 3.67 g/cm^3
m8   01001 -0.112 08016 -0.888                           $water containing source
m9   14028 0.30743 14029 0.01561 14030 0.0103 08016 0.66504
     08017 0.00025 08018 0.00137                          $glass density 2.634g/cm^3
C
C    Data cards
C
```

```
sdef   cel=1   par=2   erg=d2   ext=d3   pos=0 0 0  axs=0 0 1 rad=d4   $source is cell 1
w/energy accdng to d2 with smpling cyl height d3 center (0,0,0) in Z direction radius of
d4
C      discrete lines (in MeV) and their probabilities
si2    l 7.18000E-03 4.97730E-02 5.07420E-02 5.73000E-02 5.75050E-02 5.90280E-02
         8.41031E-03 1.09780E-01 1.18190E-01 7.18000E-03 4.97730E-02 5.07420E-02
         5.73000E-02 5.75050E-02 5.90280E-02 5.02500E-03 1.23850E-02 8.56000E-02
         1.11621E-01 1.16656E-01 1.24017E-01 1.75630E-01 1.97700E-01 2.10100E-01
         2.10600E-01 2.37140E-01 2.77430E-01 2.86500E-01 2.95901E-01 3.08291E-01
         3.62910E-01 3.71960E-01 4.19900E-01 4.24900E-01 4.87900E-01 4.95400E-01
         5.06900E-01 5.19200E-01 5.47800E-01 5.59500E-01 5.73500E-01 5.86000E-01
         6.08600E-01 6.09000E-01 6.21030E-01 6.30700E-01 6.70700E-01 6.71700E-01
         6.76100E-01 6.93900E-01 7.05800E-01 7.32500E-01 7.84090E-01 7.96550E-01
         8.60000E-01 8.69700E-01 8.71500E-01 8.82000E-01 9.07700E-01 9.12600E-01
         9.66100E-01 9.76200E-01 9.94000E-01 1.09690E+00 1.10900E+00 1.15600E+00
         1.16840E+00 1.22050E+00 1.27120E+00 1.27990E+00 1.28440E+00 1.39550E+00
         1.40050E+00 7.42000E-03 5.13540E-02 5.23890E-02 5.91590E-02 5.93830E-02
         6.09620E-02 6.67310E-02 7.18000E-03 4.97730E-02 5.07420E-02 5.73000E-02
         5.75050E-02 5.90280E-02 8.41031E-03 2.07520E-02 6.31208E-02 9.36151E-02
         1.05190E-01 1.09780E-01 1.17377E-01 1.18190E-01 1.30524E-01 1.56725E-01
         1.77214E-01 1.93150E-01 1.97958E-01 2.05990E-01 2.13936E-01 2.26300E-01
         2.40332E-01 2.61079E-01 2.91190E-01 2.94540E-01 3.07738E-01 3.33965E-01
         3.36620E-01 3.56740E-01 3.70856E-01 3.79286E-01 3.86673E-01 4.52620E-01
         4.64720E-01 4.65657E-01 4.66562E-01 4.74973E-01 4.94360E-01 5.00350E-01
         5.07800E-01 5.15104E-01 5.28572E-01 5.46160E-01 5.62413E-01 5.70890E-01
         5.79854E-01 6.00607E-01 6.24885E-01 6.33320E-01 6.42877E-01 6.63603E-01
         6.93460E-01 7.10358E-01 7.39420E-01 7.60240E-01 7.73390E-01 7.81640E-01
         7.66000E-03 5.29650E-02 5.40700E-02 6.10500E-02 6.12900E-02 6.29290E-02
         1.13805E-01 1.37658E-01 1.44863E-01 2.51474E-01 2.82522E-01 3.96329E-01
         7.66000E-03 5.29650E-02 5.40700E-02 6.10500E-02 6.12900E-02 6.29290E-02
         9.44000E-02 1.19700E-01 1.21600E-01 1.38600E-01 1.47300E-01 1.50300E-01
         1.62500E-01 1.71500E-01 2.68700E-01 3.00500E-01 3.19100E-01 3.36600E-01
         4.30500E-01 4.58000E-01 5.49900E-01 5.52000E-01 6.91900E-01 7.14200E-01
         7.60500E-01 7.79300E-01 7.83300E-01 7.90300E-01 8.76800E-01 8.99200E-01
         9.41800E-01 9.62000E-01 9.67300E-01 1.01520E+00 1.02830E+00 1.04920E+00
         1.06830E+00 1.08050E+00 1.10920E+00 1.11460E+00 1.12000E+00 1.15010E+00
         1.21540E+00 1.23100E+00 1.23680E+00 1.24180E+00 7.42000E-03 7.90000E-03
         5.13540E-02 5.23890E-02 5.40700E-02 5.46110E-02 5.91590E-02 5.93830E-02
         6.09620E-02 6.29850E-02 6.32430E-02 6.49420E-02 8.21000E-02 8.83610E-02
         9.36250E-01 9.56800E-01 1.06142E+00 1.13825E+00 1.15926E+00 1.20470E+00
         1.22661E+00 1.24762E+00 7.90000E-03 5.40700E-02 5.46110E-02 6.29850E-02
         6.32430E-02 6.49420E-02 7.16418E-02 1.12950E-01 1.36724E-01 2.08366E-01
         2.49674E-01 3.21316E-01
sp2    d 1.09136E-12 1.26792E-12 2.20954E-12 2.38201E-13 4.59622E-13 1.54761E-13
         2.78753E-10 2.29354E-12 2.46997E-13 4.45042E-07 4.27338E-07 7.44699E-07
         8.02830E-08 1.54910E-07 5.21604E-08 2.31201E-09 1.00709E-09 1.98115E-09
         6.76894E-07 7.59442E-08 3.00475E-07 2.93871E-09 8.91519E-10 2.31134E-10
         2.11983E-08 9.97180E-09 1.91511E-08 2.64154E-10 9.54255E-07 2.12644E-06
         6.50478E-10 8.48594E-09 2.74059E-09 7.39630E-10 1.65096E-10 6.60384E-11
         7.49536E-10 5.84440E-10 5.61327E-10 1.53870E-09 3.23588E-10 1.32077E-10
         1.22171E-09 6.60384E-10 2.93871E-09 1.65096E-10 8.32084E-09 7.26423E-10
         9.41048E-09 4.95288E-10 3.96231E-10 3.22268E-09 7.92461E-09 2.11323E-08
         4.95288E-11 1.81606E-09 6.60384E-10 1.27124E-09 2.09672E-08 2.54248E-09
         8.71707E-10 2.31134E-11 1.98115E-11 3.50004E-11 2.24200E-10 1.98115E-11
         6.07554E-11 9.24538E-11 1.12265E-11 8.25480E-11 7.92461E-11 9.24538E-11
         8.25480E-11 2.95057E-12 2.20590E-12 3.84410E-12 4.20093E-13 8.10180E-13
         2.74115E-13 1.22488E-12 5.75624E-02 6.36774E-02 1.10967E-01 1.19629E-02
         2.30831E-02 7.77239E-03 4.03900E-04 2.30180E-04 5.36362E-02 3.16171E-03
         3.12697E-06 2.11939E-02 4.82074E-05 2.26705E-03 1.37239E-02 1.21170E-05
         2.68833E-02 8.99004E-06 4.34301E-02 4.95104E-06 3.51784E-06 3.04011E-07
         1.38108E-04 2.08030E-03 5.21162E-06 1.17261E-06 1.21952E-02 2.17151E-06
         1.10313E-05 1.70246E-07 8.72946E-06 1.47662E-06 4.12586E-07 1.99779E-08
         4.34301E-09 2.30180E-07 2.34523E-08 2.34523E-07 1.80235E-06 1.06838E-08
         1.78063E-09 5.02052E-06 2.12808E-07 1.78063E-09 1.43319E-07 1.52005E-07
         2.32786E-06 1.37239E-06 5.94993E-06 8.33859E-09 9.20719E-08 2.29311E-07
         1.05101E-08 3.77842E-08 2.21494E-09 9.98893E-10 2.51026E-07 3.64813E-09
         2.57189E-02 2.65935E-02 4.60759E-02 5.07517E-03 9.83862E-03 3.33149E-03
```

```
         4.77832E-02 2.90925E-03 8.30518E-03 2.12912E-03 7.57381E-02 1.62528E-01
         5.89295E-03 6.21534E-03 1.07687E-02 1.18615E-03 2.29945E-03 7.78624E-04
         1.16353E-05 1.16353E-05 8.58105E-03 3.49060E-03 4.50869E-04 5.04682E-02
         1.59986E-04 8.72649E-06 4.50869E-04 1.59986E-05 1.16353E-05 1.59986E-05
         2.90883E-06 1.06172E-04 4.36325E-06 1.01809E-05 8.72649E-06 1.45442E-05
         1.59986E-04 2.76339E-04 5.81766E-06 2.18162E-05 5.52678E-05 1.71621E-03
         2.66158E-03 4.65413E-05 7.99928E-05 2.32706E-05 1.61440E-03 4.36324E-05
         2.18162E-05 1.45442E-02 5.09045E-04 8.72649E-06 1.46896E-03 1.70167E-03
         7.12664E-05 8.87193E-04 9.59914E-05 8.72649E-03 1.17967E-14 4.45935E-12
         8.95113E-15 1.55987E-14 2.14150E-12 1.23600E-12 1.70466E-15 3.28757E-15
         1.11231E-15 2.39051E-13 4.61804E-13 1.57557E-13 3.03242E-15 3.84009E-12
         9.48021E-17 1.92004E-17 3.28807E-16 1.00802E-16 6.00013E-16 4.02009E-17
         5.70013E-17 9.00020E-18 4.44010E-04 4.02463E-04 2.32288E-04 4.49261E-05
         8.67890E-05 2.96104E-05 2.52777E-05 9.07562E-04 6.89808E-06 1.52275E-03
         2.95110E-05 3.09119E-05
si3      -4.60378 4.60378                       $the lower and upper height from pos
location
si4      7.77875 9.04875                     $r1 r2, inner radius and outer radius
sp4      -21 1                          $distribute the source radialy with the correct
probability
c
f4:p 3                                  $give the photon flux for cell 3
f8:p 3                                  $give the photon counts per cm^3 for cell 3
e8   0 3999i 2.0                        $gives the energy bins for cell 3, 4000 bins at
0.5 Kev per bin
nps 200000000                             $run this many particles, 2 billion particles
c sd8 1                                 $would give the result in counts instead of counts
per cm^3
ft8 geb -0.00152 0.035018 4.188                        $brodens the results resolution to
simulate a read detector for peramiters a=1, b=2, c=3.  FWHM=a+b*SQRT(E+c*E^2), E is in
MeV.
```

Sample MCNP input deck for Cs/Sr stream in Coil 1 with HPGe detector

```
C This deck is coil 1 geometry with Cs and Sr
c
C    CCCCCCCCCCCCCCCCCCCCCCCCCCCCCCCCCCCCCCCCCCCCCCCCCCCCCCCCCCCCCCCCCCCCCCCCCCC
C    Cell cards
1    8 -1.000    -26:-33:-34:-35:-36:-37      imp:p=1     $source
2    2 -7.950    -28 33                       imp:p=1     $source tubing
4    2 -7.950    -29 34                       imp:p=1     $source tubing
5    2 -7.950    -30 35                       imp:p=1     $source tubing
6    2 -7.950    -31 36                       imp:p=1     $source tubing
7    2 -7.950    -32 37                       imp:p=1     $source tubing
8    2 -7.950    -27 26                       imp:p=1     $source tubing
3    4 -5.323     -3  -4  5                   imp:p=4     $detector
9    1 -.0012    -40 28 29 30 31 32 27 #3 #13 #14 #15 imp:p=2     $air inside shielding
10    5 -2.7      40 -39                      imp:p=1     $shielding al 0.25in
11    3 -11.34    -38 39                      imp:p=1     $shielding pb 4.0 in
12    0            38                         imp:p=0     $void
13    5 -2.7       -7 6 -8 9                  imp:p=2    $can
14    5 -2.7       -7 -10 8                   imp:p=2    $can
15    5 -2.7       -7 -9 11                   imp:p=2    $can

C    Surface cards
3    cz    3.81         $detector
4    pz    3.81         $detector
5    pz   -3.81         $detector
6    cz    3.91
7    cz    3.96
8    pz    3.91
9    pz   -3.91
10   pz    3.96
11   pz   -3.96
26   tz   0 0 0.79376 8.41375 0.635 0.635
27   tz   0 0 0.79376 8.41375 0.79375 0.79375
28   tz   0 0 -0.79376 8.41375 0.79375 0.79375
29   tz   0 0 -2.38127 8.41375 0.79375 0.79375
30   tz   0 0 2.38127 8.4175 0.79375 0.79375
31   tz   0 0 3.96878 8.4175 0.79375 0.79375
32   tz   0 0 -3.96878 8.4175 0.79375 0.79375
33   tz   0 0 -0.79376 8.41375 0.635 0.635
34   tz   0 0 -2.38127 8.41375 0.635 0.635
35   tz   0 0 2.38127 8.4175 0.635 0.635
36   tz   0 0 3.96878 8.4175 0.635 0.635
37   tz   0 0 -3.96878 8.4175 0.635 0.635
38   rpp  -21 21  -21 21  -18 18      $outer boundary
39   rpp  -11 11  -11 11  -8 8        $inside Pb boundary
40   rpp  -10 10  -10 10  -7 7        $inside Al boundary

C    Materials Cards
mode p                                                      $consider photons only
m1   007014 .72 008016 .28                                  $air, density 0.0012 g/cm^3
m2   26000 0.68 24000 0.17 28000 0.12 42000 0.02 25055 0.01 $stainless steel 316, density
7.950 g/cm^3
m3   82000 1                                                $lead, density 11.34 g/cm^3
m4   32074 1                                                $germanium, density 5.323
g/cm^3
m5   13027 1                                                $aluminum, density 2.7 g/cm^3
m6   29063 .6917 29065 .3083                                $copper, density 8.96 g/cm^3
m7   11023 0.5 53127 0.5                                    $NaI, density 3.67 g/cm^3
m8   01001 -0.112 08016 -0.888                              $water containing source
m9   14028 0.30743 14029 0.01561 14030 0.0103 08016 0.66504
     08017 0.00025 08018 0.00137                            $glass density 2.634g/cm^3
C
C    Data cards
C
```

```
sdef   cel=1   par=2   erg=d2   ext=d3   pos=0 0 0  axs=0 0 1 rad=d4   $source is cell 1
w/energy accdng to d2 with smpling cyl height d3 center (0,0,0) in Z direction radius of
d4
C      discrete lines (in MeV) and their probabilities
si2    l 1.5900E-03 1.6383E-03 1.6383E-03 1.7521E-03 1.8718E-03  $ Rb-83 Rb-84 Rb-86 Sr-
85 Rb-86
         4.1100E-03 4.2900E-03 4.4187E-03 4.6199E-03 4.8275E-03  $ Cs-131 Ba-131 Cs-134
Ba-133 Cs-134
         4.8275E-03 4.8275E-03 4.8275E-03 5.0421E-03 1.2598E-02  $ Cs-136 Ba-136m Ba-137m
Ba-140 Rb-83
         1.2598E-02 1.2598E-02 1.2649E-02 1.2651E-02 1.2651E-02  $ Rb-84 Rb-86 Rb-83 Rb-
84 Rb-86
         1.3336E-02 1.3395E-02 1.3850E-02 1.4098E-02 1.4100E-02  $ Sr-85 Sr-85 Ba-140 Rb-
86 Rb-83
         1.4107E-02 1.4107E-02 1.4165E-02 1.4957E-02 1.5830E-02  $ Rb-84 Rb-86 Rb-86 Sr-
85 Rb-86
         2.9458E-02 2.9458E-02 2.9779E-02 2.9779E-02 2.9955E-02  $ Cs-131 Cs-134 Cs-131
Cs-134 Ba-140
         3.0625E-02 3.0625E-02 3.0973E-02 3.0973E-02 3.1817E-02  $ Ba-131 Ba-133 Ba-131
Ba-133 Cs-134
         3.1817E-02 3.1817E-02 3.1817E-02 3.2194E-02 3.2194E-02  $ Cs-136 Ba-136m Ba-137m
Cs-134 Cs-136
         3.2194E-02 3.2194E-02 3.3034E-02 3.3442E-02 3.3593E-02  $ Ba-136m Ba-137m Ba-140
Ba-140 Cs-134
         3.3600E-02 3.4953E-02 3.5000E-02 3.6341E-02 3.6341E-02  $ Cs-131 Ba-133 Ba-131
Cs-134 Cs-136
         3.6341E-02 3.6341E-02 3.7761E-02 5.3161E-02 5.4889E-02  $ Ba-136m Ba-137m Ba-140
Ba-133 Ba-131
         6.6881E-02 7.8733E-02 7.9623E-02 8.0997E-02 8.2580E-02  $ Cs-136 Ba-131 Ba-133
Ba-133 Ba-131
         8.6360E-02 9.2284E-02 1.0968E-01 1.1355E-01 1.1890E-01  $ Cs-136 Ba-131 Cs-136
Ba-140 Ba-140
         1.1932E-01 1.2381E-01 1.2809E-01 1.2855E-01 1.3272E-01  $ Rb-83 Ba-131 Ba-131
Rb-83 Ba-140
         1.3361E-01 1.3736E-01 1.5325E-01 1.5715E-01 1.6061E-01  $ Ba-131 Ba-131 Cs-136
Ba-131 Ba-133
         1.6267E-01 1.6392E-01 1.6658E-01 1.7660E-01 1.8728E-01  $ Ba-140 Ba-136m Cs-136
Cs-136 Cs-136
         2.1608E-01 2.2323E-01 2.3350E-01 2.3963E-01 2.4269E-01  $ Ba-131 Ba-133 Cs-136
Ba-131 Cs-134
         2.4689E-01 2.4943E-01 2.7365E-01 2.7640E-01 2.9452E-01  $ Ba-131 Ba-131 Cs-136
Ba-133 Ba-131
         3.0240E-01 3.0285E-01 3.0487E-01 3.1550E-01 3.1550E-01  $ Cs-136 Ba-133 Ba-140
Cs-136 Ba-136m
         3.1991E-01 3.2651E-01 3.4055E-01 3.5120E-01 3.5602E-01  $ Cs-136 Cs-134 Cs-136
Ba-131 Ba-133
         3.6912E-01 3.7325E-01 3.8385E-01 3.9005E-01 4.0405E-01  $ Ba-131 Ba-131 Ba-133
Ba-131 Ba-131
         4.2373E-01 4.2757E-01 4.3759E-01 4.5142E-01 4.6126E-01  $ Ba-140 Ba-131 Ba-140
Ba-131 Ba-131
         4.6268E-01 4.6750E-01 4.7420E-01 4.7535E-01 4.8041E-01  $ Ba-131 Ba-140 Ba-131
Cs-134 Ba-131
         4.8652E-01 4.9000E-01 4.9633E-01 5.0610E-01 5.0719E-01  $ Ba-131 Cs-136 Ba-131
Ba-131 Cs-136
         5.1100E-01 5.1401E-01 5.1750E-01 5.2040E-01 5.2960E-01  $ Rb-84 Sr-85 Ba-131 Rb-
83 Rb-83
         5.3370E-01 5.3731E-01 5.4628E-01 5.5039E-01 5.5120E-01  $ Ba-131 Ba-140 Ba-131
Ba-131 Ba-140
         5.5260E-01 5.6217E-01 5.6287E-01 5.6323E-01 5.6931E-01  $ Rb-83 Rb-83 Ba-131 Cs-
134 Cs-134
         5.7269E-01 5.8504E-01 5.9650E-01 6.0470E-01 6.2011E-01  $ Ba-131 Ba-131 Ba-131
Cs-134 Ba-131
         6.4897E-01 6.5760E-01 6.6166E-01 6.7443E-01 6.8118E-01  $ Rb-83 Ba-131 Ba-137m
Ba-131 Rb-83
         6.9649E-01 7.0344E-01 7.3300E-01 7.3300E-01 7.4550E-01  $ Ba-131 Ba-131 Cs-136
Ba-136m Ba-131
```

```
         7.8592E-01 7.9015E-01 7.9585E-01 7.9745E-01 7.9937E-01  $ Ba-131 Rb-83 Cs-134
Ba-131 Rb-83
         8.0193E-01 8.1851E-01 8.1851E-01 8.3162E-01 8.4090E-01  $ Cs-134 Cs-136 Ba-136m
Ba-131 Ba-131
         8.4702E-01 8.6835E-01 8.8146E-01 9.1407E-01 9.1960E-01  $ Cs-134 Sr-85 Rb-84 Ba-
131 Ba-131
         9.2387E-01 9.5461E-01 9.6894E-01 1.0159E00 1.0386E00    $ Ba-131 Ba-131 Ba-131
Rb-84 Cs-134
         1.0464E00 1.0476E00 1.0481E00 1.0481E00 1.0770E00       $ Ba-131 Ba-131 Cs-136
Ba-136m Rb-86
         1.1679E00 1.1705E00 1.2084E00 1.2183E00 1.2354E00       $ Cs-134 Ba-131 Ba-131
Ba-131 Cs-136
         1.3216E00 1.3419E00 1.3652E00 1.5381E00 1.5513E00       $ Cs-136 Ba-131 Cs-134
Cs-136 Cs-136
         1.5513E00 1.8970E00                                     $ Ba-136m Rb-84
sp2    d 8.1469E-14 4.4210E-18 1.2339E-26 7.9234E-16 1.0776E-26  $ Rb-83 Rb-84 Rb-86 Sr-
85 Rb-86
         6.8211E-41 1.5270E-41 6.9742E-08 2.8274E-08 3.0847E-04  $ Cs-131 Ba-131 Cs-134
Ba-133 Cs-134
         2.1227E-28 1.4924E-28 4.2220E-03 1.1666E-26 5.6689E-13  $ Cs-136 Ba-136m Ba-137m
Ba-140 Rb-83
         5.0338E-17 1.3985E-25 1.0863E-12 9.7613E-17 2.7147E-25  $ Rb-84 Rb-86 Rb-83 Rb-
84 Rb-86
         8.5116E-15 1.6416E-14 9.6154E-28 1.2339E-25 2.8854E-13  $ Sr-85 Sr-85 Ba-140 Rb-
86 Rb-83
         2.5388E-17 7.0746E-26 2.3527E-25 4.3872E-15 6.4494E-26  $ Rb-84 Rb-86 Rb-86 Sr-
85 Rb-86
         1.6702E-40 1.6094E-07 3.0934E-40 3.2189E-07 1.1342E-26  $ Cs-131 Cs-134 Cs-131
Cs-134 Ba-140
         3.4573E-41 5.7375E-08 6.3927E-41 1.0599E-07 6.4109E-04  $ Ba-131 Ba-133 Ba-131
Ba-133 Cs-134
         4.2453E-28 1.8931E-28 8.4034E-03 1.1776E-03 7.8224E-28  $ Cs-136 Ba-136m Ba-137m
Cs-134 Cs-136
         3.5000E-28 1.5508E-02 4.4734E-28 8.2066E-28 1.1266E-07  $ Ba-136m Ba-137m Ba-140
Ba-140 Cs-134
         1.1082E-40 3.8360E-08 2.3211E-41 4.3186E-04 2.8499E-28  $ Cs-131 Ba-133 Ba-131
Cs-134 Cs-136
         1.2767E-28 5.6835E-03 3.0413E-28 3.6359E-09 1.2797E-43  $ Ba-136m Ba-137m Ba-140
Ba-133 Ba-131
         9.4062E-28 9.1741E-43 4.3320E-09 5.6316E-08 1.7530E-44  $ Cs-136 Ba-131 Ba-133
Ba-133 Ba-131
         1.0190E-27 7.3042E-43 4.1152E-29 1.5110E-29 5.2983E-29  $ Cs-136 Ba-131 Cs-136
Ba-140 Ba-140
         4.8556E-16 3.6170E-41 1.7530E-44 4.5521E-17 1.7661E-28  $ Rb-83 Ba-131 Ba-131
Rb-83 Ba-140
         2.6529E-42 4.6747E-44 1.1307E-27 2.1913E-43 1.0665E-09  $ Ba-131 Ba-131 Cs-136
Ba-131 Ba-133
         4.9961E-27 6.7578E-28 7.2505E-29 1.9596E-27 7.0545E-29  $ Ba-140 Ba-136m Cs-136
Cs-136 Cs-136
         2.4542E-41 7.4405E-10 1.5677E-29 3.0093E-42 5.6330E-05  $ Ba-131 Ba-133 Cs-136
Ba-131 Cs-134
         7.8885E-43 3.5119E-42 2.1751E-27 1.1845E-08 2.0685E-43  $ Ba-131 Ba-131 Cs-136
Ba-133 Ba-131
         5.8788E-30 3.0308E-08 3.4596E-27 3.9193E-30 4.7305E-31  $ Cs-136 Ba-133 Ba-140
Cs-136 Ba-136m
         9.7981E-29 3.8626E-05 8.2892E-27 1.1395E-43 1.0260E-07  $ Cs-136 Cs-134 Cs-136
Ba-131 Ba-133
         1.6946E-44 1.7530E-41 1.4782E-08 2.3373E-45 1.6361E-42  $ Ba-131 Ba-131 Ba-133
Ba-131 Ba-131
         2.5118E-27 1.1920E-43 1.5306E-27 5.0837E-44 7.0120E-44  $ Ba-140 Ba-131 Ba-140
Ba-131 Ba-131
         5.8434E-44 7.8493E-31 2.9217E-45 3.9163E-03 4.0904E-43  $ Ba-131 Ba-140 Ba-131
Cs-134 Ba-131
         2.6062E-42 1.5677E-29 5.8434E-41 2.3373E-45 1.9008E-28  $ Ba-131 Cs-136 Ba-131
Ba-131 Cs-136
         2.2762E-16 4.9572E-14 1.7530E-45 1.5174E-12 1.0015E-12  $ Rb-84 Sr-85 Ba-131 Rb-
83 Rb-83
```

```
         1.7530E-45 1.9623E-26 4.3825E-45 2.6879E-45 5.2983E-30  $ Ba-131 Ba-140 Ba-131
Ba-131 Ba-140
         5.4170E-13 2.8830E-16 4.4994E-45 2.2478E-02 4.1389E-02  $ Rb-83 Rb-83 Ba-131 Cs-
134 Cs-134
         1.9517E-43 1.4901E-42 2.0452E-45 2.6180E-01 1.7940E-42  $ Ba-131 Ba-131 Ba-131
Cs-134 Ba-131
         2.8830E-15 4.3241E-45 3.6577E-01 1.6479E-43 1.0622E-15  $ Rb-83 Ba-131 Ba-137m
Ba-131 Rb-83
         1.8114E-43 8.0054E-45 3.9193E-30 2.7031E-31 1.7530E-45  $ Ba-131 Ba-131 Cs-136
Ba-136m Ba-131
         2.9217E-45 2.2305E-14 2.2908E-01 4.4994E-44 8.0420E-15  $ Ba-131 Rb-83 Cs-134
Ba-131 Rb-83
         2.3417E-02 1.7441E-26 2.1963E-27 2.8458E-43 2.3373E-45  $ Cs-134 Cs-136 Ba-136m
Ba-131 Ba-131
         8.0471E-07 5.9484E-18 2.9722E-16 5.7849E-44 1.1102E-44  $ Cs-134 Sr-85 Rb-84 Ba-
131 Ba-131
         8.9988E-43 4.0904E-44 4.5578E-44 1.8130E-18 2.6824E-03  $ Ba-131 Ba-131 Ba-131
Rb-84 Cs-134
         1.1278E-43 1.6536E-42 1.3521E-26 2.2030E-27 1.4215E-21  $ Ba-131 Ba-131 Cs-136
Ba-136m Rb-86
         4.8417E-03 1.9867E-45 2.1620E-45 5.8434E-46 3.9389E-27  $ Cs-134 Ba-131 Ba-131
Ba-131 Cs-136
         9.7981E-30 1.3440E-45 8.1544E-03 1.9596E-29 2.9395E-30  $ Cs-136 Ba-131 Cs-134
Cs-136 Cs-136
         2.0273E-31 3.2694E-18                                  $ Ba-136m Rb-84
si3      -4.60378 4.60378                      $the lower and upper height from pos
location
si4      7.77875 9.04875                     $r1 r2, inner radius and outer radius
sp4      -21 1                         $distribute the source radialy with the correct
probability
c
f4:p 3                                 $give the photon flux for cell 3
f8:p 3                                 $give the photon counts per cm^3 for cell 3
e8   0 3999i 2.0                       $gives the energy bins for cell 3, 4000 bins at
0.5 Kev per bin
nps 200000000                            $run this many particles, 2 billion particles
c sd8 1                                $would give the result in counts instead of counts
per cm^3
 ft8 geb 0.000405 0.00124 0.185                        $brodens the results resolution to
 simulate a read detector for peramiters a=1, b=2, c=3.  FWHM=a+b*SQRT(E+c*E^2), E is in
                                          MeV.
```

APPENDIX B

Sample ORIGEN input deck for cerium

```
-1
-1
-1
 RDA  Irradiation of 50mg Ce
 RDA
 RDA
 LIB  0  1 2 3  204 205 206  9  50 0 1 1
 PHO     101 102 103  10
 INP  1   1  -1  -1   1   1
 BUP
 IRF 0.517  3.9E13  1 2 3 2
 DEC 1          2 3 3 0
 DEC 2          3 4 3 0
 DEC 1          4 5 4 0
 DEC 1.1        5 6 4 0
 DEC 7          6 7 4 0
 DEC 30         7 8 4 0
 BUP
 OPTL 4*8 5 8 5 5 20*8
 OPTA 4*8 6 8 8 8 8 16*8 8 8 8
 OPTF 4*8 8 8 8 21*8
 OUT     8   1  -1   0
 END
1 80160 0.02756 80170 0.0000105 80180 0.0000566 0 0.0
1 70140 0.004822 70150 0.0000178 581360 0.0000298 581380 0.0000405
1 581400 0.01427 581420 0.00179 010010 0.001395 010020 1.604E-7
 0
```

Sample ORIGEN input deck for ytterbium

```
-1
-1
-1
 RDA  Irradiation of 50mg Yb
 RDA
 RDA
 LIB  0  1 2 3  204 205 206  9  50 0 1 1
 PHO     101 102 103  10
 INP  1   1  -1  -1   1   1
 BUP
 IRF 0.067  4.0E12  1 2 3 2
 DEC 1          2 3 3 0
 DEC 2          3 4 3 0
 DEC 3          4 5 3 0
 DEC 5          5 6 3 0
 DEC 1          6 7 4 0
 DEC 30         7 8 4 0
 BUP
 OPTL 4*8 5 8 5 5 20*8
 OPTA 4*8 6 8 8 8 8 16*8 8 8 8
 OPTF 4*8 8 8 8 21*8
 OUT     8   1  -1   0
 END
1 701680 0.0000241 701700 0.000563 701710 0.002644 701720 0.00404
1 701730 0.002986 701740 0.00589 701760 0.00236 70140 0.004483
1 80160 0.02563 80170 0.00000976 80180 0.0000527 70150 0.00001656
1 010010 0.00129 010020 1.489E-7 0 0.0 0 0.0
 0
```

APPENDIX C

C.1 Plots showing statistical analysis of experimental data

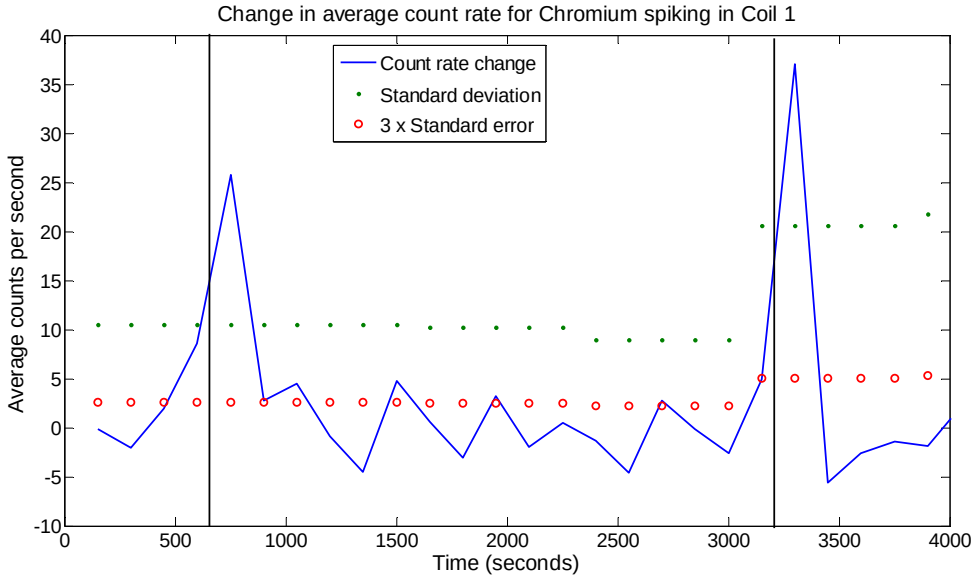

The difference in the average count rate from one point to the next is compared with the standard deviation and 3x standard error to determine when the activity increase is significant.

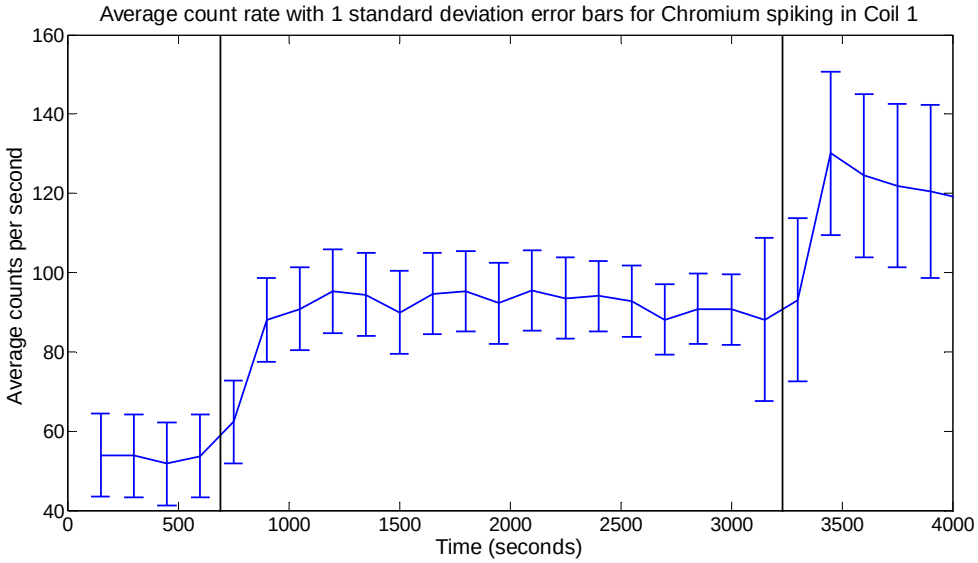

Averaged total spectrum count rate vs. time with error bars of one standard deviation for chromium spiking experiment in Coil 1.

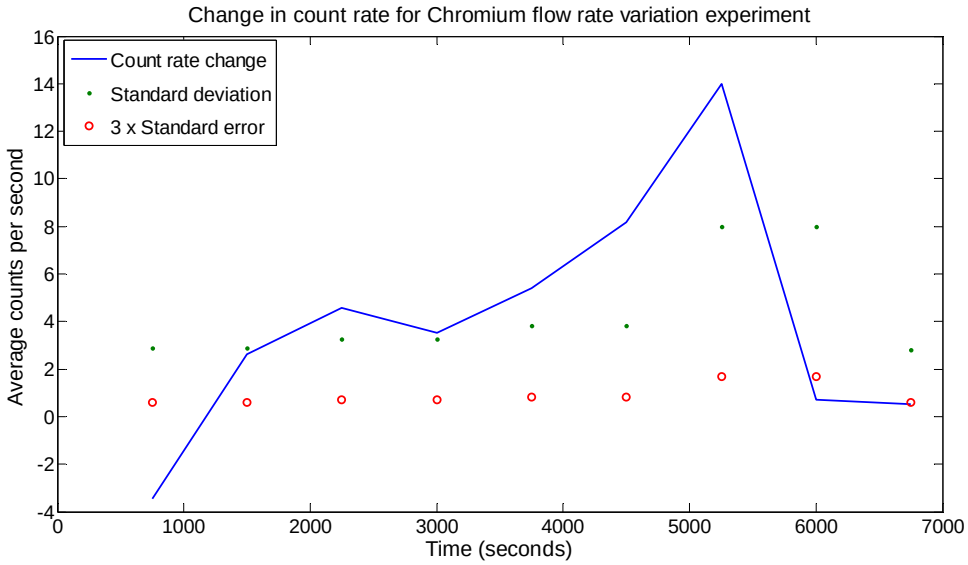

The difference in the average count rate from one point to the next is compared with the standard deviation and 3x standard error to determine when the activity increase is significant.

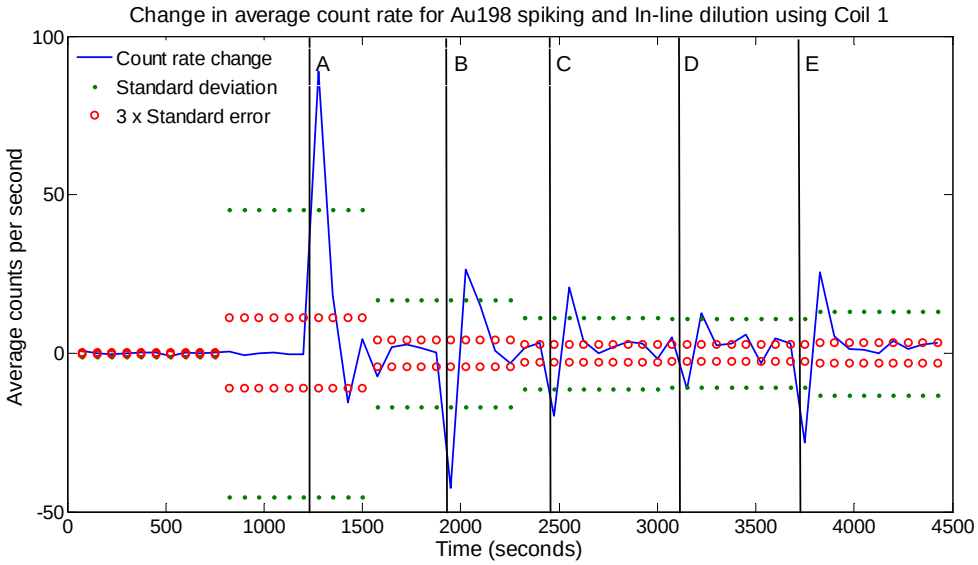

The difference in the average count rate from one point to the next is compared with the positive and negative standard deviation and 3x standard error to determine when the activity increase or decrease is significant.

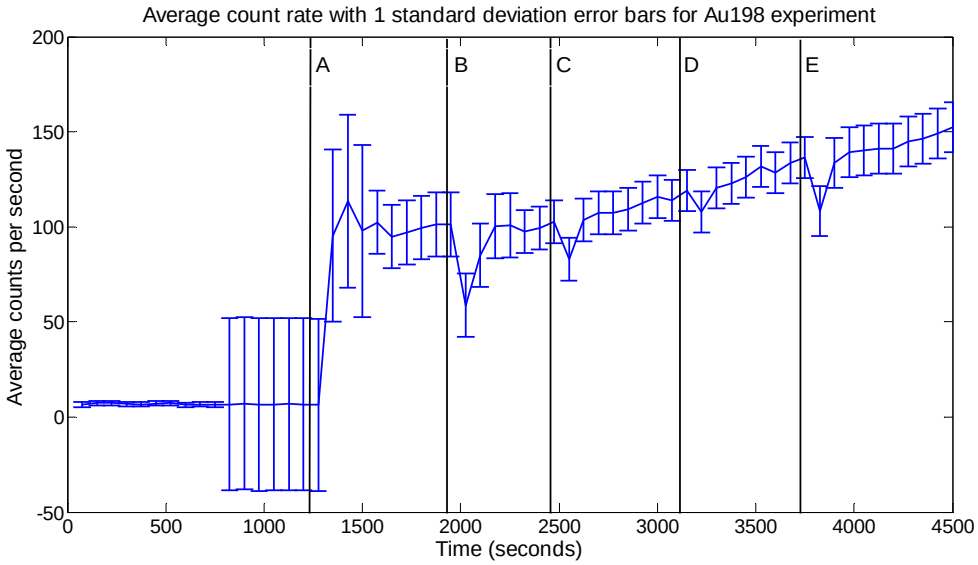

Averaged total energy spectrum count rate for Au198 experiment as a function of time with error bars of 1 standard deviation.

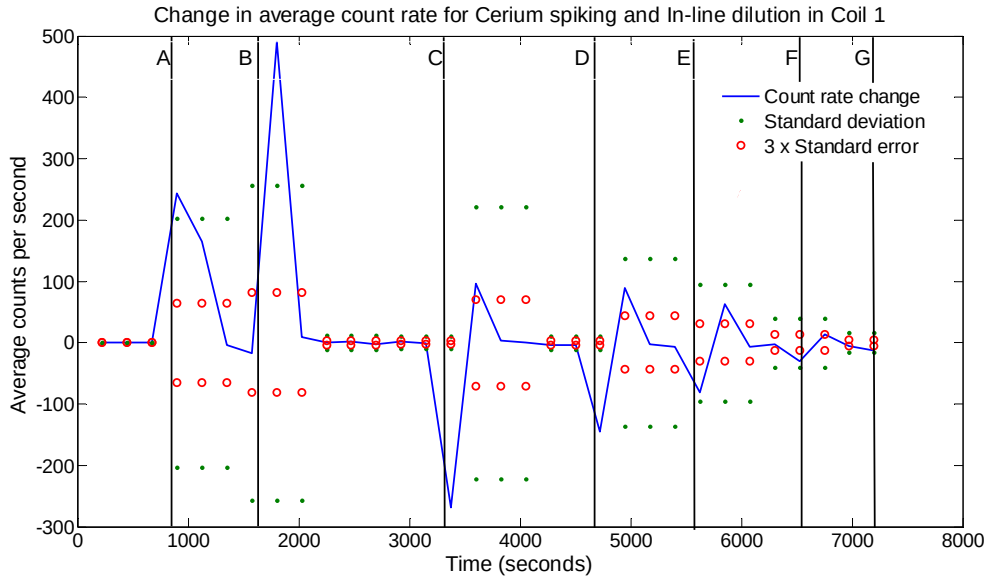

The difference in the average count rate from one point to the next is compared with the positive and negative standard deviation and 3x standard error to determine when the activity increase or decrease is significant.

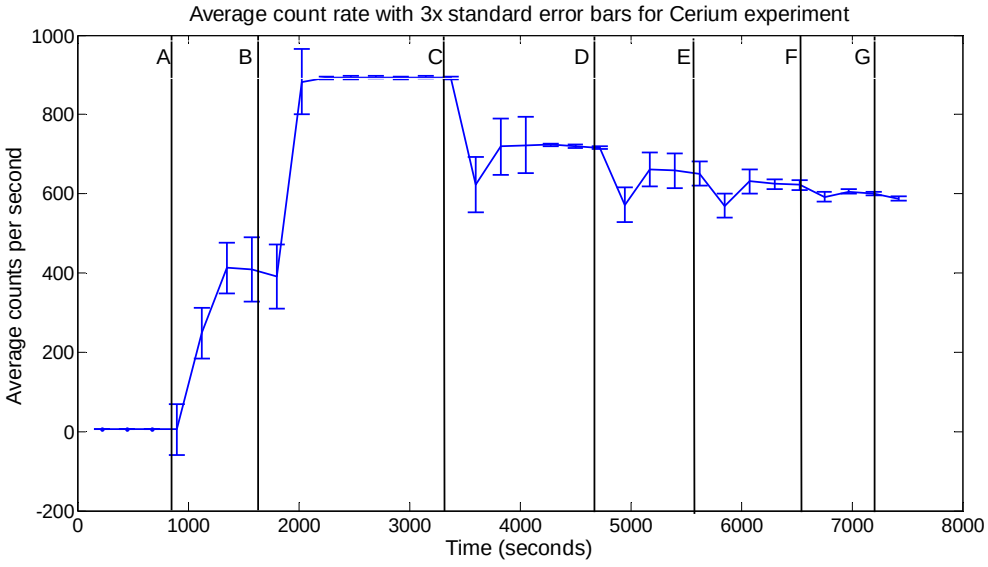

Averaged total energy spectrum count rate as a function of time for cerium experiment with error bars of three times the standard error.

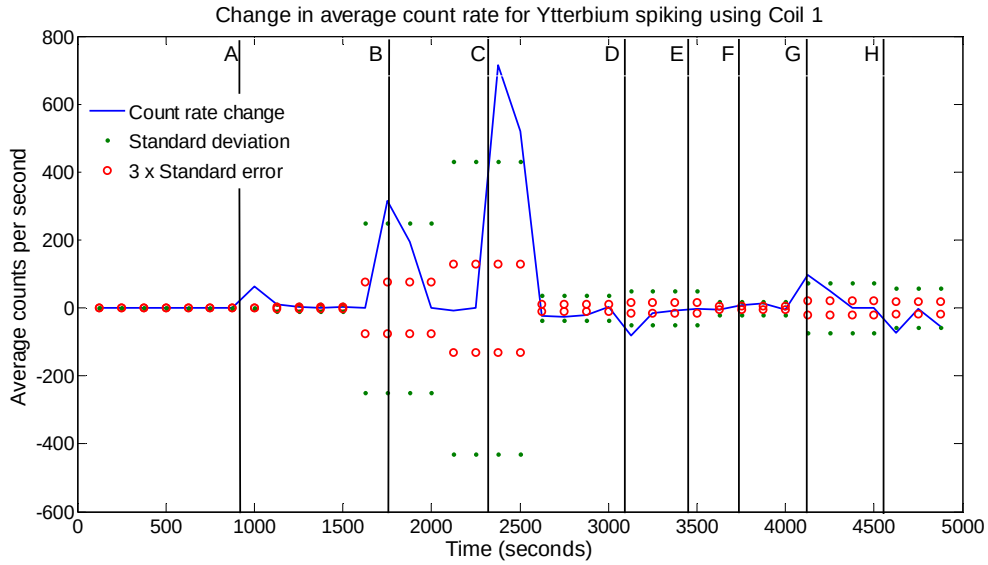

The difference in the average count rate from one point to the next is compared with the positive and negative standard deviation and 3x standard error to determine when the activity increase or decrease is significant.

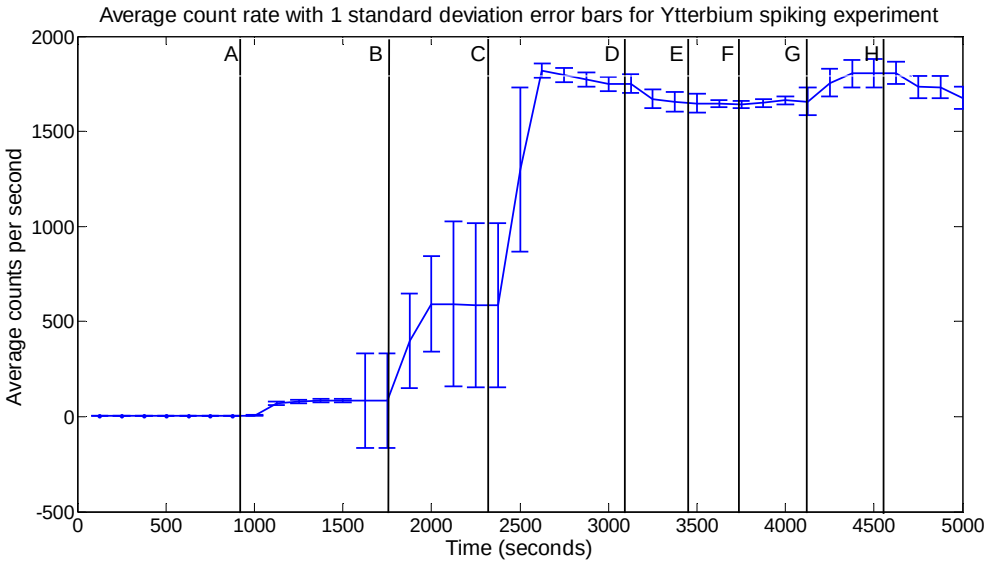

Averaged total energy spectrum count rate as a function of time for ytterbium experiment with error bars of 1 standard deviation.

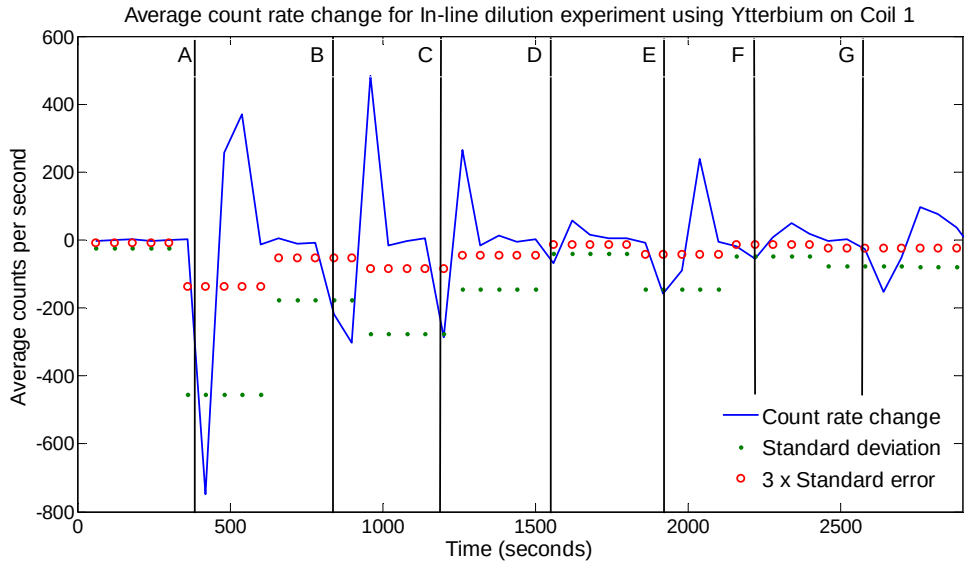

The difference in the average count rate from one point to the next is compared with the negative standard deviation and 3x standard error to determine when the activity decrease is significant.

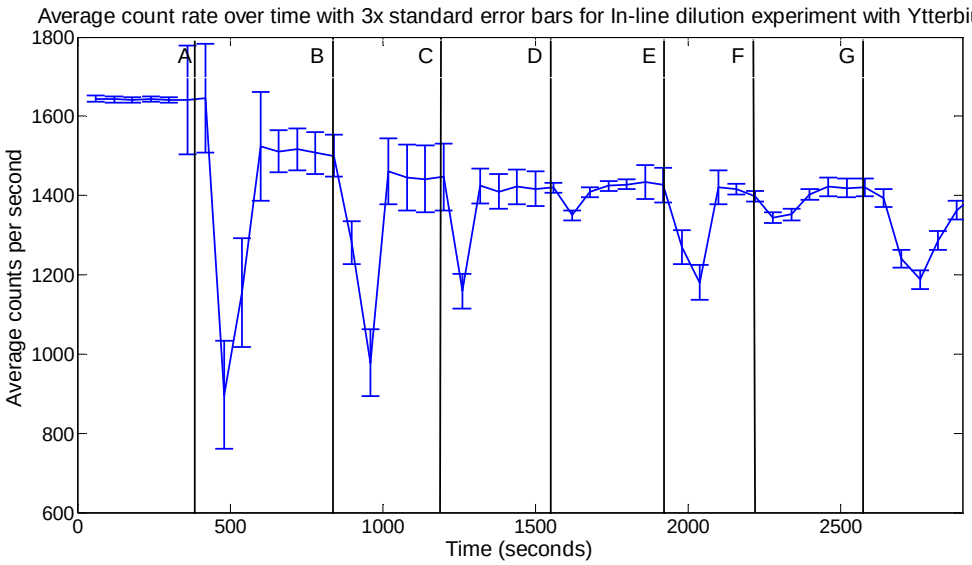

Averaged total spectrum count rate vs. time for ytterbium in-line dilution experiment using coil 1 with error bars of three times the standard error.

Results of peak ratio comparisons for fully filled vs. partially filled pipe condition for ytterbium experiment					
	peak 1	peak 2	peak 3	peak 4	peak 5
Partial filled/total FWHM area	0.146	0.183	0.177	0.193	0.299
Fully filled/total FWHM area	0.151	0.187	0.166	0.197	0.298
difference	0.005	0.004	0.011	0.0043	0.0015
3 x standard error	0.009	0.012	0.032	0.0152	0.0153
Partial filled/total area	0.065	0.081	0.078	0.0852	0.132
Fully filled/total area	0.066	0.081	0.072	0.0856	0.129
difference	0.0011	0.0002	0.0062	0.0004	0.0028
3 x standard error	0.0055	0.0060	0.0135	0.0067	0.0064

C.2 Geometry comparison experiments

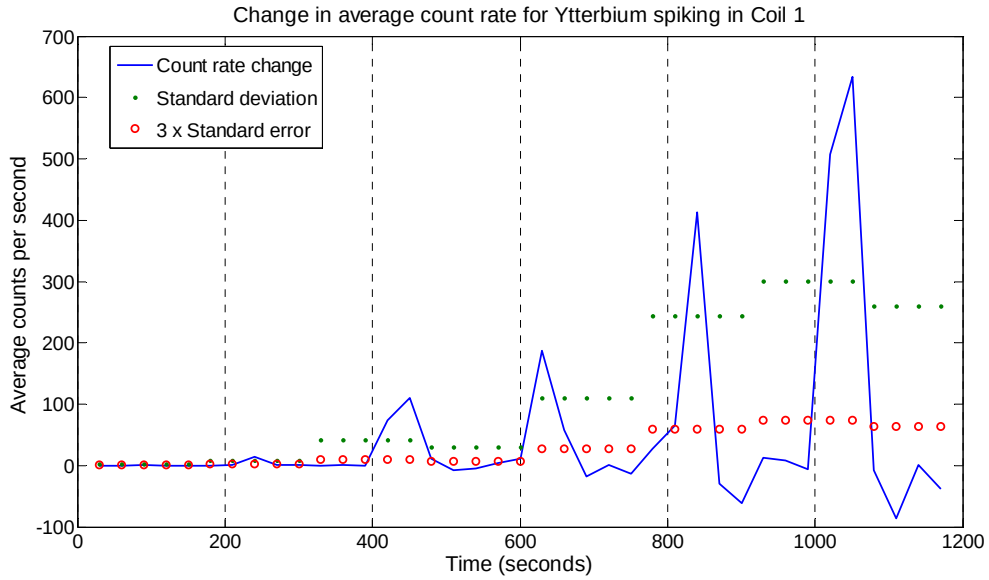

The difference in the average count rate from one point to the next is compared with the standard deviation and 3x standard error to determine when the activity increase is significant.

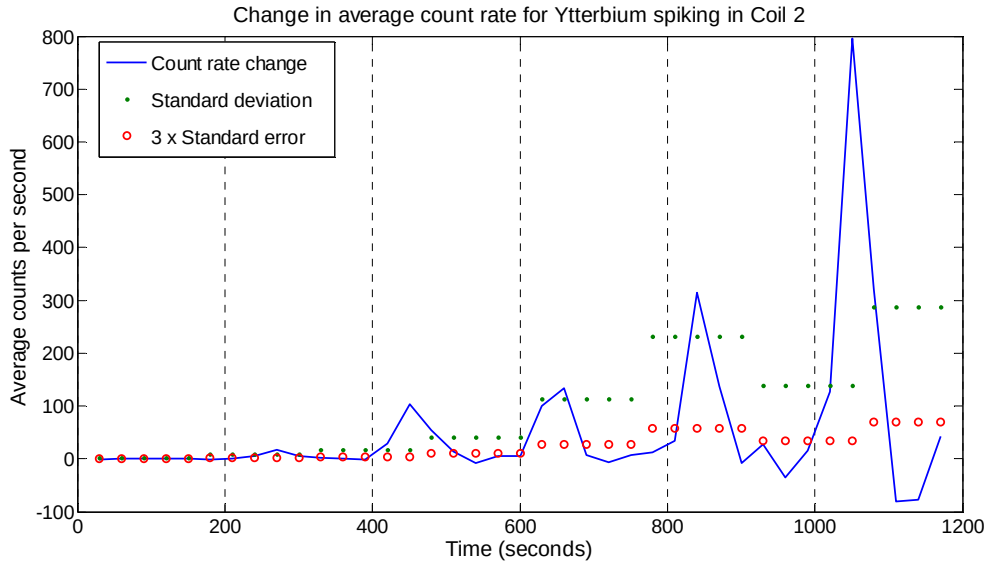

The difference in the average count rate from one point to the next is compared with the standard deviation and 3x standard error to determine when the activity increase is significant.

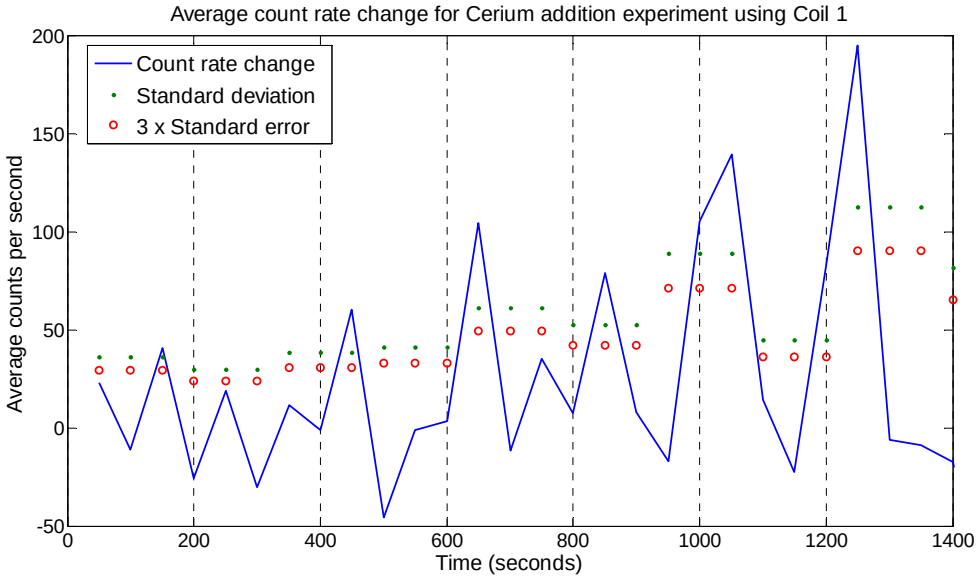

The difference in the average count rate from one point to the next is compared with the standard deviation and 3x standard error to determine when the activity increase is significant.

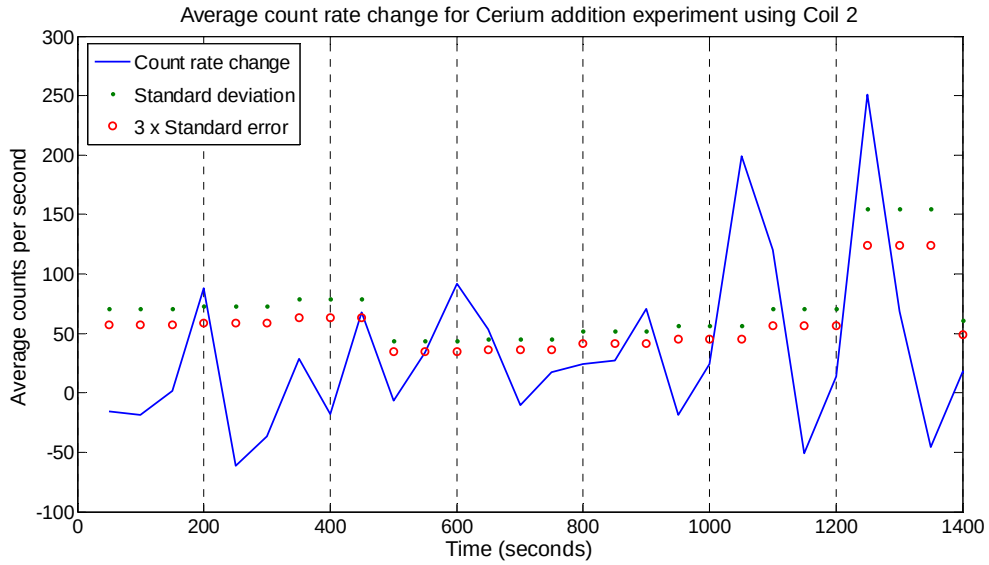

The difference in the average count rate from one point to the next is compared with the standard deviation and 3x standard error to determine when the activity increase is significant.

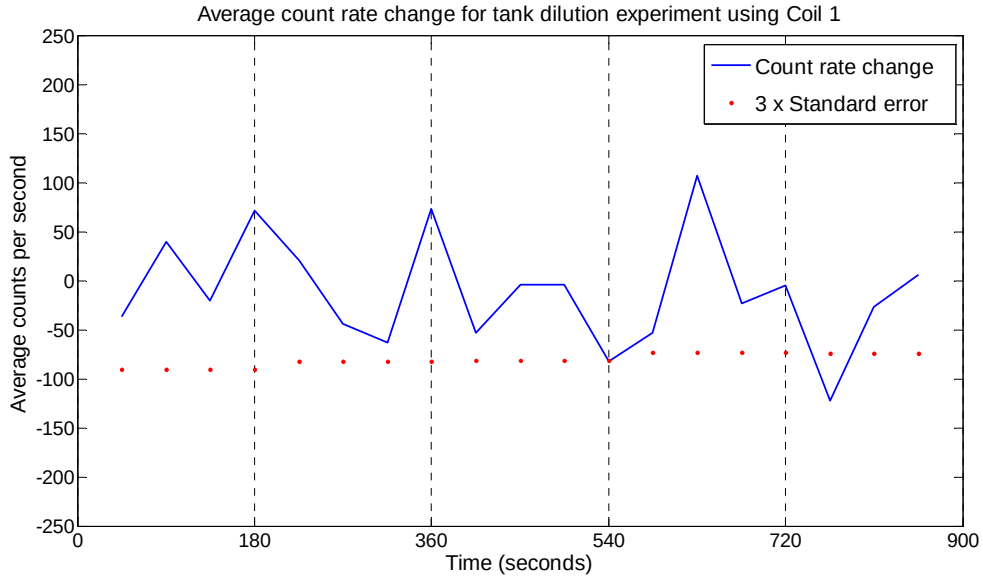

The difference in the average count rate from one point to the next is compared with the negative 3x standard error to determine when the activity decrease is significant.

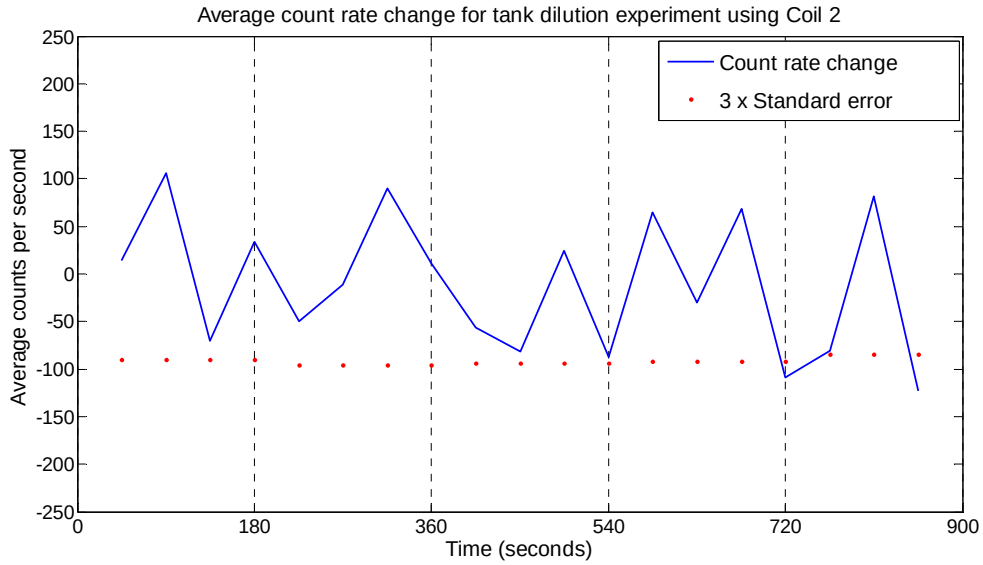

The difference in the average count rate from one point to the next is compared with the negative 3x standard error to determine when the activity decrease is significant.

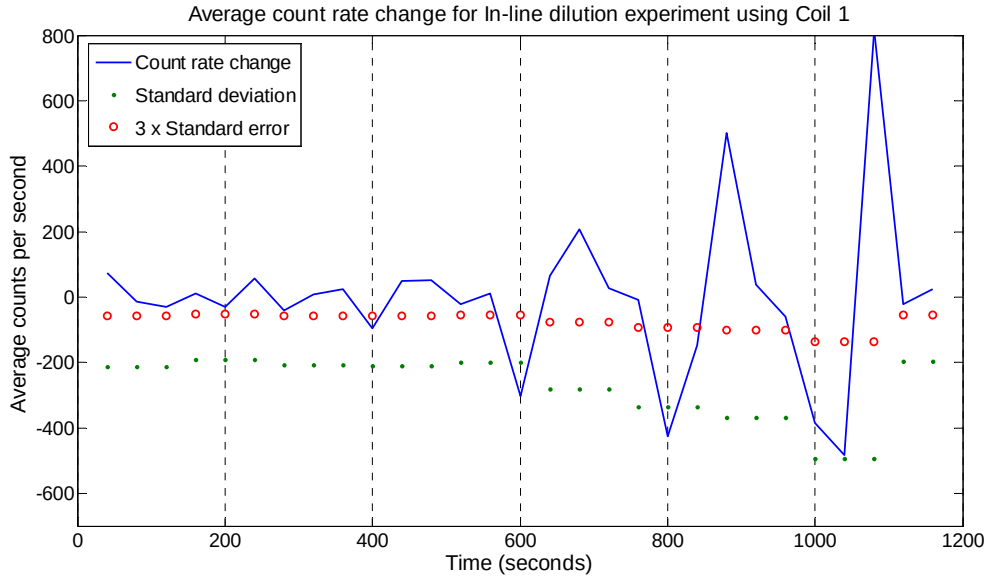

The difference in the average count rate from one point to the next is compared with the negative standard deviation and 3x standard error to determine when the activity decrease is significant.

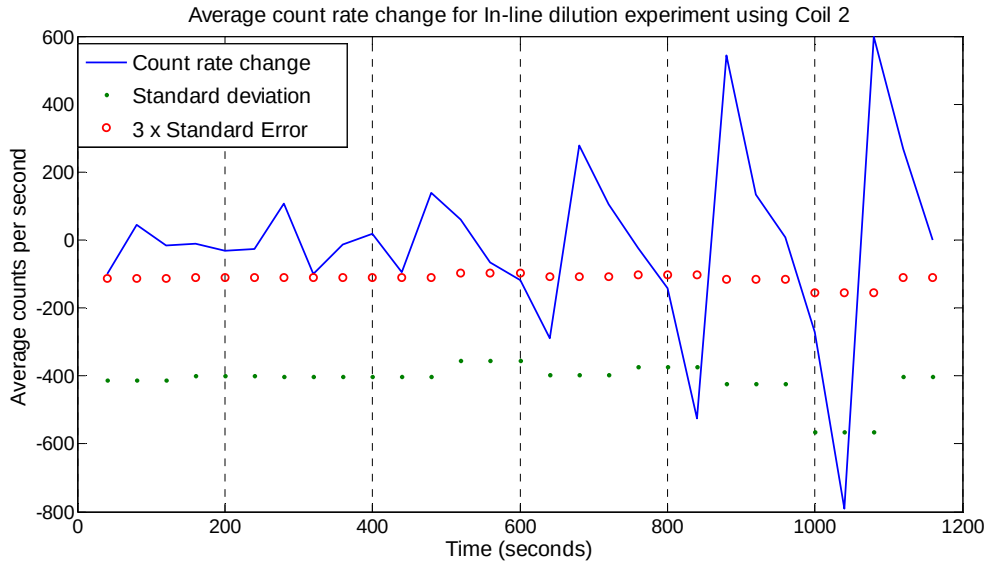

The difference in the average count rate from one point to the next is compared with the negative standard deviation and 3x standard error to determine when the activity decrease is significant.

C.3 Variable flow rate experiments using Coil 2

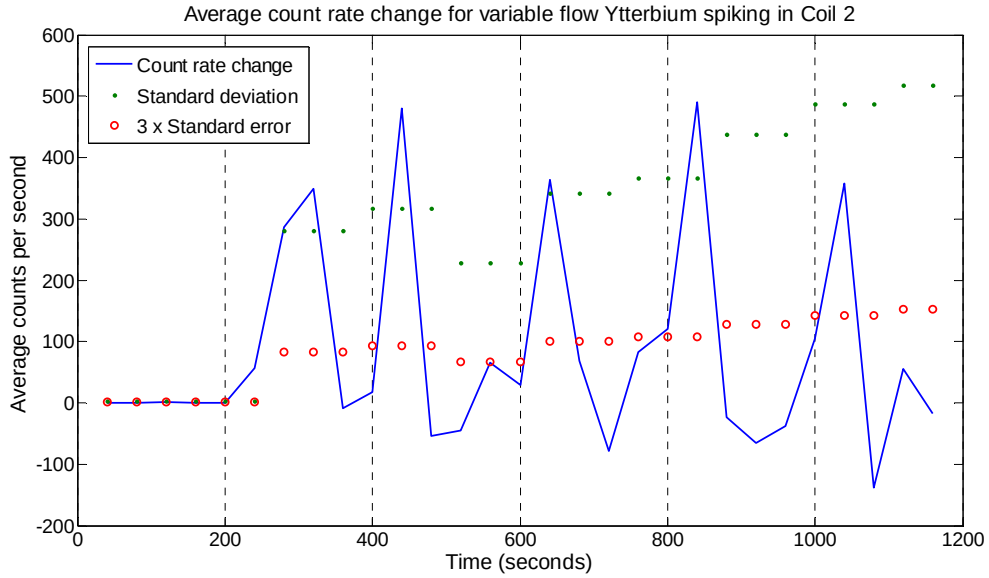

The difference in the average count rate from one point to the next is compared with the standard deviation and 3x standard error to determine when the activity increase is significant.

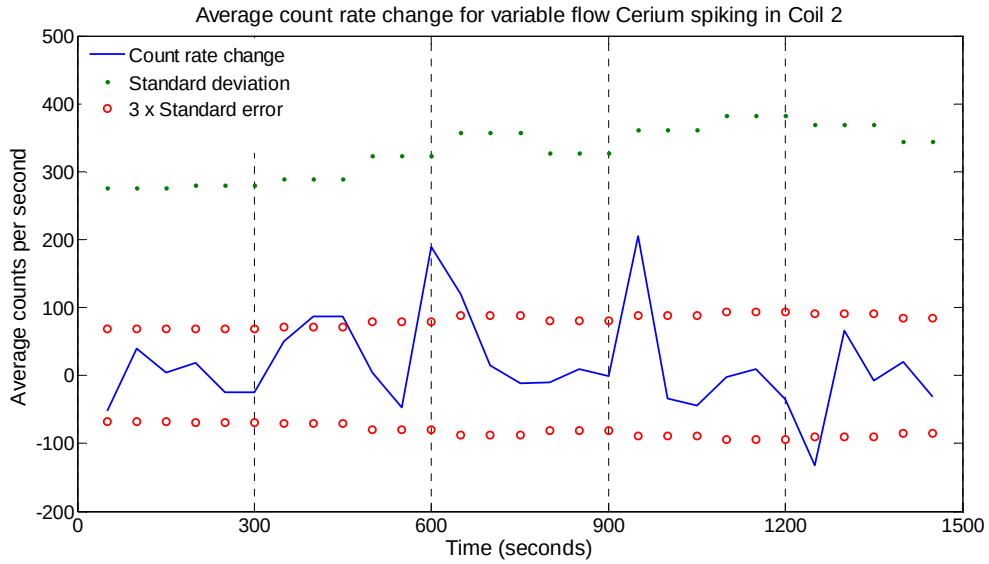

The difference in the average count rate from one point to the next is compared with the standard deviation and the positive and negative 3x standard error to determine when the activity increase or decrease is significant.

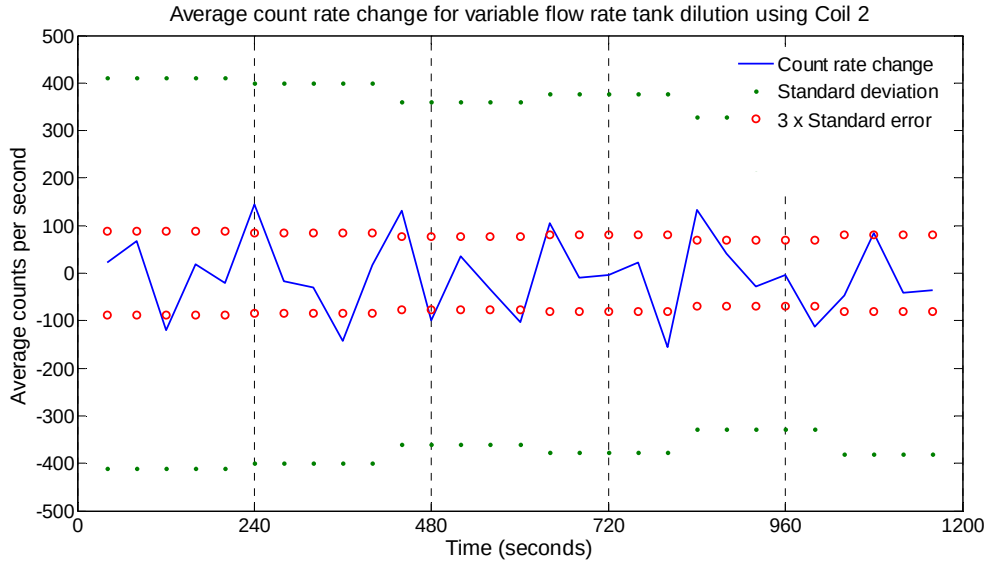

The difference in the average count rate from one point to the next is compared with the positive and negative standard deviation and 3x standard error to determine when the activity increase or decrease is significant. (no significant points were identified in this particular case)

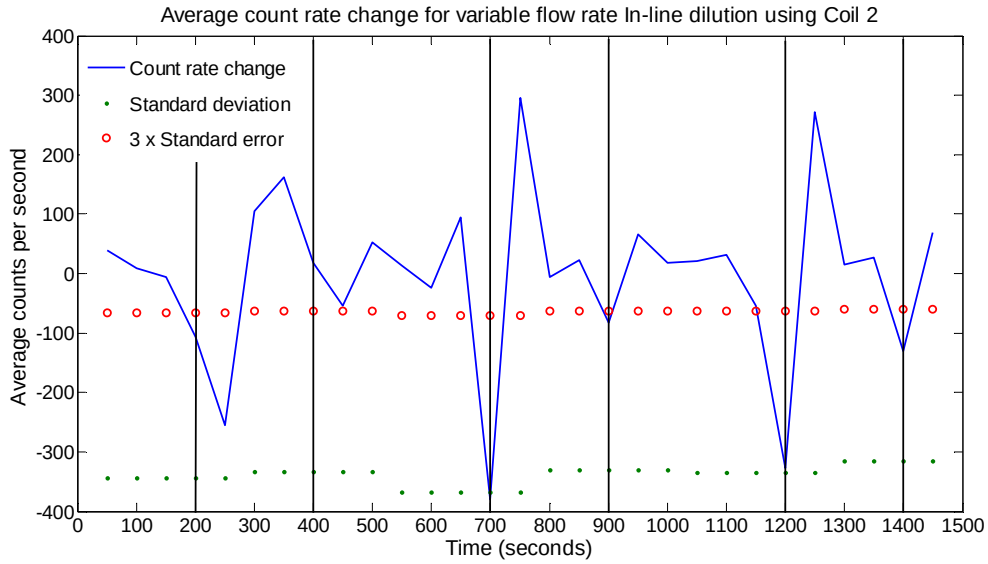

The difference in the average count rate from one point to the next is compared with the negative standard deviation and 3x standard error to determine when the activity decrease is significant.

APPENDIX D

MCNP results

Simulation of cerium spiking into system containing ytterbium in Coil 1.

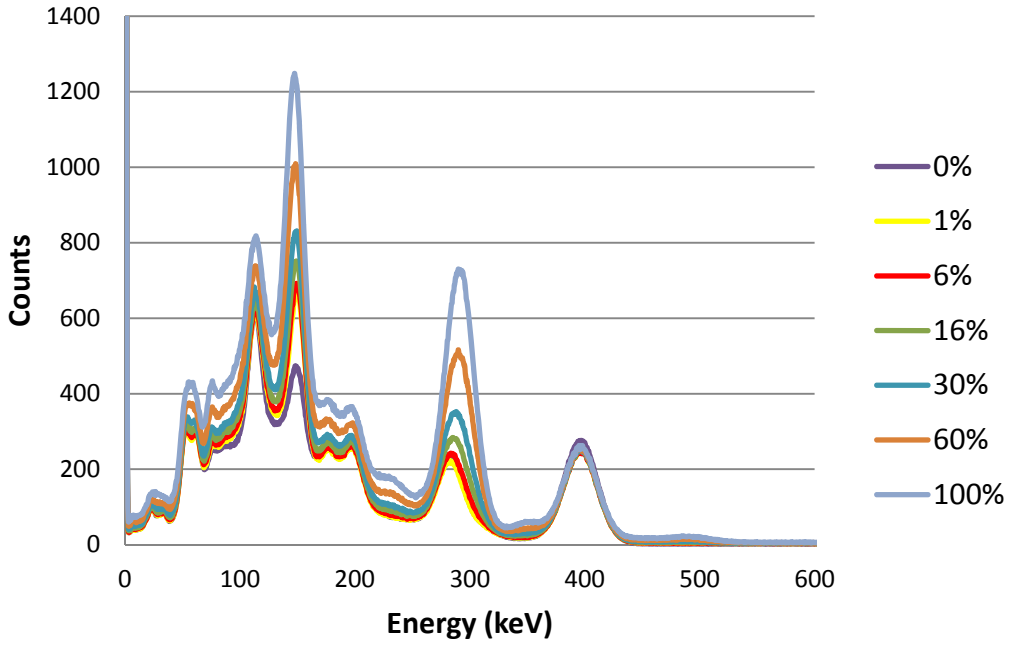

Experimental results for cerium spiking into system containing ytterbium in Coil 1.

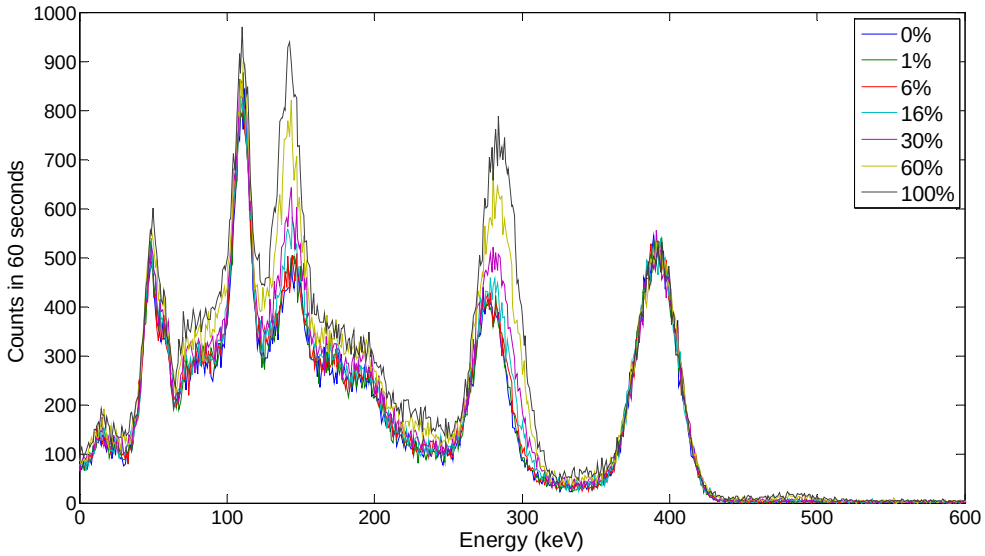

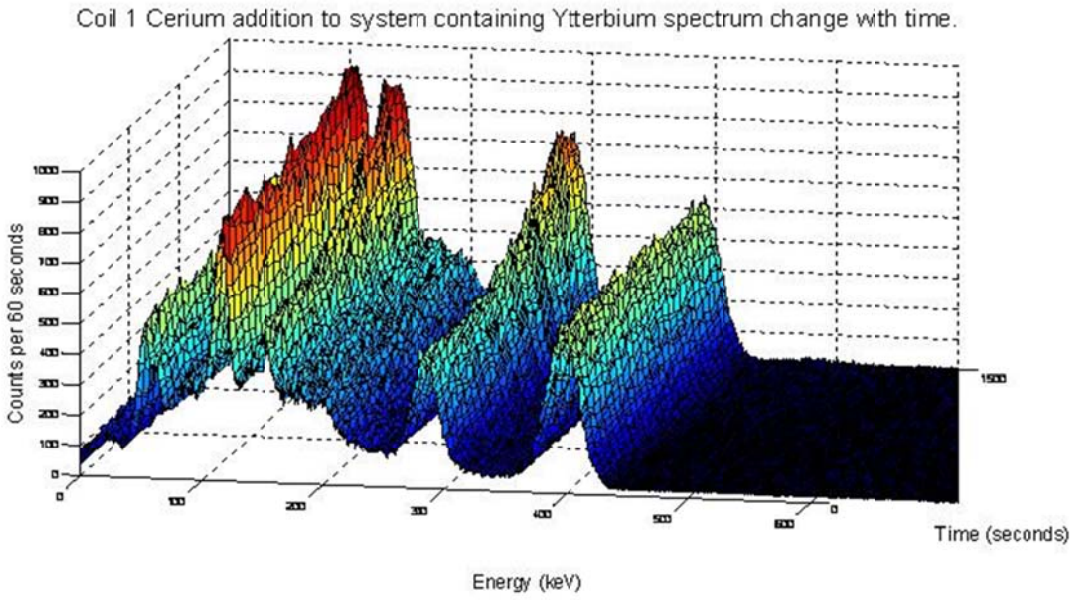

Simulation of cerium spiking into system containing ytterbium in Coil 2.

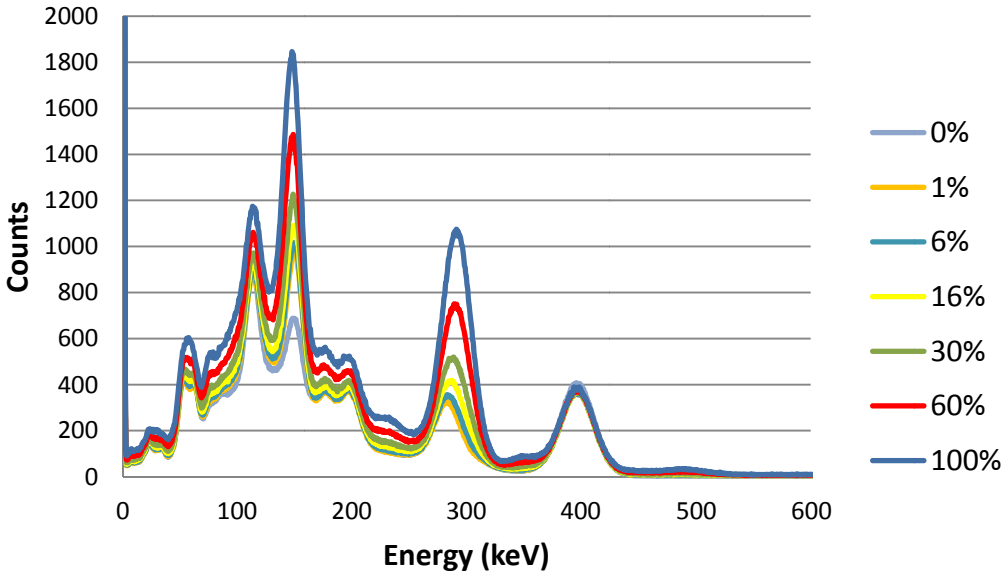

Experimental results for cerium spiking to system containing ytterbium in Coil 2.

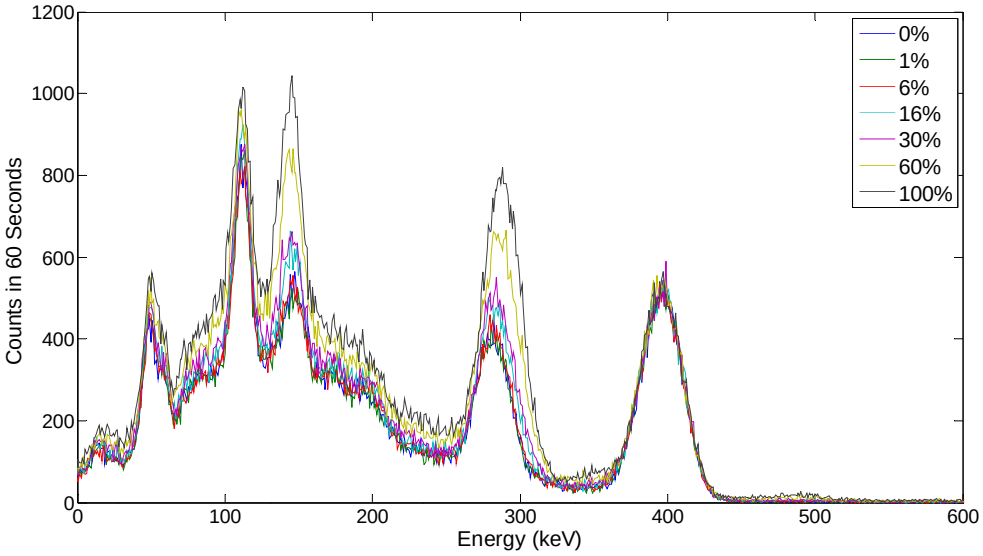

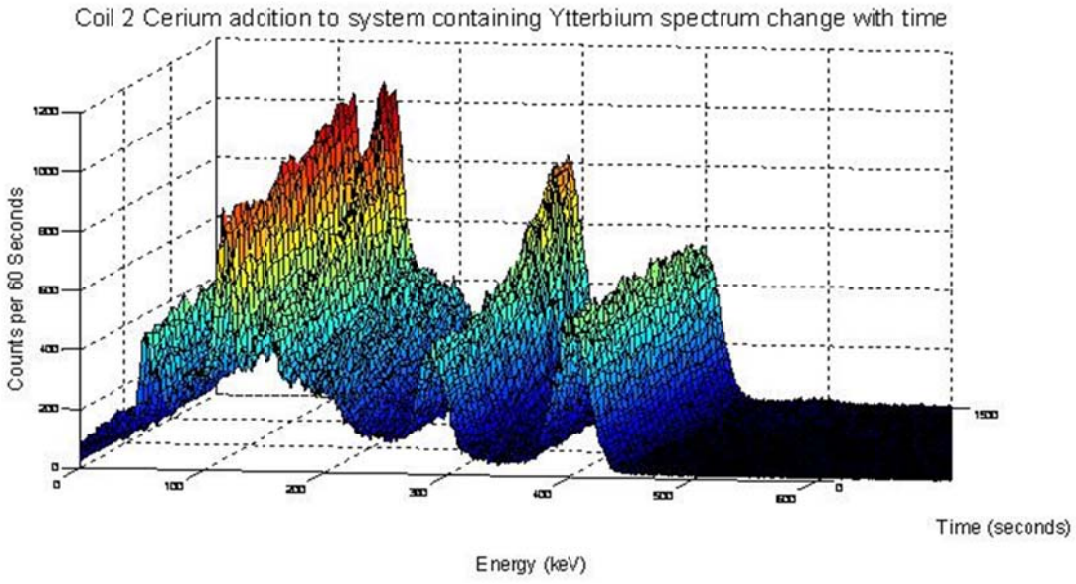

Simulation of cerium spiking to system containing ytterbium in Coil 3.

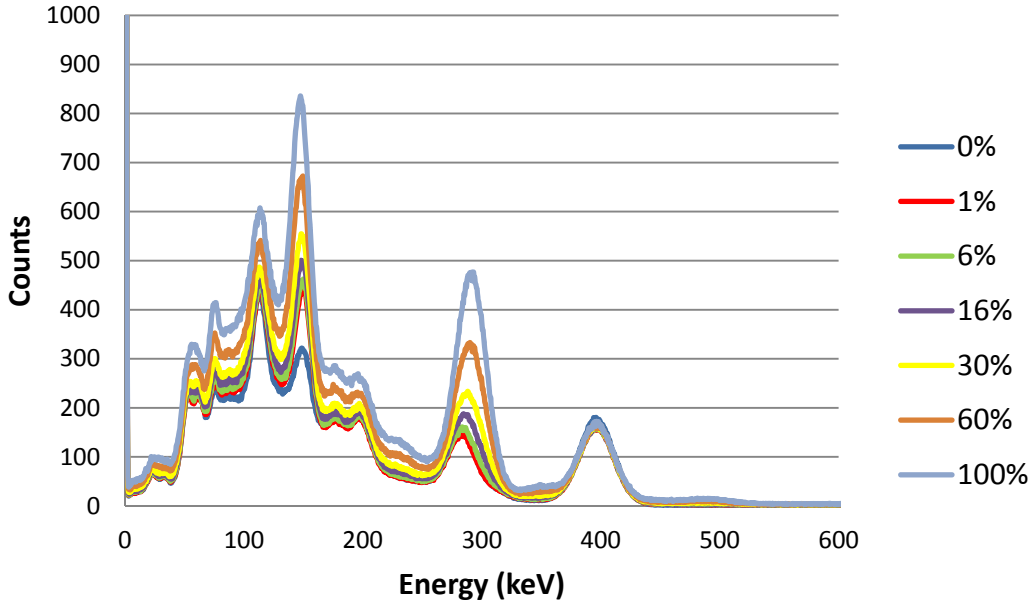

Simulation of cerium addition to system containing ytterbium in Coil 1 using HPGe detector.

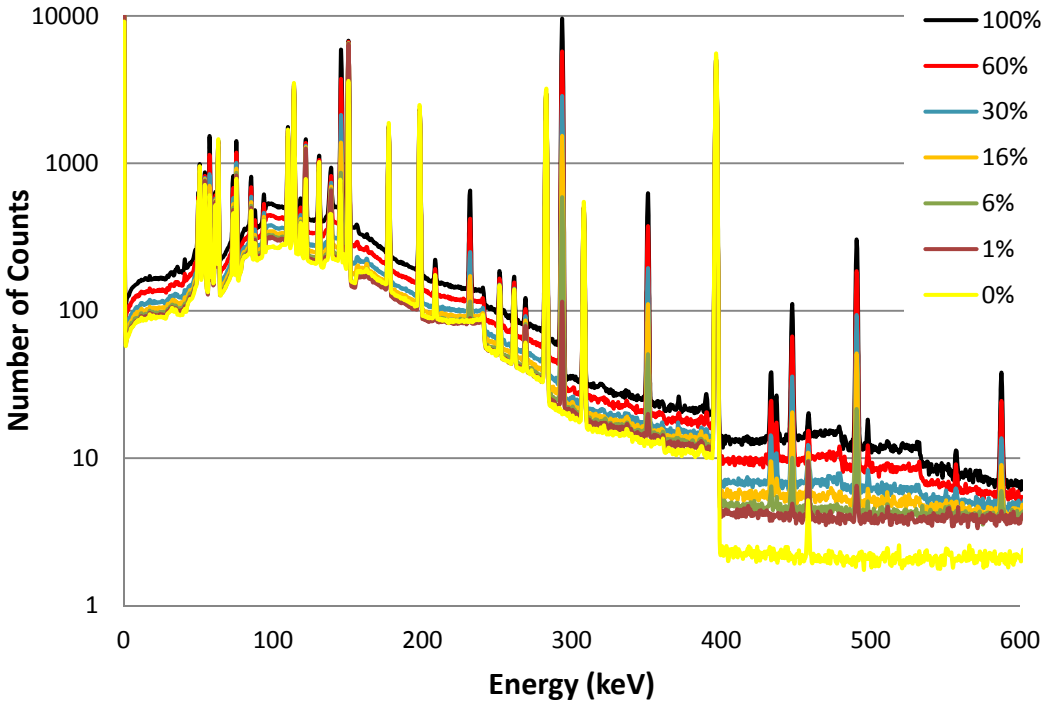

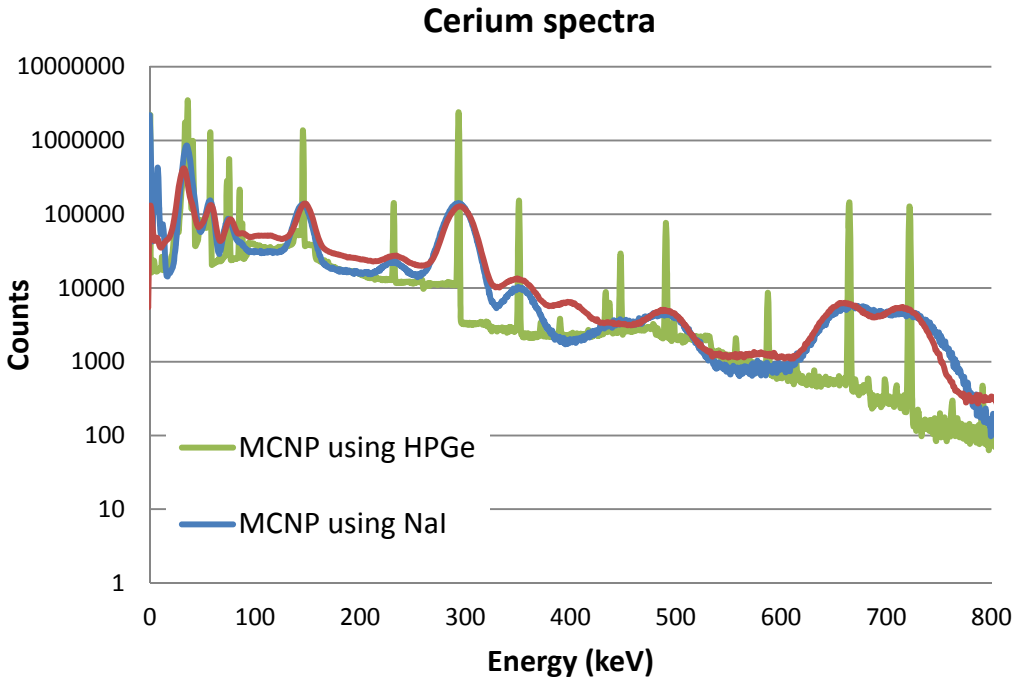
Cerium spectra
10000000
1000000
100000
10000
1000
100
10
1
Counts
MCNP using HPGe
MCNP using NaI
0
100
200
300
400
500
600
700
800
Energy (keV)

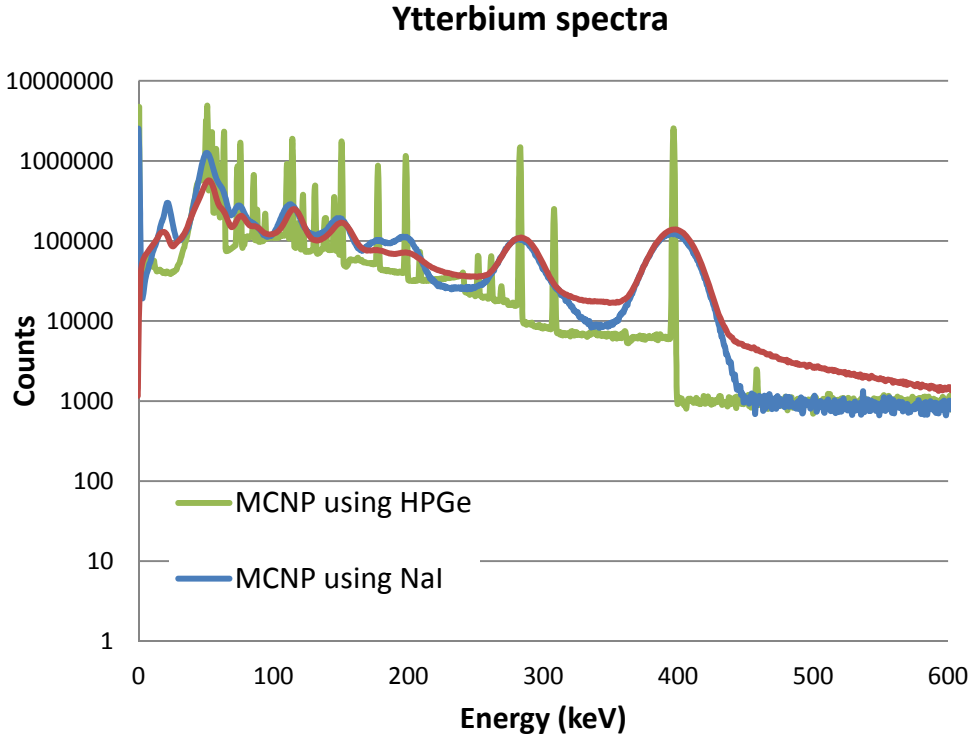
Ytterbium spectra
10000000
1000000
100000
10000
1000
100
10
1
Counts
MCNP using HPGe
MCNP using NaI
0
100
200
300
400
500
600
Energy (keV)

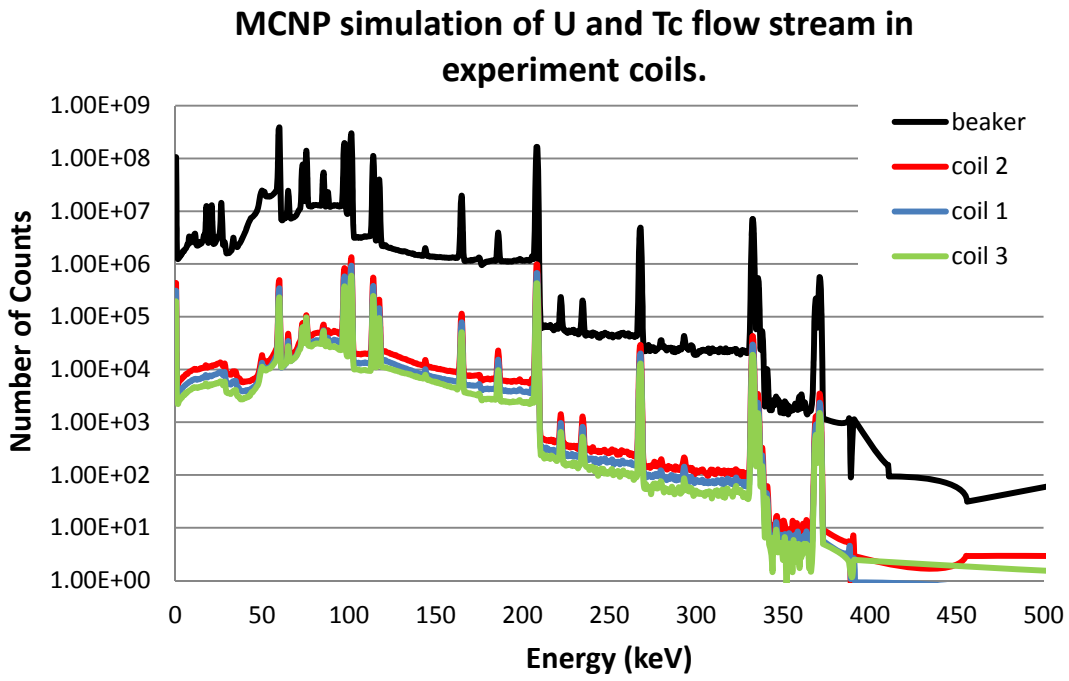
MCNP simulation of U and Tc flow stream in experiment coils.
Number of Counts
1.00E+09
1.00E+08
1.00E+07
1.00E+06
1.00E+05
1.00E+04
1.00E+03
1.00E+02
1.00E+01
1.00E+00
0
50
100
150
200
250
300
350
400
450
500
Energy (keV)
beaker
coil 2
coil 1
coil 3

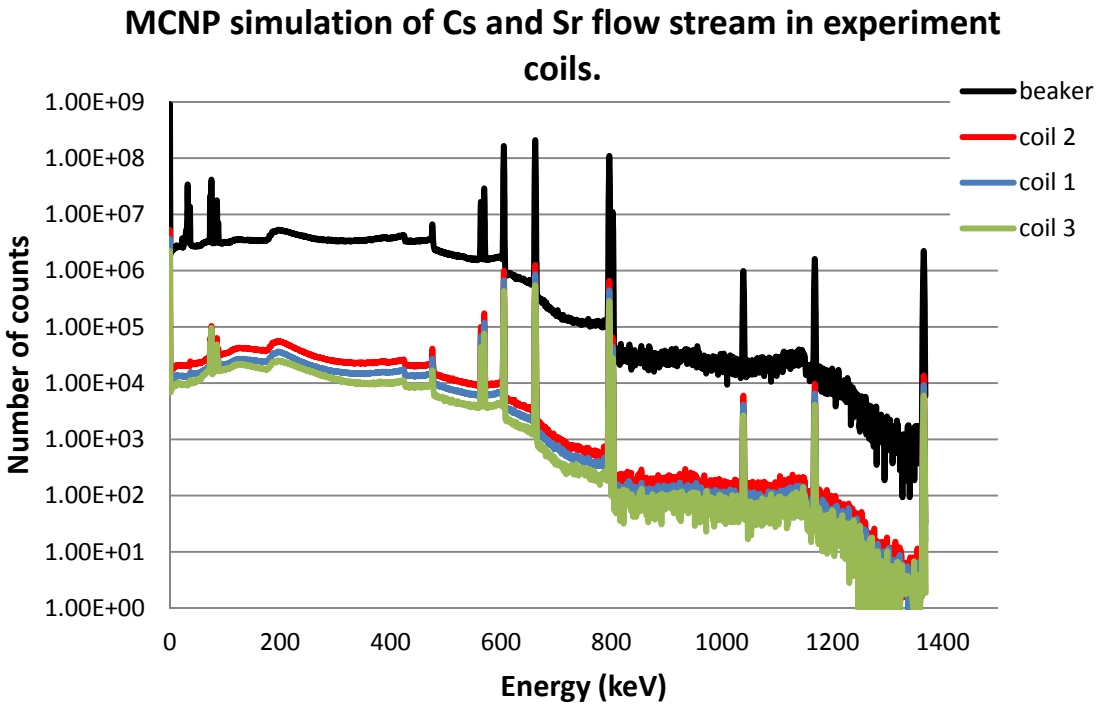
MCNP simulation of Cs and Sr flow stream in experiment coils.
Number of counts
1.00E+09
1.00E+08
1.00E+07
1.00E+06
1.00E+05
1.00E+04
1.00E+03
1.00E+02
1.00E+01
1.00E+00
0
200
400
600
800
1000
1200
1400
Energy (keV)
beaker
coil 2
coil 1
coil 3

VITA

Name:	Thomas Russell Hogelin
Address:	Department of Nuclear Engineering Texas A&M University, 3133 TAMU College Station, TX 77843-3133
Email Address:	TomHogelin@tamu.edu
Education:	B.M.E., Mechanical Engineering, Auburn University, 2006 M.S., Nuclear Engineering, Texas A&M University, 2010